RESILIENCE AND CONNECTIVITY OF CORAL REEFS AT MULTIPLE SPATIAL SCALES THROUGHOUT THE WIDER CARIBBEAN BASIN

John P. Rippe

A dissertation submitted to the faculty at the University of North Carolina at Chapel Hill in partial fulfillment of the requirements for the degree of Doctor of Philosophy in the Department of Marine Sciences.

Chapel Hill
2019

Approved by:

Karl D. Castillo

Adrian Marchetti

John F. Bruno

Sarah W. Davies

Scott M. Gifford

ABSTRACT

John P. Rippe: Resilience and connectivity of coral reefs at multiple spatial scales throughout the wider Caribbean basin
(Under the direction of Karl Castillo)

As reports of coral reef decline across the globe continue to mount, it is critical that coastal managers and researchers understand not only the environmental factors that jeopardize coral health, but also the biological and evolutionary forces that strengthen their resilience. Warming oceans are often cited as the most pressing threat to coral reefs, as high temperatures degrade the delicate symbiosis between corals and their single-celled algal partners. This symbiotic breakdown inhibits coral growth and, in severe cases, can lead to widespread mortality. Additionally, rising ocean temperatures have also been shown to significantly increase the virulence and distribution of coral pathogens, which have caused several major coral mortality events throughout the Caribbean region over the past three decades.

Adopting an interdisciplinary approach that incorporates coral skeletal analysis, disease ecology and population genetics, this research explores the physiological resilience of corals in the wider Caribbean basin to these compounding climate threats and evaluates the patterns by which population connectivity may bolster the long-term evolutionary resilience of corals across a cascade of spatial scales. First, we compared the differential response of inner and outer reef corals across the Florida Keys Reef Tract to a major ongoing coral disease outbreak (Chapter 1). Recent research has shown that inner reef corals are better suited to cope with environmental stress due to their exposure to dynamic nearshore conditions, and indeed we found significantly lower disease

incidence and mortality at inner reef sites. We then investigated the extent to which this enhanced resilience translates to differences in growth patterns between inner and outer reef corals on the Florida Keys Reef Tract (Chapter 2) and across the western Caribbean basin (Chapter 3) and, in doing so, characterized the environmental drivers behind the observed coral growth trends. Lastly, we explored the genetic structure of a foundational coral species across the wider Caribbean and Gulf of Mexico region to infer a network of population connectivity that may enhance the exchange of adaptive genetic variation throughout the species range (Chapter 4).

To my wife and my dog.

ACKNOWLEDGEMENTS

This is one of those things in life that truly cannot be achieved individually. I owe thanks to each and every person who has had a hand in helping me get to this point and who has supported me along the way. First and foremost, to my advisor Karl Castillo, whose infectious joy and enthusiasm for science is a constant reminder to never stop cherishing the journey and to always appreciate the fortune in being able to do this job for a living. I am immensely grateful also to Sarah Davies, who in addition to being a great friend has been instrumental in helping me navigate the unique and often amorphous challenges of a career in academia. Thank you also to the rest of my graduate committee, Adrian Marchetti, John Bruno and Scott Gifford, for your sage wisdom and guidance along the way.

To my amazing friends and colleagues, Colleen Bove, Justin Baumann, Hannah Aichelman, Brooke Benson, Nicola Kriefall, Dan Wuitchik, Alex Hounshell, Jill Arriola, Molly Bost, Kelsey Jesser, Carter Smith and the many others, thank you for exemplifying and sharing with me the passion and excitement that I love about the scientific endeavor. And finally to my family, Allie, Mom, Dad, Matt, Mom-in-law, Dad-in-law, Jessie and Hurley, your endless love and support truly keeps everything in perspective and has made this journey so much better for it. I would not be here without you.

TABLE OF CONTENTS

LIST OF TABLES

LIST OF FIGURES

LIST OF ABBREVIATIONS AND SYMBOLS

ACCRETE	Acidification, Climate and Coral Reef Ecosystems Team
AIC	Akaike's Information Criterion
AMO	Atlantic Multidecadal Oscillation
AMOVA	Analysis of molecular variance
ANOVA	Analysis of variance
AR	Alligator Reef
ARMA	Autoregressive moving average
AVHRR	Advanced Very High Resolution
BAH	Bahamas
BAR	Barbados
BEL	Belize
BH	Basin Hill Shoals
BS	Bache Shoals
BTRC	Bocas del Toro Reef Complex
CF	Carysfort Reef
CI	Confidence interval
CR	Cheeca Rocks
CT	X-ray computed tomography
CUR	Curaçao
CV	Coefficient of variation
DHW	Degree heating week
DiProPerm	Distance-Projection-Permutation

DPF	Days post fertilization
DS	Dark spots
DWD	Distance weighted discrimination
ENA	Excluding null allele
ES	Eastern Sambo
FGB	Flower Garden Banks
FKRT	Florida Keys Reef Tract
FLK	Florida Keys
FR	Fowey Rocks
FRRP	Florida Reef Resilience Program
GAM	Generalized additive model
GHRSST	Group for High Resolution Sea Surface Temperature
HSD	Honest significant difference
HWE	Hardy-Weinberg equilibrium
IR	Inner reef
LD	Linkage disequilibrium
LK	Lower Keys
LME	Linear mixed effect
MBRS	Mesoamerican Barrier Reef System
MEX	Mexico
MLRF1	Molasses Reef oceanographic and meteorology buoy
MMM	Maximum monthly mean
MUR	Multi-scale ultra-high resolution

NOAA	National Oceanographic and Atmospheric Administration
OISST	Optimally interpolated sea surface temperature
OR	Outer reef
PAN	Panama
PCA	Principal component analysis
PCoA	Principal coordinates analysis
PLD	Pelagic larval duration
PR	Puerto Rico
QA	Quality assurance
ROI	Region of interest
SE	Standard error
SST	Sea surface temperature
UK1	Upper Keys
USVI	US Virgin Islands
UV	Ultraviolet
WP	White plague
WS	White syndrome
WW	West Washerwoman

A_R	Allelic richness
Ω_{arag}	Saturation state of seawater with respect to aragonite
E	Simpson's evenness index
F_{ST}	Fixation index

G''_{ST}	Hedrick's fixation index
H_E	Expected heterozygosity
H_O	Observed heterozygosity
K_d490	Diffuse attenuation coefficient at 490 nm
N_A	Number of alleles
N_{PA}	Number of private alleles
P_{ID}	Probability of identity

INTRODUCTION

Over the past three decades, coral reefs in the Caribbean basin have experienced severe reductions in live coral cover, biodiversity, and structural complexity. A recent region-wide survey reveals a nearly 60% loss of coral cover since the 1970s (Jackson, Donovan, Cramer, & Lam, 2014). Far beyond just the aesthetic beauty of the ocean's most productive and diverse ecosystem, what is at stake is the primary source of nutrition for millions of people residing in coastal nations, natural barriers that protect coastlines from damaging wave action and storm surge, and a valuable ecological attraction that sustains local economies via a multibillion dollar eco-tourism industry. Therefore, as reports of decline continue to mount, researchers and managers are pressed to develop action plans that identify and protect the valuable reefs we have left. Such a challenge requires that we understand not only the environmental factors that jeopardize coral reef health, but also the biological and evolutionary forces that strengthen their resilience.

Most frequently implicated in the demise of coral reefs globally is the rapid warming of atmospheric and ocean temperatures over the course of the last four decades. All major reef-building corals rely heavily on a symbiotic relationship between the host cnidarian and a single-celled dinoflagellate of the family *Symbiodiniaceae*, which resides in the gastroderm of the coral polyp. In some species, photosynthetic products from resident symbionts have been shown to provide more than 90% of the coral's nutritional requirements, thereby allowing tropical corals to thrive in largely oligotrophic environments (Muscatine & Porter, 1977). However, prolonged

exposure to abnormally high water temperatures causes this symbiosis to break down and can lead to the expulsion of symbionts from the coral host in a process known as bleaching. Severe or repeated bleaching starves the coral of its primary source of nutrition and can ultimately lead to colony mortality.

Catastrophic mass bleaching events have become a common occurrence in recent years as global temperatures continue to rise. The first such event to occur at a global scale transpired during the 1997/1998 El Niño interval, during which approximately 16% of all corals on the planet perished (Wilkinson & Souter, 2008). Two additional global bleaching events have occurred in the years since, with the most recent beginning in the summer of 2014 and continuing until 2017. While total estimates of global coral loss are still being tallied from this most recent event, early reports from the Great Barrier Reef indicate roughly a quarter of corals on the reef have succumbed bleaching-induced mortality (Australian Institute of Marine Science, 2016), hinting at the potential severity of damage expected in areas of the world that have not yet been comprehensively assessed.

Importantly, however, the effect of rising temperatures is not limited to the acute impacts of bleaching and mortality during extreme temperature anomalies. Several studies have revealed a chronic decline in the growth rate of living corals during the modern era of climate warming (Castillo, Ries, & Weiss, 2011; De'ath, Lough, & Fabricius, 2009). The explicit cause of the decline remains largely unknown; however, a number of empirical studies have demonstrated direct correlation between coral growth rates and annual or seasonal ocean temperatures (Castillo, Ries, Weiss, & Lima, 2012; Lough & Barnes, 2000; Pratchett et al., 2015). *Ex situ* experiments have shown that growth rates tend to increase with rising temperatures up to a threshold of thermal tolerance beyond which growth rates begin to decline (Castillo, Ries, Bruno,

& Westfield, 2014; Jokiel & Coles, 1977). It is under these extreme thermal conditions that the delicate symbiosis between coral and algal symbiont breaks down and bleaching becomes an added threat to colony survival.

Rising temperatures have also been shown to increase coral susceptibility to pathogens (Ruiz-Moreno et al., 2012), particularly on reefs with high coral cover (Bruno et al., 2007). In fact, the most perilous threat to the Florida Keys Reef Tract since 2014 has been an ongoing coral disease outbreak affecting at least 23 species of coral and causing mortality rates often exceeding 60% of infected colonies (Precht, Gintert, Robbart, Fura, & Van Woesik, 2016).

As oceans continue to warm and coral diseases become more frequent throughout the next century, successful management and conservation of coral reefs requires an understanding of the extent to which coral reefs are resilient to these growing threats. Yet, there are many ways to evaluate and understand coral resilience. Survivorship and the rate of coral growth are perhaps the most explicit measures of resilience, as they directly reflect the health and productivity of the organism as a whole. If measured through time, growth rates offer insight into coral health during various periods of environmental change.

The resilience of coral reefs can also be understood from an evolutionary perspective. In particular, effective management of coral reefs relies on a sound understanding of the level to which spatially discrete populations are linked by dispersal throughout their range. Connectivity via larval dispersal fosters the exchange of genetic variants, which acts to increase genetic variation population-wide and facilitate the spread of advantageous alleles within and between reefs. Genetic connectivity primes populations to adapt to a range of environmental pressures across the extent of the species distribution. In this way, understanding the source-sink dynamics

of larval supply and dispersal across a seascape provides insight into valuable reef areas for protection and can greatly enhance the effectiveness of marine conservation planning.

This PhD project characterizes the physiological and evolutionary resilience of Caribbean coral reefs by addressing two principal questions: ***(1) How does the physiological resilience of corals to the effects of climate change vary across multiple spatial scales in the wider Caribbean?*** This first question will be addressed in three separate chapters. Chapter 1 focuses on variability in the resistance of corals to a severe and ongoing disease outbreak on the Florida Keys Reef Tract based on their proximity to shore. Chapter 2 evaluates resilience by means of century-scale records of coral growth from the Florida Keys Reef Tract. Long- and short-term patterns of coral growth were assessed throughout the reef system with particular attention paid to the dichotomy between the inner and outer reef zone and how proximity to shore influences growth. Chapter 3 expands on this concept to compare coral growth patterns on three separate reef ecosystems that span the latitudinal range of the W Caribbean basin: the Florida Keys Reef Tract, the Belize Barrier Reef System, and the Bocas del Toro Reef Complex, Panama. Coral growth records were correlated with corresponding records of environmental parameters to characterize the principal drivers of coral growth in the Anthropocene.

(2) What is the nature and extent of genetic connectivity across the wider Caribbean? This second question is addressed in a final chapter that describes the large-scale patterns of genetic connectivity throughout the wider Caribbean basin. Specifically, Chapter 4 describes the population genetic patterns of the mountainous star coral, *Orbicella faveolata*, across the full geographic extent of the wider Caribbean basin.

CHAPTER 1: DIFFERENTIAL DISEASE INCIDENCE AND MORTALITY OF INNER AND OUTER REEF CORALS OF THE UPPER FLORIDA KEYS IN ASSOCIATION WITH A WHITE SYNDROME OUTBREAK[1]

Introduction

Ocean warming and acidification are widely recognized as posing the most significant risks to coral reef health and resilience on a global scale (Hoegh-Guldberg et al., 2007). In addition to these abiotic factors, corals are also faced with the persistent threat of disease, which can cause localized mortality at levels comparable to mass bleaching events (Aronson & Precht, 2001). The Florida Keys Reef Tract (FKRT), in particular, has experienced several major disease outbreaks over the past four decades that have drastically altered the health and composition of the reef community (Porter et al., 2001).

The earliest reports of disease on the FKRT documented the occurrence of what was described as coral "plague" at Carysfort Reef in the upper Keys, which manifested as an advancing line of infection causing rapid tissue mortality in six species of reef-building corals (Dustan, 1977). Similar disease symptoms, aptly termed plague type II, reemerged in the same region two decades later and spread throughout the FKRT, this time infecting at least 17 species of corals (L. L. Richardson, Goldberg, Carlton, & Halas, 1998). Since then, reports of new, virulent coral diseases on Caribbean reefs have increased considerably (Aronson & Precht, 2001; Goreau et al., 1998; Weil, 2004). These include the spread of white band and white pox diseases,

[1] This chapter previously appeared as an article in the Bulletin of Marine Science. The original citation is as follows: Rippe, J.P., Kriefall, N.G., Davies, S.W. and Castillo K.D. "Differential disease incidence and mortality of inner and outer reef corals of the upper Florida Keys in association with a white syndrome outbreak." *Bulletin of Marine Science* 95, no. 2 (Apr 2019): 305-316.

which have decimated populations of *Acropora palmata* and *A. cervicornis* (Aronson & Precht, 2001), the ubiquitous, albeit less destructive, incidence of black band, yellow band and dark spots diseases (Gil-Agudelo, Smith, Garzón-Ferreira, Weil, & Petersen, 2004; Kuta & Richardson, 1996), and most recently, a new outbreak of white plague-like symptoms on the FKRT that is unprecedented in its virulence and scale of damage (Precht et al., 2016).

This most recent outbreak was first identified in 2014 off the coast of Virginia Key, and, over the course of three years, it has radiated to the northern and southern reaches of the FKRT (Muller, van Woesik, & Sartor, 2018; Precht et al., 2016). Although efforts are still underway to fully understand the etiology of the epidemic, local monitoring teams have reported previously characterized symptoms of white plague as well as several uncharacterized diseases that include "white blotch," "white bleaching band" and symptoms resembling rapid tissue loss, which have collectively affected at least 20 species of corals on the FKRT (Lunz, Landsberg, Kiryu, & Brinkhuis, 2017). Here, we capitalized on an existing long-term monitoring effort to evaluate post-coring regrowth rate, disease incidence and mortality outcomes of two abundant reef-building coral species, *Siderastrea siderea* and *Pseudodiploria strigosa*, at two cross-shore transects in the upper FKRT. Using images taken during three annual site visits from 2015 to 2017, we tested our hypothesis that the effects of the recent disease outbreak would differ between inner and outer reef sites due to cross-shore differences in environmental conditions.

Materials and Methods

Two pairs of inner and outer reef sites in the upper Florida Keys Reef Tract (FKRT) were visited in April 2015, April 2016 and October 2017 (Figure 1.1). Inner reef sites, Basin Hill Shoals (BH) and Cheeca Rocks (CR), are located on the seaward boundary of Hawk Channel and

are characterized as isolated high-relief patch reef structures interspersed among unconsolidated sand and seagrass. By comparison, outer reef sites were located outside the Carysfort (CF) and Alligator Reef (AR) Sanctuary Preservation Areas and comprise part of the continuous barrier reef system that borders the offshore edge of the continental shelf along the extent of the FKRT. Vertical relief at these sites is primarily attributable to the limestone remains of relict reef structures with relatively sparse distributions of live coral (Marszalek, Babashoff, Noel, & Worley, 1977). Similar to the patterns documented by Ruzicka et al. (2013) in a Keys-wide survey of reef community structure, the inner patch reef sites had greater live coral cover with many large (> 1 m diameter) colonies of mounding corals, while the outer reef sites were dominated primarily by octocorals and macroalgae.

On the initial site visits in 2015, as part of an associated investigation of historical coral growth trends (Rippe et al., 2018), skeletal cores were extracted from visibly healthy colonies of *Siderastrea siderea* and *Pseudodiploria strigosa* at each of the four study sites. Five colonies of each species were sampled at both CF and BH, four colonies of each species were sampled at AR, while five colonies of *S. siderea* and four colonies of *P. strigosa* were sampled at CR (Supplemental Table S1.1). Concrete plugs were inserted and cemented into drilled holes with Z-Spar® underwater epoxy to protect the coral colonies from erosion and further physical damage. To document tissue regrowth rates over the coring site, a 20 x 20 cm quadrat was centered on the core extraction site, and an initial image was captured using a GoPro® camera (i.e. Figure 1.2). On subsequent visits, cored colonies were located and analogous images re-captured to yield three annual photographs per colony. Using ImageJ software (Rasband), we outlined the margin of living tissue encircling the coring hole in each image to calculate total exposed surface area, standardized using the quadrat. Across each annual interval, the difference in area was calculated

as the total percent change divided by the number of days between successive images to yield an average regrowth rate for each colony. The effect of *Year*, *Reef zone* and *Species* on regrowth rate was assessed using a three-way ANOVA in R (R Core Team, 2017).

Mortality and disease occurrence were assessed qualitatively for each of the imaged corals at each time point during the study period. Coral colonies were evaluated as living (< 5% tissue loss), dead (> 95% tissue loss) or partially dead (5-95% tissue loss) based on estimated percentages of tissue loss visible in the images. Disease state was evaluated as either present or absent, and specific symptoms were identified based on recently published accounts of coral diseases on the FKRT (Porter et al., 2011; Precht et al., 2016). Because the etiology of the current disease outbreak remains largely uncharacterized, we use the term "white plague" and "white syndrome" to refer to any white plague-like symptoms affecting *P. strigosa* and *S. siderea*, respectively.

Ambient environmental conditions at each site were compared using high-resolution satellite-derived daily sea surface temperature (SST) and ocean color data collected from 2003-2016 and 2012-2017, respectively. SST data were obtained at 1-km resolution from the Group for High Resolution Sea Surface Temperature (GHRSST) Level 4 Multi-scale Ultra-high Resolution (MUR) SST Analysis dataset. To characterize ocean color, we used Level 2 chlorophyll *a* and K_d490 data (~750 m resolution) collected from the Visible Infrared Imaging Radiometer Suite sensor aboard the Suomi NPP satellite and compiled by NOAA CoastWatch/OceanWatch. K_d490 represents the diffuse attenuation coefficient at 490 nm wavelength (blue-green region), which can be used as a proxy for water column turbidity (Shi & Wang, 2010).

Lastly, to place our findings within the context of overall coral disease trends in the area, we analyzed publicly-available observations from annual surveys conducted by Florida Reef Resilience Program (FRRP) in the upper Keys region from 2014 – 2016; FRRP surveys were not conducted in the area in 2017 and thus could not be included in the analysis (Florida Reef Resilience Program). Disease prevalence was measured as the total percentage of symptomatic corals (any disease) at each site, and ordinary kriging was used to spatially interpolate between survey sites. Results were then plotted on a 400 x 400 cell raster grid overlaying our study region. Analyses were performed using the *gstat* package in R (Pebesma, 2004; R Core Team, 2017). Importantly, of all disease observations in the FRRP survey dataset, 87.3% were of dark spots disease, while only 1.8% were of white plague-related disease (i.e., white plague, white blotch and patchy necrosis) and 8.2% were of unknown disease. Thus, the spatial and temporal patterns revealed by this dataset largely reflect those of dark spots disease, not of white plague-related symptoms.

Statistical analysis

The relative effect of *Year*, *Reef zone* (i.e., inner and outer reef), and *Species* on the tissue condition of the colonies (i.e., living, partial mortality, full mortality) was assessed using an ordinal logistic regression model implemented with the *MASS* package in R (Venables & Ripley, 2002). A binomial generalized linear model was then used to assess the relative effect of *Year*, *Species*, *Reef zone* and post-coring tissue *Regrowth* rate on the occurrence of white plague-like symptoms. *Regrowth* was included in this model to determine whether coring operations may have heightened susceptibility of corals to this disease outbreak. Note, because symptoms were perfectly separated across reef zones in our samples (i.e., white plague-like symptoms were not

observed at inner reef sites for either species), a penalized regression was used to more reasonably reflect the true population level effect of *Reef zone* on disease occurrence. The penalty term was computed using the cross-validation procedure implemented with the *glmnet* package in R (Friedman, Hastie, & Tibshirani, 2010).

Results and Discussion

The three-year photographic time-lapse presented here revealed a striking distinction in the prevalence of white plague-like symptoms and mortality across inner and outer reef habitats of the upper Florida Keys. Between the initial site visits in May 2015 and final return in October 2017, all previously-labeled *Pseudodiploria strigosa* colonies that were found (3 of 3) and two-thirds of *Siderastrea siderea* colonies (4 of 6) that were found at outer reef sites exhibited complete mortality (Figure 1.3). Three of the four dead *S. siderea* colonies had exhibited symptoms of white syndrome in 2016; no other colonies of either species showed any signs of disease in 2016 before succumbing. The two surviving colonies of *S. siderea* that were found had experienced partial tissue mortality associated with white syndrome that continued through 2017.

Notably, none of the previously cored *P. strigosa* colonies at CF could be located in 2017; however, every *P. strigosa* colony that the dive team encountered was dead, suggesting that this species had been severely impacted at this site between 2016 and 2017. Moreover, of the five *P. strigosa* colonies imaged at this site one year earlier (2016), two had completely died and two exhibited partial mortality associated with an infection of white plague. Without thorough benthic surveys, it is difficult to assign an exact measure to the past extent of this species at this site. However, like many outer reef areas of the Florida Keys Reef Tract (Ruzicka et al., 2013), this site near Carysfort Reef was largely dominated by octocorals and macroalgae with few

isolated colonies of stony corals in areas of hard substrate. We estimate that < 50 dead colonies of *P. strigosa* were encountered across this site, and < 10 were larger than 0.5 m in diameter. During the study period, no colonies of either species showed any sign of recovery from infection by white plague or white syndrome.

Conversely, all *S. siderea* colonies (7 of 7) and all but two colonies of *P. strigosa* (5 of 7) that were found at inner reef sites in 2017 were healthy without tissue loss (Figure 1.3). Two inner reef colonies of *P. strigosa* experienced significant partial mortality between 2016 and 2017, but did not show any signs of disease. Thus, we cannot be certain whether the tissue mortality observed here resulted from temperature-induced bleaching, disease infection or an unknown cause. Interestingly, all colonies of *S. siderea* at BH exhibited early stage symptoms of dark spots disease by 2017, but none had experienced associated tissue mortality (i.e. Figure 1.2). All colonies of both species found at CR were visibly healthy and showed no evidence of disease throughout the sampling period.

Modeling results reinforce the observed differences in mortality and incidence of white plague-like symptoms between inner and outer reef sites. The risk of mortality was found to be significantly higher at outer reef sites (log odds 95% CI: 3.21-9.32) and as *Year* increased (log odds 95% CI: 28.24-31.93 (2015 to 2016); 34.22-36.45 (2016 to 2017)), but did not differ significantly between species (log odds 95% CI: -3.28-0.26). Likewise, logistic regression also indicated that the incidence of white plague-like symptoms was significantly higher at outer reef sites and as *Year* increased. Estimates of effect sizes and the associated standard error of independent variables from penalized regression models cannot be interpreted reliably due to the substantial bias introduced by the penalization procedure (Goeman, 2010). However, because the cross-validation procedure removed *Species* and *Regrowth* from the best-fit model, we can

conclude that neither factor had a significant effect on the occurrence of white plague-like symptoms.

Similar to our observations, FRRP surveys revealed an increase in overall coral disease frequency from 2014 to 2016 (Figure 1.4). Note, because the large majority of disease observations in this dataset were of dark spots disease (87.3%), the prevalence of disease at inner patch reef sites in the FRRP data reflects our observation of dark spots disease at the northern inner reef site (BH). Interestingly, FRRP surveys did not report significant incidence of white plague-related disease within our study region by 2016 (< 3.1% at only two sites). According to anecdotal accounts, symptoms of the current outbreak had been observed as far south as Davis Reef (see Figure 1.1) by January 2017 (Florida Department of Environmental Protection); however, reports from the upper Keys region at this time were inconsistent, so it is conceivable that FRRP sites had not yet been significantly impacted.

Coring operations did not influence disease incidence or mortality given the healthy status of most cored colonies in 2016 (one year post-coring, Figure 1.3), and as verified by logistic modeling results. *S. siderea* regrew significantly faster than *P. strigosa* (0.068% day^{-1} ± 0.01 and 0.027% day^{-1} ± 0.01, respectively; Table 1.1), an effect that was compounded by year of observation (2015-16 or 2016-17; Table 1.1). Notably, no significant differences were found between regrowth rates of inner and outer reef colonies (0.052% day^{-1} ± 0.01 and 0.043% day^{-1} ± 0.01, respectively; Table 1.1), despite differences in disease incidence and mortality between reef zones (Figure 1.3).

Preliminary evidence suggests that the onset of the current outbreak was likely associated with record high summer temperatures experienced across the FKRT in 2014, preceded by abnormally warm winter and summer seasons (Precht et al., 2016). Temperature has been shown

to enhance the virulence of *Vibrio coralliilyticus*, a ubiquitous bacterial pathogen known to cause fatal infections of corals and other marine organisms (Kimes et al., 2012). Furthermore, during the 2005 bleaching event on the FKRT, Brandt and McManus (2009) found that the frequency of white plague and dark spots disease was positively correlated with bleaching extent, and that black band disease incidence was highest during the period of warmest temperatures.

Importantly, environmental conditions vary considerably between inner and outer reef habitats, and there is evidence that such differences have implications on reef resilience to environmental stress (Kenkel et al., 2013). Inner patch reefs are generally exposed to higher dissolved nutrient concentrations, turbidity and greater temperature variability than outer bank barrier reefs on the FKRT (Lirman & Fong, 2007; Soto, Muller Karger, Hallock, & Hu, 2011), which, rather counterintuitively, correlates with higher coral cover (Lirman & Fong, 2007). Likewise, our analysis of temperature and ocean color conditions illustrates clear differences in temperature variability, mean chlorophyll-a and turbidity between the two inner and two outer reef sites examined in this study. We found that mean annual SST from 2003-2016 was similar between all sites (IR: 26.94 ± 0.11° C, OR: 26.96 ± 0.10° C), but mean annual SST range was significantly higher at inner reef sites (IR: 9.47 ± 0.31° C, OR: 8.90 ± 0.33° C). Moreover, between 2012-2017, the two inner reef sites exhibited significantly higher levels of chlorophyll-a (IR: 2.02 ± 0.09 mg m^{-3}, OR: 1.39 ± 0.05 mg m^{-3}) and higher turbidity (IR: 0.27 ± 0.02 m^{-1}, OR: 0.17 ± 0.02 m^{-1}) than the outer reef sites.

Inner reef corals on the FKRT have demonstrated greater tolerance to experimental heat stress than their outer reef counterparts (Kenkel et al., 2013), and recent research has shown that high chlorophyll-a levels, typical of inner reef waters, are associated with lower prevalence of bleaching and disease during thermal stress events (van Woesik & McCaffrey, 2017). Likewise,

under the combined stress of heating and inoculation with a known disease-causing agent, outer reef colonies of *Porites astreoides* from the FKRT were found to exhibit a two- to four-fold increase in the expression of genes related to innate immune response (Haslun, Hauff-Salas, Strychar, Ostrom, & Cervino, 2018). Inner reef colonies exhibited lower levels of immune-related gene expression independent of treatment, suggesting greater resistance to biotic stress (Haslun et al., 2018). Consistent with these patterns, our findings of lower disease-associated mortality at inner reef sites suggest that the physiological or environmental factors underlying inner reef coral resilience to biotic and abiotic stress may also be buffering these areas from the more severe impacts of the current disease epidemic. However, better etiological understanding of this outbreak is necessary to substantiate this hypothesis.

It is also important to note that CR, one of the two inner reef sites (Figure 1.1), has been identified as one of the most resilient patch reef communities on the FKRT. Manzello, Enochs, Kolodziej, and Carlton (2015) found that *Orbicella faveolata* colonies at CR have significantly greater calcification rates than those at an adjacent outer reef site, and in a recent study, this coral community was found to experience only minimal mortality during repeat thermal stress events in 2014 and 2015 (Gintert et al., 2018). Thus, it is possible that the superior fitness of corals at this site under average and anomalous growing conditions may also be reducing their susceptibility to disease.

This study adds to reports documenting the recent spread of coral disease throughout the FKRT. We find that corals living on outer reef sites have been more severely affected by disease than their inner reef counterparts, highlighting the potential role of habitat differences in protecting inner reef corals from the severity of this outbreak. It is critical, however, to emphasize the spatial and temporal limits of this study, as this data was collected during the

initial three years (2015-2017) of an ongoing disease event and from only two inner-outer reef transects on the FKRT. In fact, as of August 2018, symptoms of white syndrome have been observed at CR and at a nearby inner patch reef site adjacent to Hens and Chickens Reef, causing substantial mortality in *Pseudodiploria spp.*, *Colpophyllia natans*, *Dichocoenia stokesii*, and *Montastraea cavernosa* (D. Manzello, personal communication). Thus, as monitoring efforts on the FKRT continue to elucidate the mechanisms underlying coral disease dynamics, it will be important to resolve whether the patterns observed here reflect a true disparity in resistance that has prevented or at least delayed the onset of disease or, rather, if it has arisen coincidentally during the course of the ongoing outbreak.

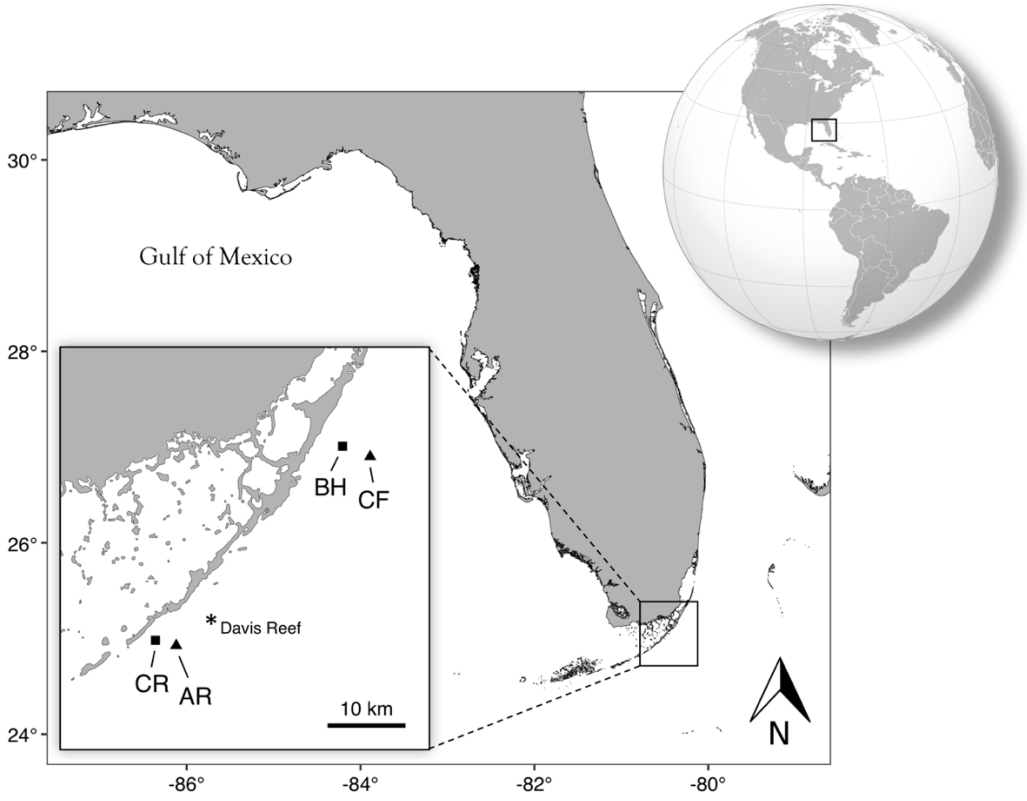

Figure 1.1. Inner-outer reef survey sites in the upper Florida Keys. Squares and triangles represent inner and outer reef sites, respectively. Site abbreviations are as follows: Basin Hill Shoals (BH), Carysfort Reef (CF), Cheeca Rocks (CR) and Alligator Reef (AR). Davis Reef, referenced in the text, is indicated with an asterisk.

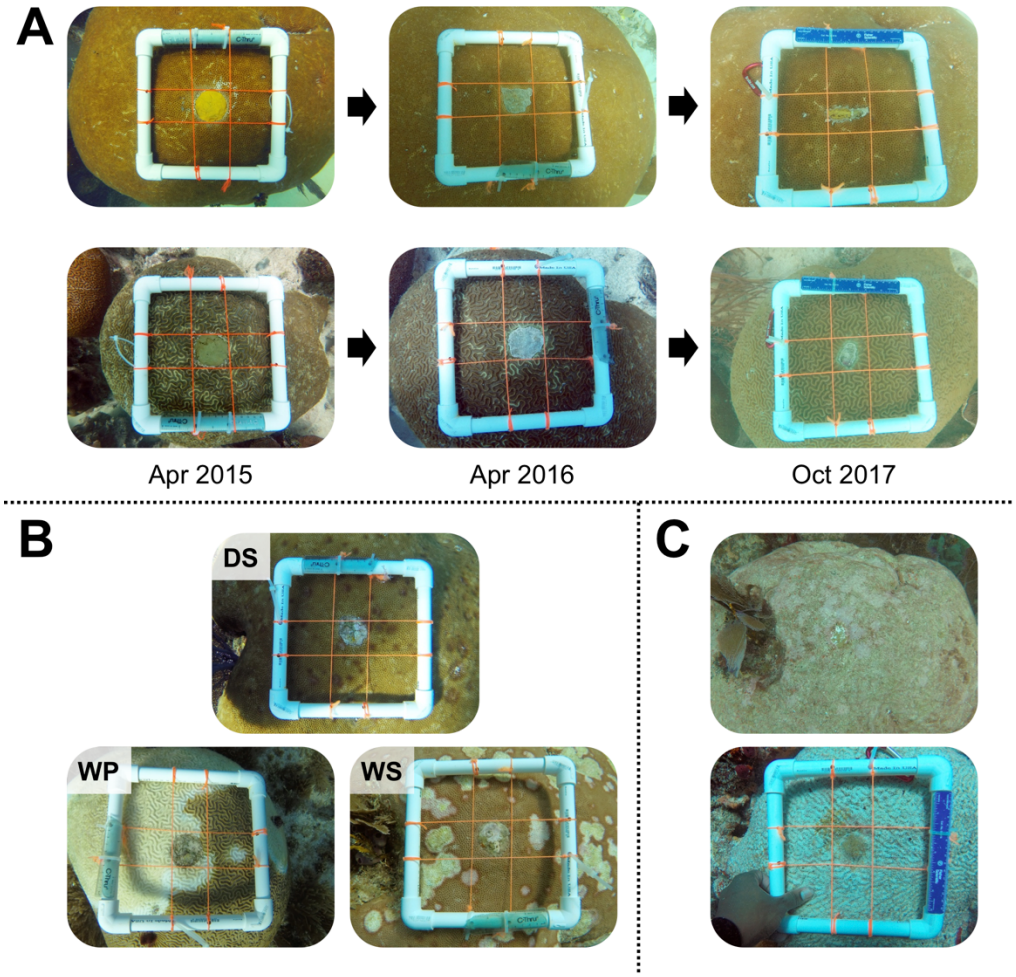

Figure 1.2. Disease occurrence and mortality assessed from 2015-2017. A Tissue regrowth following coring was tracked for the study species, *Siderastrea siderea* (top) and *Pseudodiploria strigosa* (bottom). Colonies exhibiting **B** symptoms of: dark spots (DS), white plague (WP), and white syndrome (WS), and **C** mortality were recorded during each site visit.

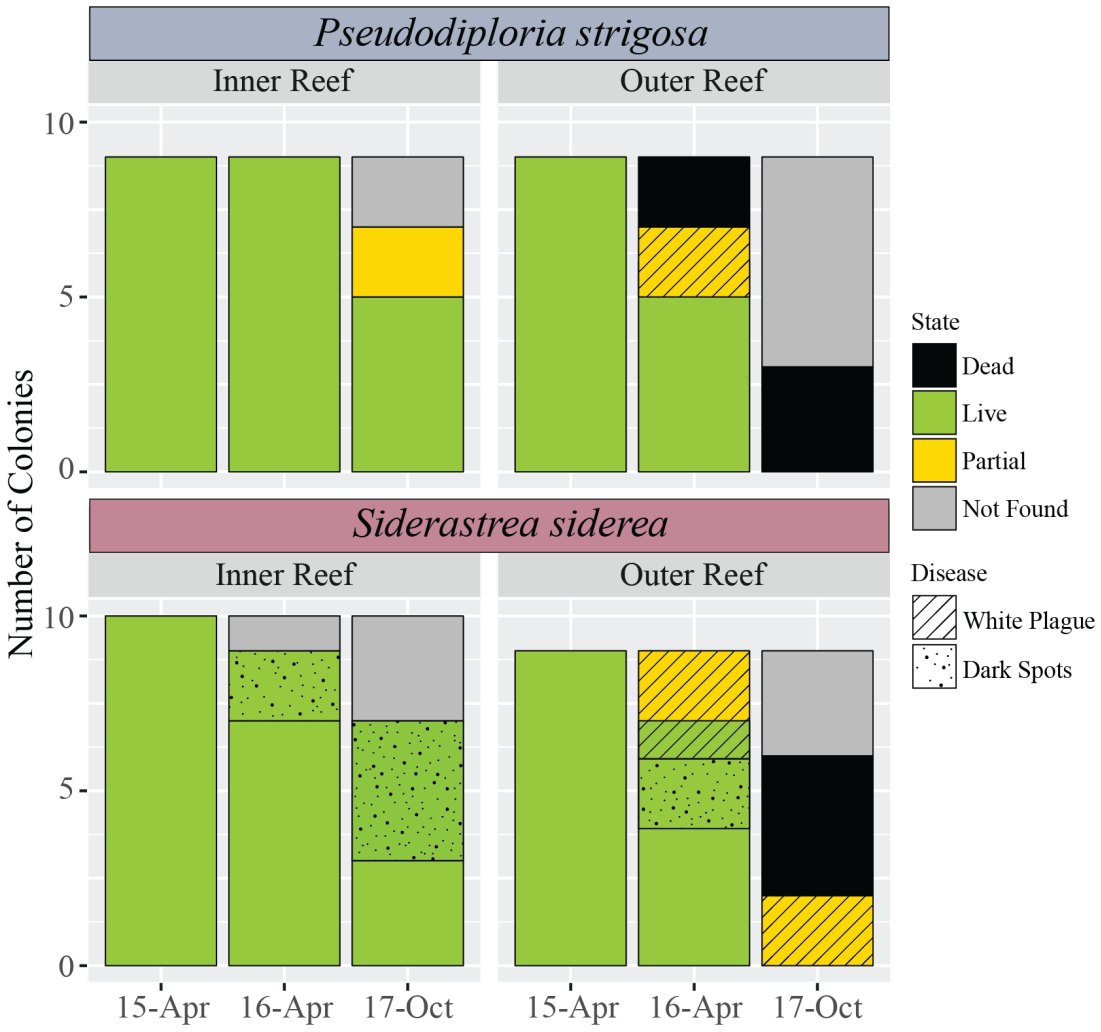

Figure 1.3. Outer reef corals exhibit greater disease prevalence and mortality. Total count of *P. strigosa* (top) and *S. siderea* (bottom) colonies exhibiting disease and mortality during each site visit. Colors denote the state of mortality (green: > 95% living tissue, yellow: 5-95% living tissue, black: < 5% living tissue, gray: not found). Diagonal and spotted patterns denote symptoms of white plague or syndrome and dark spots disease, respectively.

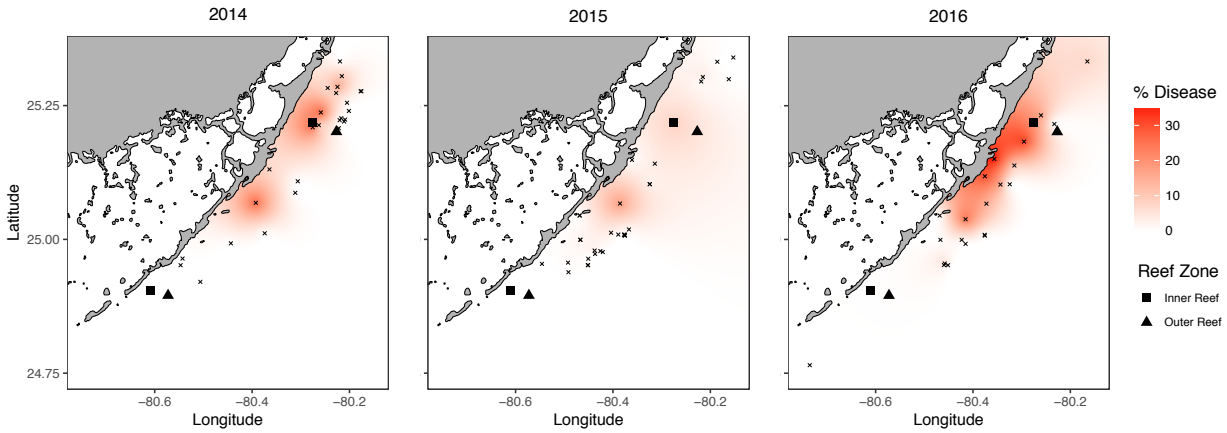

Figure 1.4. Coral disease frequency reported by Florida Reef Resilience Program (FRRP). Sites associated with the current study are depicted as in Figure 1.1. FRRP survey sites are depicted as ×s. Color intensity reflects the total percentage of symptomatic corals (*any disease*) at each site, estimated across the seascape using spatial interpolation. Of all disease observations, 87.3% were of dark spots disease, 1.8% were of white plague-related disease (i.e., white plague, white blotch and patchy necrosis) and 8.2% were of unknown disease.

Variable	*df*	*SS*	*F*	*p*
Species	1	0.01920	7.632	0.0087**
Reef Zone	1	0.00161	0.639	0.4289
Year	1	0.00852	3.389	0.0732
*Species*Reef Zone*	1	0.00235	0.934	0.3398
*Species*Year*	1	0.01190	4.729	0.0358*
*Reef Zone*Year*	1	0.00002	0.007	0.9349
Residuals	39	0.09810		

Table 1.1. Tissue regrowth rates following coring operations. Regrowth rates are defined as the mean percent change in exposed surface area of the coring hole per day and are compared between species (*Pseudodiploria strigosa* or *Siderastrea siderea*), reef zones (inner or outer), and years (2015-16 and 2016-17) with a three-way ANOVA. Asterisks indicate significant differences, accompanied by the level of significance (*$p < 0.05$, **$p < 0.01$).

CHAPTER 2: CORALS SUSTAIN GROWTH BUT NOT DENSITY ACROSS THE FLORIDA KEYS REEF TRACT DESPITE ONGOING WARMING[2]

Introduction

As the most thoroughly monitored coral reef ecosystem in the wider Caribbean, the Florida Keys Reef Tract (FKRT) has unfortunately become a paradigm for the severe decline of coral reefs across the region throughout the last four decades. Following the near extirpation of acroporids in the 1970s and 1980s, a further decline in stony coral cover on the order of 40% since 1996 has driven an ecological shift on the FKRT towards greater dominance of octocorals, macroalgae and sponges (M. Miller, Bourque, & Bohnsack, 2002; Ruzicka et al., 2013; Somerfield et al., 2008). This deterioration of the stony coral community has been attributed primarily to chronically warming waters (Causey, 2001; Manzello, 2015), acute high and low temperature stress events (Colella, Ruzicka, Kidney, Morrison, & Brinkhuis, 2012; Kemp et al., 2011; Lirman et al., 2011), and widespread disease (Porter et al., 2001; Precht et al., 2016).

Yet, sustained reductions in coral cover have been unevenly skewed towards outer reef environments, highlighting a unique cross-shelf distinction on the FKRT (Ruzicka et al., 2013). Inner patch reefs along the seaward boundary of Hawk Channel, a 10 m deep channel running 2-3 km offshore of the Florida Keys archipelago, maintain 15-17% stony coral cover despite their proximity to the highly variable water conditions associated with Florida Bay (Ruzicka et al.,

[2] This chapter previously appeared as an article in Global Change Biology. The original citation is as follows: Rippe J.P., Baumann J.H., De Leener D.N., Aichelman H.E., Friedlander E.B., Davies S.W., and Castillo K.D. "Corals sustain growth but not density across the Florida Keys Reef Tract despite ongoing warming. *Global Change Biology*, 24, no. 11 (Nov 2018): 5204-5217.

2013). By comparison, outer reef sites, which are bank-barrier reefs located 8-9 km offshore along the edge of the shelf predominantly immersed in the clear waters of the Florida Current, have been reduced to ≤5% coral cover and continue to experience significant mortality of important reef-building coral species (Ruzicka et al., 2013).

Depending on geographic context, two theories are often proposed to explain differences in ecology and resilience of corals at inner versus outer reef sites. In some cases, observations of higher coral cover (Lirman & Fong, 2007; Thomson & Frisch, 2010), greater colony size and growth rates (Manzello et al., 2015; Soto et al., 2011), elevated bleaching resistance (Barshis et al., 2013; Palumbi, Barshis, Traylor-Knowles, & Bay, 2014), and stable growth trajectories (Carilli, Donner, & Hartmann, 2012; Castillo et al., 2012) on nearshore reefs suggest that consistent exposure to a highly variable environment preconditions resident coral populations toe better cope with ocean warming and the increasing frequency of high temperature stress events. However, conflicting reports of reduced coral cover (De'ath & Fabricius, 2010), degraded thermal tolerance (Carilli, Norris, Black, Walsh, & McField, 2010), and slower coral growth rates (Cooper, De'ath, Fabricius, & Lough, 2008) suggest that exposure to high levels of suspended sediments and nutrients associated with local human development reduces the fitness of nearshore corals. It is more likely that the evolutionary or acclimatory advantage gained by living in a variable thermal environment co-occurs with the negative impacts of terrestrial runoff, and the balance of these factors determines the relative condition of the reef community.

Sclerochronology, or the use of coral skeletal cores to examine historic trends in growth, provides a useful tool in diagnosing reef health in space and time, and therefore can reveal differences in the sensitivity of sampled reef areas to their changing environments. Early studies from the upper Florida Keys report long-term growth trends of the *Orbicella* species complex,

drawing qualitative comparisons between skeletal extension rates and anthropogenic factors related to human development in south Florida (Hudson, 1981; Hudson, Hanson, Halley, & Kindinger, 1994). More recent analysis of *Orbicella faveolata* from the same region reveals that opposing trends in skeletal density and extension rates over time correlate significantly with the Atlantic Multidecadal Oscillation index (Helmle, Dodge, Swart, Gledhill, & Eakin, 2011). Additionally, baseline calcification rates were found to be significantly greater at an inner reef site of the upper Florida Keys relative to a nearby outer reef site (Manzello et al., 2015). These findings support the premise that there may be a physiological growth advantage for corals living in inner patch reef environments of the FKRT (Anthony, 2006).

Notably, the long-term stability of extension and calcification rates reported for *O. faveolata* on the FKRT (Helmle et al., 2011) deviates from coral growth trends on other reef systems. In the Pacific, Southeast Asia and Red Sea, for example, calcification rates of *Porites* spp. and *Diploastrea heliopora* have declined alongside rising ocean temperatures over the past three decades (Cooper et al., 2008; De'ath et al., 2009; Tanzil et al., 2013; Tanzil, Brown, Tudhope, & Dunne, 2009).

Similarly, multiple studies on the Belize Mesoamerican Barrier Reef System (MBRS) have revealed long-term declines in the extension rates of *Siderastrea siderea* and *Pseudodiploria strigosa*; although, the trend in this case varied based on proximity to shore and the spatial scale of investigation (Baumann et al., 2018; Castillo et al., 2012). Along a single inner-outer reef transect on the southern MBRS, forereef colonies of *S. siderea* were found to exhibit a long-term decline in extension rates, while those from nearshore and backreef environments maintained stable growth trajectories (Castillo et al., 2011; Castillo et al., 2012). Carilli et al. (2010) also observed long-term declines in the extension rate of *O. faveolata* at

nearby reefs in southern Belize and Honduras, but not at offshore atolls or in eastern Honduras. The authors of these studies suggest that the trends may arise due to local water quality dynamics or due to lower resilience of forereef corals to rising ocean temperatures. However, further investigation of *S. siderea* and *P. strigosa* conducted at the scale of the entire Belize MBRS, revealed a contrasting pattern in which declining extension rates were observed only for colonies at nearshore sites, but not for colonies farther from shore (Baumann et al., 2018). Such complexity of coral growth trajectories throughout the MBRS reflects the delicate balance between the historical advantage of residing in a variable nearshore environment and the deteriorating conditions associated with terrestrial runoff and continual ocean warming.

Here, we assess growth trajectories of two abundant and ubiquitous Caribbean reef-building coral species (*Siderastrea siderea* and *Pseudodiploria strigosa*) from four inner-outer reef transects spanning ~200 km of the FKRT. Comparing long- and short-term patterns in extension, density and calcification, we demonstrate that these two coral species have largely sustained extension and calcification rates throughout the FKRT, but have experienced a chronic reduction in skeletal density over the past century. These results suggest that a subtropical climate may buffer corals on the FKRT from warming-induced declines in extension and calcification rates, as is observed in other reef systems, but we propose that declining density may indicate underlying vulnerability to changing carbonate chemistry on the FKRT.

Materials and Methods

Study design

In May 2015 and 2016, skeletal cores were collected from colonies of the reef-building corals, *Siderastrea siderea* and *Pseudodiploria strigosa*, from four pairs of inner-outer reef sites

spanning the Florida Keys Reef Tract (FKRT; Figure 2.1). From south to north, inner reef sites include W Washerwoman (WW), Cheeca Rocks (CR), Basin Hill Shoals (BH) and Bache Shoals (BS). Outer reef sites include E Sambo (ES), Alligator Reef (AR), Carysfort Reef (CF) and Fowey Rocks (FR). In total, 39 *S. siderea* cores and 31 *P. strigosa* cores were collected from 3 to 5 m depth. Cores were extracted using a CS Unitec Model 2 1335 0010 hydraulic drill affixed with hollow extension rods and a 5 cm diameter wet diamond core bit. At each of the eight sites, five healthy colonies of each species were selected randomly for coring. Health was assessed qualitatively by visual inspection, and only colonies without evidence of significant mortality were sampled. In some cases, less than five colonies of *S. siderea* and *P. strigosa* were sampled, either because the dive team was unable to locate five colonies of sufficient size at certain sites or because coring efforts were halted due to inclement weather. Notably, large colonies of *P. strigosa* were relatively rare at the four outer reef sites, whereas colonies of *S. siderea* were ubiquitous across the entire reef tract (Table 2.1).

Cores were extracted from the vertical growth axis of each colony and were between 12 and 70 cm in length, encompassing 16-137 and 14-89 years of growth for *S. siderea* and *P. strigosa*, respectively. After extraction, a concrete plug was inserted and secured in the drilled hole with Z-Spar® underwater epoxy to protect the colony from erosion and further physical damage. The collected cores were then stored in capped PVC tubes filled with 100% ethanol (EtOH) and transported to the University of North Carolina at Chapel Hill where they were air dried in preparation for sclerochronology development.

Sclerochronology development

To assess coral skeletal growth histories, we use a procedure adapted from Castillo et al. (2011). All cores were scanned using X-ray computed tomography (CT) on a Siemens Biograph

CT scanner at the Biomedical Research Imaging Center, University of North Carolina at Chapel Hill. Coral cores were oriented lengthwise in rows of 4 to 5 on the scanning table, and equipment parameters were set to 120 kV, 250 mAs and 0.6 mm slice thickness with images reconstructed at 0.1 mm increments using the H70h "Very Sharp Spine" window. All images were exported from the scanner as DICOM files, which were then 3-dimensionally reconstructed using the open-access Horos v2.0.2 medical image viewing software. High- and low-density bands were visualized using a 10-mm thick 'Mean' projection oriented as a rectangular prism through the center of each core (Figure S2.1).

All boundaries between semiannual density bands were delineated manually and three sets of linear transects were drawn down the length of the cores using the Region of Interest (ROI) tool in Horos (Figure S2.1). Each set of transects was drawn within the exothecal space between corallite walls in order to standardize density measurements and to avoid aberrant density spikes in areas where the transect may otherwise have crossed a high-density corallite wall. Density and calcification measurements are therefore lower than would be expected if all features of the skeletal architecture were taken into account. Importantly, it has been shown that individual colonies may vary in their timing of high- and low-density band deposition due to intraspecific differences in tissue thickness and morphology (Barnes & Lough, 1993, 1996; Carricart-Ganivet, Vásquez-Bedoya, Cabanillas-Terán, & Blanchon, 2013; Taylor, Barnes, & Lough, 1993). Thus, to approximate a consistent time standard between cores, we begin all chronologies at the top of the first fully deposited high- or low-density band beneath the band of terminal growth. Additionally, because cores were collected in subsequent years, the most recent year of growth (2015) was not included for cores collected in 2016 in order to keep the beginning of chronologies uniform throughout the study.

By-pixel density measurements were extracted from linear transects and average density was calculated for each semiannual high- and low-density band. Following previously established protocol (DeCarlo et al., 2015), nine coral standards of known density were included in every scanning session to convert density measurements from CT Hounsfield units to g cm^{-3}. Average density of each standard was assessed in Hounsfield units using Horos and a standard curve was created for all cores scanned in the corresponding session (Figure S2.2). Linear extension was measured in Horos as the width of each annual density band couplet, and calcification (g cm^{-2}) was calculated as the product of density and linear extension.

Statistical analysis

The following section describes the suite of statistical analyses undertaken to evaluate the patterns by which each growth parameter (i.e., extension, density and calcification) varies spatially across the FKRT and temporally throughout the last century.

Mean growth parameters were calculated for each coral species within each site by averaging annual measurements of extension, density and calcification across time. Additionally, as a coarse representation of colony size, the physical length of each core sample was measured and averaged within sites.

Variability in annual extension, density and calcification within and between individual coral colonies was evaluated using two complementary methods. First, the coefficient of variation (CV) was calculated for each colony to determine the scale at which each growth parameter varied between years. CV is measured as the ratio of the standard deviation to the mean ($CV = s/\bar{x} * 100\%$). Additionally, spatial autocorrelation was calculated to assess similarity in growth patterns between coral colonies in close geographic proximity (i.e., within

the same site). Positive values indicate significant correlation between colonies within specified distance classes. Spatial autocorrelation was evaluated using a permutation-based Mantel test (n=1000), and the resulting correlogram was fitted with a non-parametric correlation spline and 95% confidence interval determined by bootstrapping (n=1000). The Mantel test was conducted using an increment of 10 km to create 13 uniformly spaced pairwise distance classes. Analyses of spatial autocorrelation were performed in the *ncf* package in R (Bjornstad, 2009; R Core Team, 2017). In this analysis, we employ a 30-year threshold in order to compare sufficiently long-term chronologies while also retaining a large majority of sampled cores. Only cores longer than 30 years were included in the spatial autocorrelation analysis (58 of 67 samples).

To determine whether the overall "shape" (or multi-dimensional characteristics) of coral growth records differed between inner and outer reef zones, we used the concept of object-oriented data analysis, which treats each growth record as a multi-dimensional data object (see An et al. (2016) for a detailed description). Within this framework, similar to principal component analysis (PCA), the annual growth measurements of each chronology exist in *d*-dimensional space, where *d* is the number of years included in the analysis. In this case, rather than finding the coordinate axes which represent the maximum amount of overall variation within the data, as in PCA, a method known as Distance Weighted Discrimination (DWD) was used to compute the vector which best separates the two specified classes of corals (i.e., inner and outer reef) (Marron, Todd, & Ahn, 2007). Since the data exists in such high dimension, we expect there to be a direction which separates the two classes almost perfectly regardless of whether a difference actually exists. To remedy this, we conducted a Direction-Projection-Permutation (*DiProPerm*) statistical test (S. Wei, Lee, Wichers, & Marron, 2016) to evaluate whether the vector separating the two groups appears to be better than one would expect solely

due to the high dimensionality of the data. The test is conducted by randomly relabeling the class of each core sample (i.e., inner and outer reef) and refitting the DWD direction 1,000 times. A *p*-value is then calculated as the percentage of iterations that are separated better than the DWD direction of the original data. Note, as with the analysis of spatial autocorrelation, only the most recent 30 years of growth are compared, and all shorter cores are not included in this analysis for the reasons described above.

Lastly, temporal trends in growth were assessed in two steps, first using linear mixed effect (LME) modelling, generally following the statistical protocol of Castillo et al. (2011), and second using generalized additive modelling to capture short-term fluctuations in growth. For both approaches, in order to account for the hierarchical nature of the dataset, mean-standardized annual values of linear extension, density and calcification measured within each core were treated as the units of observation, while the cores themselves were treated as sampling units and were incorporated as random effects. Consistent with Castillo et al. (2011), the variable *Year* in all LME models was centered to minimize correlation between random slopes and intercepts, and the residual correlation structure of individual cores was described using an autoregressive moving-average model of order (*p*,*q*). An interaction term between *Reef Zone* and *Year* is included as a model predictor in order to compare linear trends in growth between reef zones (Appendix S1).

Basic generalized additive models (GAM) for extension, density and calcification were implemented in the *mgcv* package in R (R Core Team, 2017; Wood, Pya, & Säfken, 2016), incorporating an adaptive smoothing spline of *Year* as a fixed effect predictor and *Core* as a random effect. Adaptive smoothing allows the degree of smoothing to vary with the covariates to be smoothed and is therefore well suited to capture rapid fluctuations in growth. The smoothing

basis ($k = 25$) was selected following the protocol recommended by Wood (2017), whereby k was increased progressively ($k = 5, 10, 15, 20, 25$) until the effective degrees of freedom stabilized at a value sufficiently lower than $k - 1$. Once the models were fitted to the data, time intervals of significant change were computed using the first derivative of the fitted trend spline, following the methods of Bennion, Simpson, and Goldsmith (2015). In short, a finite differences approximation of the first derivative is calculated at fixed time points along the model prediction with an associated 95% confidence interval. Where the confidence interval of the derivative curve excludes 0 (i.e., zero slope), we conclude that significant change in growth is observed at that time point. These intervals of significant change are indicated on all GAM plots as thick green (increasing) and red (decreasing) segments.

Results

Mean growth and variability within sites

To compare baseline growth parameters between all sampling sites, we calculated site-wide mean rates of extension, density and calcification for each species (Table 2.1). On average, extension and calcification rates were significantly greater for *Pseudodiploria strigosa*, and skeletal density was greater for *Siderastrea siderea* throughout the FKRT ($p < 0.001$ for each parameter). Mean extension of *S. siderea* was relatively consistent across all sites on the FKRT, while extension of *P. strigosa* was greatest at the two sites within the middle upper Keys transect (UK2; i.e., Cheeca Rocks and Alligator Reef) and lowest at W Washerwoman (lower Keys). Between inner and outer reef sites within each transect, skeletal density of both species was generally greater on the outer reef with only one exception – within the southern upper Keys transect (UK1), density of *P. strigosa* colonies was greater on the inner reef (Cheeca Rocks;

1.124 ± 0.030) than on the outer reef (Alligator Reef; 1.049 ± 0.042). Similar to extension, site-wide averages of annual calcification rates were relatively consistent for *S. siderea*, but varied considerably between sites with no discernible pattern for *P. strigosa.* Mean calcification of *P. strigosa* was greatest at Fowey Rocks (0.637 ± 0.034) and lowest at W Washerwoman (0.461 ± 0.019).

Annual extension and calcification rates were found to vary substantially within and between all sampled colonies, regardless of their geographic proximity. Average interannual coefficients of variation (CV) in extension for each core were 20.5% (10.7 – 33.0%) and 18.0% (9.8 – 33.9%) for *S. siderea* and *P. strigosa*, and in calcification were 20.1% (11.6 – 35.0%) and 18.6% (11.1 – 29.7%) for *S. siderea* and *P. strigosa*, respectively. By comparison, interannual variability in density was considerably lower, with an average CV of 6.8% (3.2 – 17.1%) and 12.1% (5.1 – 20.2%) for *S. siderea* and *P. strigosa*, respectively (Figure S2.3). Additionally, spatial autocorrelation between standardized annual extension, density and calcification of both species was assessed for the most recent 30 years of data (i.e., 1985-2014). Between the three growth parameters, no Mantel *r* statistics calculated for any of the 13 distance classes spanning the FKRT were found to be significant after Bonferroni correction, suggesting no evidence of spatial correlation between nearby colonies (Figure S2.4).

Coral growth trajectories on the Florida Keys Reef Tract

Long-term linear trends reveal that skeletal density of both species significantly decreases through time, while extension and calcification rates are neither increasing nor decreasing (Figure 2.2). We find no evidence to suggest that temporal patterns in extension, density or calcification differ significantly between inner and outer reef sites at the scale of the FKRT ($p >$

0.05 for all parameters; Figure 2.2, S2.5). Generalized additive model results also demonstrate little apparent difference in long- or short-term trends between reef zones in either species and, in fact, highlight the considerable colony-level variation in growth through time (Figure 2.3). Even accounting for short-term fluctuations, model predictions explain only 5.58% and 4.70% of the deviance in the chronologies of annual extension rate for *S. siderea* and *P. strigosa*, respectively.

Note, although a declining long-term trend in density and stable extension rates could be expected to cause a corresponding decline in calcification based on the direct relationship of the parameters, we find that the variation in calcification rates is driven primarily by variation in extension for these two species (Figure S2.6). Therefore, despite the slope estimates of calcification trending negative, we cannot conclude at the 95% confidence level that calcification rates have declined over our period of investigation.

We also compared growth chronologies of each species between the four inner-outer reef site pairs, highlighting the along-shore variability in coral growth trends along the FKRT (Figure S2.7). The extension rate of both species declined significantly in the lower Keys transect (LK) during the 1997-98 mass bleaching event and had still not fully recovered by 2014. Declining extension of *S. siderea* at the northern upper Keys transect (UK3) drives a corresponding reduction in calcification since 2001. Additionally, calcification of *P. strigosa* at the middle upper Keys transect (UK2) has declined significantly since 1980.

Extreme temperature events differentially impact Pseudodiploria strigosa

Generalized additive model results reveal the short-term response of *P. strigosa* to two documented extreme temperature events on the FKRT. In 1969-70, the extension rates of inner reef *P. strigosa* were depressed in association with a cold-water bleaching event (Hudson, Shinn,

Halley, & Lidz, 1976). Similarly, in 1997-98, the extension rates of outer reef *P. strigosa* were depressed in association with a Caribbean-wide warm-water bleaching event (Causey, 2001). *Siderastrea siderea* did not demonstrate the same reduction in extension in association with extreme temperature events at the scale of inner and outer reef zones (Figure 2.3).

Discussion

This study reveals that the contrasting trends in coral cover and resilience previously observed between inner and outer reefs of the Florida Keys Reef Tract (FKRT) do not translate to clear reef zone differences in long-term growth for *Siderastrea siderea* and *Pseudodiploria strigosa* at the scale of the entire FKRT system. Rather, linear modelling indicates that long-term trends of all growth parameters are virtually indistinguishable between inner and outer reef colonies. Multi-dimensional DWD and *DiProPerm* analyses corroborate this result, offering no evidence that annual growth differs significantly between reef zones in the most recent 30 years (Figure 2.2).

The long-term growth trends observed here largely reflect those previously reported for *Orbicella faveolata* from the upper Keys, with extension and calcification remaining stable and density declining significantly over time (Figure 2.2) (Helmle et al., 2011). However, the lack of reef zone differences contradicts previous observations from the Belize MBRS, which demonstrate variable declines in extension rates based on proximity to shore (Baumann et al., 2018; Castillo et al., 2012). As hypothesized by Helmle et al. (2011), it is possible that the disparity between growth patterns on the FKRT and the MBRS may be attributed to the subtropical nature of the Florida Keys, in that mean temperature conditions on the FKRT have

not yet crossed a critical optimum that would lead to extended declines in coral growth on a reef zone scale.

Previous research has shown that coral extension and calcification rates are correlated with temperature in a parabolic fashion. At moderate temperatures, coral growth accelerates with increasing temperature (Lough & Barnes, 2000); however, once a thermal optimum is reached, calcification declines with further warming (Castillo et al., 2014; Jokiel & Coles, 1977). Recent theory supports the existence of such an optimum based on physiological factors known to regulate biomineralization (Wooldridge, 2013). Moreover, a comprehensive record of *Porites* growth rates from the Great Barrier Reef reflect this pattern temporally, with an extended period of increasing calcification until 1990 followed by a drastic decline throughout the modern era of climate warming (De'ath et al., 2009).

Historical *in situ* measurements of seawater temperature on the FKRT show that conditions have warmed ~0.8°C over the course of the last century (see Figure 2.4) (Kuffner, Lidz, Hudson, & Anderson, 2015), which is in line with the estimated global ocean warming rate of 0.11°C per decade since 1970 (Rhein et al., 2013). Mean annual temperatures, however, remain considerably cooler and recent warming trends (1985-2009) are slower on the FKRT than on reefs in more tropical regions of the wider Caribbean (Chollett, Müller-Karger, Heron, Skirving, & Mumby, 2012; Chollett, Mumby, Müller-Karger, & Hu, 2012). In a broad-scale analysis of the physical environment throughout the Caribbean basin, Chollett, Mumby, et al. (2012) show that the mean annual temperature of high-latitude regions (including the FKRT, Bahamas and western Cuba banks) was 26.05°C from 1993 to 2008. Conversely, coastal waters around Belize, Panama and the Lesser Antilles had mean annual temperatures of 27.60, 27.01, and 27.15°C, respectively, during this period.

Notably, the warming trend on the FKRT, and throughout the Caribbean, is especially pronounced in summer months, which has led to more days per year spent above extreme temperature thresholds (Kuffner et al., 2015; Manzello, 2015). Tropical and subtropical reef environments also differ in the degree, frequency and duration of these extreme temperature events, which are factors known to weaken coral health and increase the likelihood of bleaching (Manzello, Berkelmans, & Hendee, 2007). Using the Belize MBRS for comparison, previous work has shown that outer reef sites experienced 20.0-40.1 days per year of recorded average temperatures above the local bleaching threshold of >29.7°C between 2003-2012 (Aronson, Precht, Toscano, & Koltes, 2002; Baumann et al., 2016). During the same time period, a permanent monitoring station at Molasses Reef (MLRF1), an outer reef site on the FKRT, recorded only 13.2 days per year with average temperatures >29.7°C (Baums, Miller, & Hellberg, 2005). Moreover, if we consider the metric found to correlate best with bleaching occurrence specifically on the FKRT (i.e., number of days annually >30.5°C; Manzello et al., 2007), we find that MLRF1 recorded on average only 7.3 days per year above this locally-derived bleaching threshold during the same time period of comparison.

As global ocean temperatures continue to rise in the future, coral reefs will be faced with the combined effects of warmer average conditions and the increased frequency of high temperature events (van Hooidonk, Maynard, & Planes, 2013). At present, however, high-latitude reefs that currently experience less extreme summer temperatures and relatively cooler annual temperatures may still fall beneath the thermal optimum beyond which coral growth is expected to decline. In accordance with this notion, previous work from western Australia found that *Porites* colonies from two southern sites (i.e., highest latitudes) have exhibited an increase in calcification rates with warming over the last century, while those from more tropical regions

have shown no change (Cooper, O'Leary, & Lough, 2012). In addition, a recent study conducted in Bermuda, the northernmost reef system in the Atlantic basin, predicts that calcification rates of two dominant corals may in fact increase with moderate increases in ocean temperature over the next century, though only under conservative warming scenarios (Courtney et al., 2017). Similarly, *S. siderea* and *P. strigosa* colonies sampled here appear able to sustain baseline extension and calcification rates through present day, regardless of their reef zone origin and despite persistent warming on the FKRT (Kuffner et al., 2015; Manzello, 2015).

However, exceptions to this pattern occur when extreme temperature events punctuate the prevailing subtropical climate on the FKRT. As has been reported extensively, anomalously warm SSTs are increasing in frequency worldwide, causing more frequent recurrence of major coral bleaching events (van Hooidonk et al., 2013). Moreover, corals on the FKRT are occasionally faced with intrusions of anomalously cold water from the neighboring Florida Bay. Florida Bay is a wide, shallow embayment extending south from the mainland peninsula of Florida and west behind the shelter of the Florida Keys (Figure 2.1). Bay waters are subjected to extreme seasonal fluctuations in temperature and salinity, as well as elevated suspended sediment and nutrient concentrations associated with freshwater outflow from the Everglades ecosystem (Boyer, Fourqurean, & Jones, 1999). Under average weather conditions, tidal water exchange from Florida Bay has a relatively marginal impact on reefs beyond the boundary of the Middle Keys (Szmant & Forrester, 1996). However, during severe winter cold fronts that draw polar air masses across the region, pulses of bay water can reach surrounding inner reef areas of the upper Keys and, in some cases, cause catastrophic mortality in the reef community (Colella et al., 2012; Kemp et al., 2011; Lirman et al., 2011).

The coral growth records presented here indicate that two particular extreme temperature events induced short-term reductions in extension rates of *P. strigosa* at the scale of entire reef zones (Figure 2.3B). The first instance was a cold-water bleaching event in 1969-70, which reportedly caused 80-90% coral mortality at Hens and Chickens Reef, an inner patch reef in the upper Keys (Hudson et al., 1976). Long-term growth trends indicate the impact of this event spanned inner reef sites across the FKRT, causing a significant drop in the extension rate of *P. strigosa* colonies at these sites. A similar growth response is observed in association with the severe 1997-98 warm-water bleaching event, during which extension rates of *P. strigosa* colonies at outer reef sites were significantly depressed. This pattern suggests that, although extensive bleaching was reported throughout the FKRT in 1997-98, outer reef areas were particularly impacted by this event, echoing the continued decline of stony coral communities on the outer reef since 1998 (Ruzicka et al., 2013). Some have shown that higher turbidity associated with inner reef areas acts to attenuate UV radiation through the water column, thereby reducing coral susceptibility to bleaching (Morgan, Perry, Johnson, & Smithers, 2017). Additionally, a number of coral genera have demonstrated capacity to mitigate the negative effects of thermal stress via heterotrophy (Grottoli, Rodrigues, & Palardy, 2006). One or both of these factors may have lessened bleaching severity or accelerated the recovery of inner reef corals.

Interestingly, a number of other major bleaching events are not evident in the long-term growth records, namely the 2004-05 warm-water and 2009-10 cold-water events, both of which caused extensive coral bleaching and mortality on the FKRT (Colella et al., 2012; Manzello et al., 2007; Wagner, Kramer, & Van Woesik, 2010). The absence of clear reductions in extension rate at the reef zone scale suggests that the impact of these events may not have been as

widespread or as severe as the 1969-70 or 1997-98 events. Alternatively, inherent spatial variation in bleaching susceptibility and impact may hinder reliable correlation of acute stress events with long term growth records. However, as extreme temperature anomalies become more frequent on the FKRT (Manzello, 2015), repeated exposure to these thermal stress events may begin to push conditions beyond their thermal optima and lead to future reductions in coral extension rates.

The long-term decline in skeletal density observed for both species throughout the FKRT highlights the complexity of the coral growth response to the impacts of climate change. Together, skeletal density and extension control the rate of calcification, or the annual amount of skeleton accreted by the coral, which is important in determining whether coral reefs are in a state of net framework construction or erosion (Eyre et al., 2018). Small changes to reef-wide calcification budgets can have direct implications on habitat function and viability; however, growing evidence indicates that density and extension are affected independently by different parameters of environmental change (Lough & Barnes, 2000; Mollica et al., 2018).

Early research revealed variations in density based on hydraulic energy of the reef setting, such that denser skeletons strengthened coral colonies exposed to higher wave activity (Scoffin, Tudhope, Brown, Chansang, & Cheeney, 1992). Reduced skeletal density has also been attributed to elevated nutrients and poor water quality associated with heavy influence from nearby human development (Carricart-Ganivet & Merino, 2001; Dunn, Sammarco, & LaFleur Jr, 2012; Edinger et al., 2000). Accordingly, we find that average density of both species is significantly lower at inner reef sites at all but one of the cross-shore transects across the FKRT (Table 2.1), implying that these factors may limit baseline coral density. However, we have no reason to believe that hydraulic energy on the FKRT has increased significantly over the past

century, and in fact, water quality has improved throughout the FKRT since 1995 (reduced turbidity and organic carbon) (Briceño & Boyer, 2014), which would be expected to stimulate an increase in skeletal density through time.

Rather, we hypothesize that the long-term reduction in coral density may reflect changing carbonate chemistry on the FKRT over the past century. Recent analysis of *Porites* growth from the central Pacific reveals a strong sensitivity of skeletal density, but not extension, to aragonite saturation state (Ω_{arag}) and ocean acidification (Mollica et al., 2018; Tambutté et al., 2015). Likewise, density has been shown to decrease from high to low Ω_{arag} along a natural pH gradient in Puerto Morelos, Mexico and in Milne Bay, Papua New Guinea (Crook, Cohen, Rebolledo-Vieyra, Hernandez, & Paytan, 2013; Fabricius et al., 2011). Our findings also reflect those of Helmle et al. (2011), which demonstrated significant correlation between declining trends in skeletal density of *O. faveolata* on the FKRT and modelled Ω_{arag}.

In situ monitoring efforts are beginning to unravel the complex biogeochemical mechanisms driving daily and seasonal fluctuations in carbonate chemistry on the FKRT, revealing, in particular, that inner reef areas are elevated in Ω_{arag} relative to outer reef areas in the upper Keys, but depleted by comparison in the lower Keys (Manzello, Enochs, Melo, Gledhill, & Johns, 2012). Independently, we would expect this to cause an associated *increase* in mean skeletal density at inner reef sites in the upper Keys, rather than the reduction observed here. However, within the local setting of elevated nutrients and suspended particulate matter in inner reef areas, coral growth patterns likely reflect the interaction of these factors, which in this instance, may have opposing effects on skeletal density.

Importantly, while we hypothesize that the observed density decline may reflect long-term acidification, some have found that scleractinian corals are able to regulate the internal pH

conditions at the site of calcification at relatively low energetic cost (McCulloch, Falter, Trotter, & Montagna, 2012; Ries, Cohen, & McCorkle, 2009). This suggests that corals may be able to maintain calcification rates at current levels of acidification; although, it is argued that this physiological buffering capacity is dependent on the ability of corals to adapt simultaneously to increasing temperature stress (McCulloch et al., 2012). Here, corals on the FKRT have been able maintain calcification despite a long-term reduction in density, but to truly elucidate the cause of the observed growth trends, continued research and long-term records of Ω_{arag} in the nearshore reef environment are necessary. Regardless, if the observed reduction in density continues, it is likely that coral skeletons will become more porous in the future, potentially making them more susceptible to chemical and biological erosion (Barkley et al., 2015; Highsmith, 1981).

Site-wide averages of growth parameters suggest that the baseline calcification rate for *P. strigosa* is greatest at the northernmost outer reef site (i.e., Fowey Rocks); however, the sampled colonies at this site were the smallest in size (Table 2.1). During the course of sampling, the dive team encountered numerous larger, older colonies of *P. strigosa* (100+ years) throughout the sampling site, but all had experienced recent mortality and were virtually extirpated, presumably during the 2014-2015 bleaching event (*pers. obs.*). It is possible that the colonies which were able to survive this event may be especially well adapted and productive in their environment, and are therefore able to maintain comparably high calcification rates.

This finding, however, highlights a critical implication regarding the use of coral cover versus growth rates as indices of overall reef health. Because only living colonies were sampled for this analysis, the growth trends reported here represent only those individuals that have survived the major mortality events occurring over the past several decades and are therefore distinctly resilient to environmental change. Additionally, in comparison to other species, it is

important to note that *S. siderea* is particularly robust to thermal stress, allowing the species to persist ubiquitously throughout the Caribbean basin and as far north as Onslow Bay, North Carolina (34.5°N) (Macintyre & Pilkey, 1969). Its resilience to both cold- and warm-water stress has allowed it to become one of the most abundant species on the FKRT (Florida Fish and Wildlife Conservation Commission, 2016) and explains why the bleaching-associated growth rate reductions observed in *P. strigosa* are not reflected for *S. siderea*. Consequently, coral growth trends do not reflect the health of the entire coral reef community. Subtler environmental changes that may have significant consequences for more susceptible individuals or species might not be fully captured in the skeletal growth records of the sampled colonies.

Overall, this study provides a comprehensive assessment of past and current growth dynamics of two important reef-building species that are ubiquitous across the FKRT. In particular, we find that:

- *S. siderea* and *P. strigosa* have been able to sustain baseline rates of extension and calcification despite recent bleaching events and chronic ocean warming.
- *P. strigosa* has experienced two significant, acute reductions in extension associated with major coral mortality events.
- Skeletal density of both species has declined significantly over the past century.

The complex growth dynamics observed here highlight the importance of measuring each component of coral growth to fully understand the past and future trajectories of coral reefs in the modern era of climate change. Stable calcification rates suggest that the local climate may buffer corals from chronic growth declines associated with climate warming, such as those observed on other Caribbean reefs and globally. Furthermore, we posit that declining density may point to the susceptibility of corals to changing carbonate chemistry on the FKRT, and

suggest that corals may experience further skeletal weakening in the future. Additional investigation of coral growth trends for other, perhaps more susceptible species, coupled with targeted analysis of environmental correlates is encouraged to test this hypothesis and provide a more comprehensive understanding of the trajectory of the reef community as a whole.

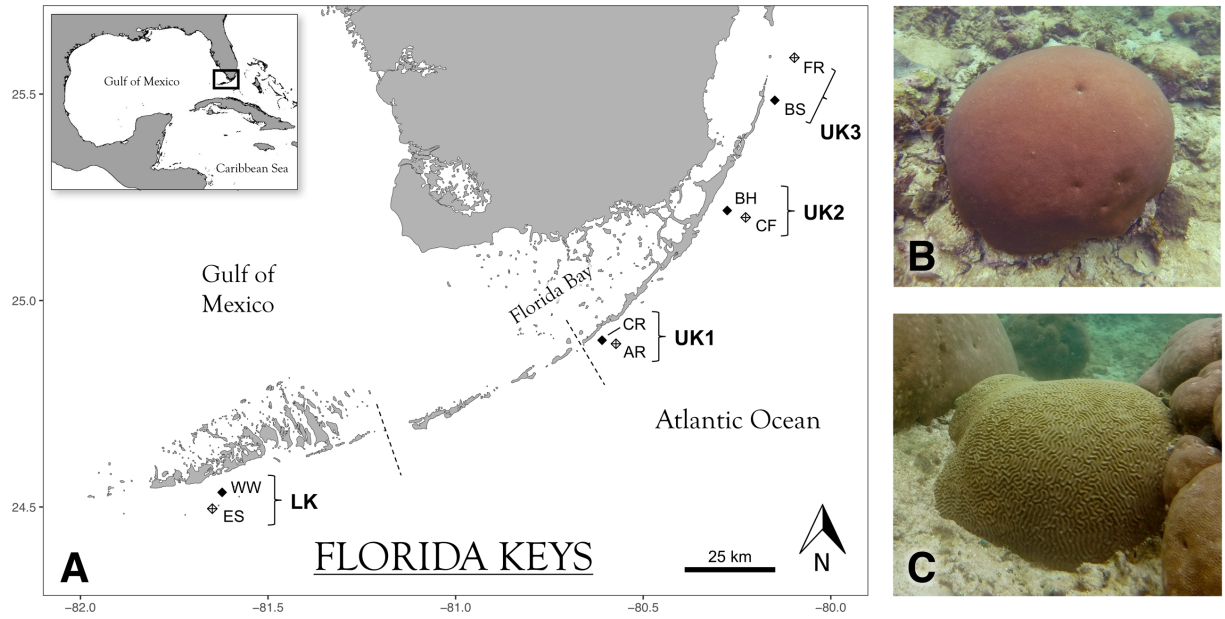

Figure 2.1. Map of sampling sites (A) and study species (B, C). Solid and crosshatch diamonds represent inner and outer reef sites, respectively. Dashed lines depict the approximate boundaries between the Lower, Middle and Upper Keys. Site and transect abbreviations are as follows: Lower Keys (LK) – West Washerwoman (WW), Eastern Sambo (ES); Upper Keys 1 (UK1) – Cheeca Rocks (CR), Alligator Reef (AR); Upper Keys 2 (UK2) – Basin Hills (BH), Carysfort Reef (CF); Upper Keys 3 (UK3) – Bache Shoals (BS), Fowey Rocks (FR). The two study species are pictured on the right: *Siderastrea siderea* (top) and *Pseudodiploria strigosa* (bottom).

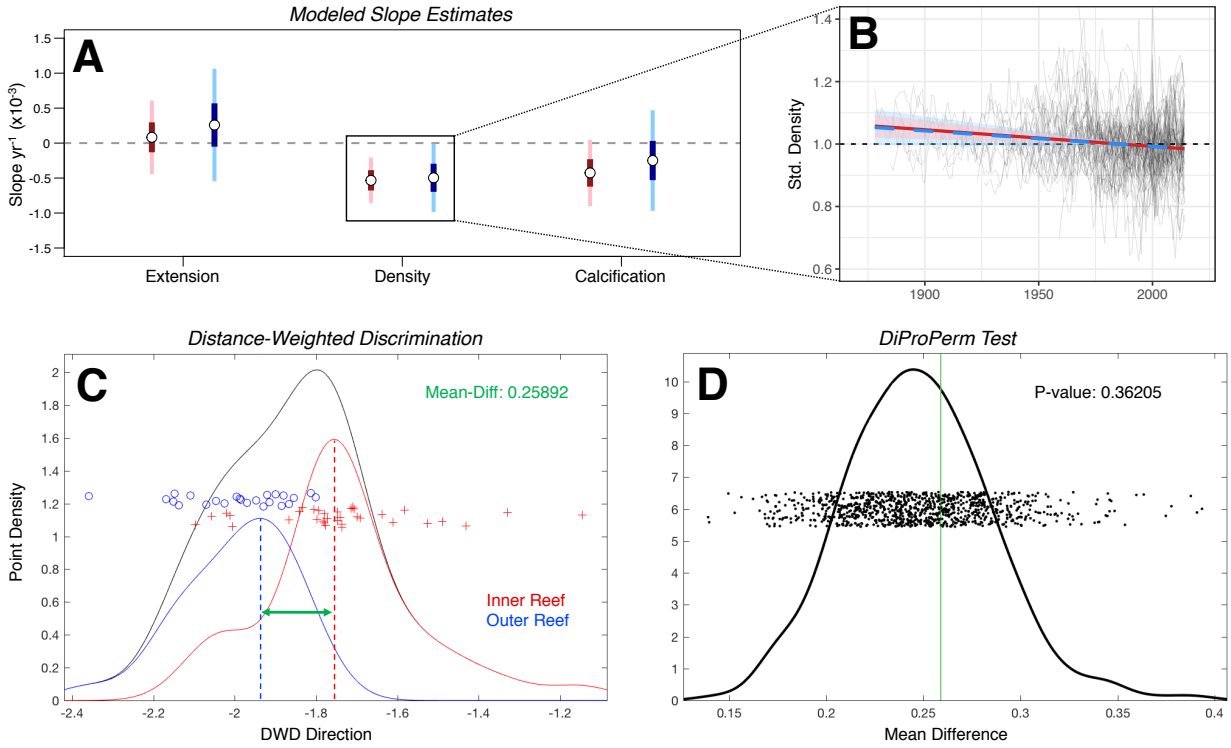

Figure 2.2. Long-term growth patterns do not differ between reef zones. (A) Modeled estimates of linear trends in extension, density and calcification for the inner (red) and outer reef (blue). Dark- and light-colored bars represent 50% and 95% confidence intervals, respectively. (B) Modeled linear trends with 95% confidence intervals overlaying individual chronologies of mean-standardized skeletal density (gray). Line colors correspond to inner and outer reef slope estimates displayed in Panel A. (C) *Extension* chronologies of inner and outer reef cores were also compared using Distance Weighted Discrimination (DWD). Red crosses (inner reef) and blue circles (outer reef) represent the relative position of each core chronology along the DWD axis, and the mean difference between the two groups was calculated. (D) The significance of the difference between the inner and outer reef cores along the DWD axis was evaluated using a DiProPerm test. Each point signifies a mean-difference calculation after each of 1000 permutations of randomly relabeling the data and refitting the DWD direction. The green line denotes the mean difference between the true groups (inner and outer reef) in the data. Curves in Panels C and D represent the density of points along the x-axes. All analyses pictured were performed on the full dataset including mean-standardized annual measurements of both study species together.

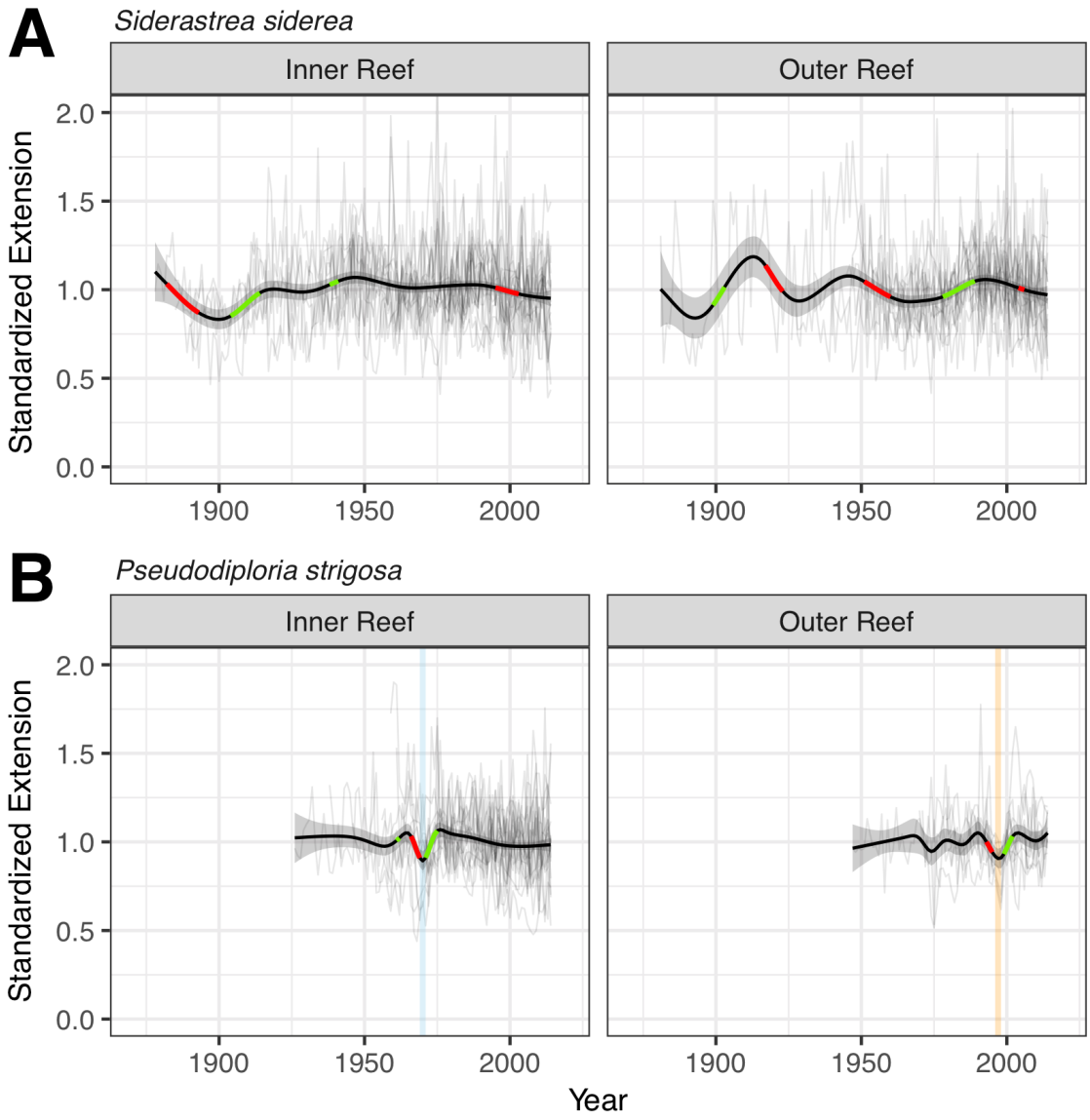

Figure 2.3. Sensitivity to extreme thermal events differs between species and reef zones. Generalized additive model predictions (±2 SE) overlay individual core chronologies of standardized annual extension (light gray), organized by reef zone and species. Green and red segments denote regions of the curve that are significantly increasing and decreasing, respectively. The light blue and orange vertical lines indicate two previously reported major bleaching events in the FL Keys: 1969-70 cold water (blue) and 1997-98 warm water (orange).

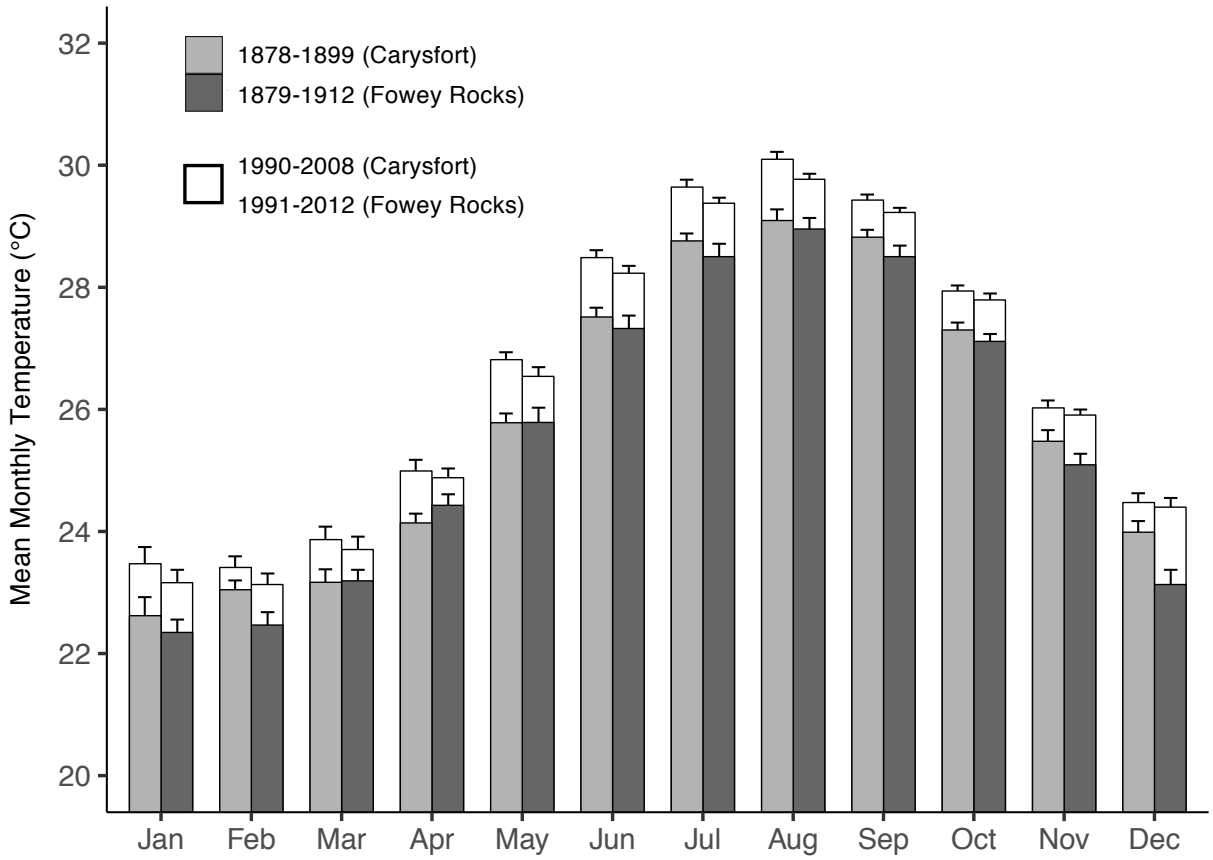

Figure 2.4. Century-scale warming on the FKRT. Stacked bar plots depict the difference between current and historic *in situ* temperatures at Carysfort Reef and Fowey Rocks on the FKRT. White bars reflect the increase in mean monthly temperatures from the late 1800s (colored bars) to modern day. Historic temperatures were documented by lighthouse keepers at each site and represent the oldest temperature records from the FKRT. Recent temperatures were recorded by fixed loggers as part of two large-scale monitoring efforts in the region. This figure has been adapted from Kuffner et al. (2015) with permission from the authors.

Siderastrea siderea						
Site	**N**	**Size (cm)**	**Age (yr)**	**Extension (cm yr^{-1})**	**Density (g $cm^{-3}yr^{-1}$)**	**Calcification (g $cm^{-2}yr^{-1}$)**
W Washerwoman	5	24.0	56.4	0.38 (±0.01)	1.34 (±0.01)	0.51 (±0.01)
E Sambo	5	49.8	82.8	0.36 (±0.01)	1.35 (±0.01)	0.48 (±0.01)
Cheeca Rocks	5	58.4	106.8	0.36 (±0.01)	1.38 (±0.01)	0.50 (±0.01)
Alligator Reef	4	23.8	45.5	0.34 (±0.02)	1.46 (±0.02)	0.49 (±0.02)
Basin Hills	5	38.9	91.2	0.34 (±0.01)	1.45 (±0.01)	0.48 (±0.01)
Carysfort Reef	5	32.3	61.0	0.38 (±0.01)	1.49 (±0.02)	0.57 (±0.01)
Bache Shoals	4	35.3	52.5	0.36 (±0.01)	1.38 (±0.01)	0.50 (±0.02)
Fowey Rocks	5	19.7	34.4	0.38 (±0.02)	1.42 (±0.02)	0.54 (±0.02)

Pseudodiploria strigosa						
Site	**N**	**Size (cm)**	**Age (yr)**	**Extension (cm yr^{-1})**	**Density (g $cm^{-3}yr^{-1}$)**	**Calcification (g $cm^{-2}yr^{-1}$)**
W Washerwoman	5	20.7	34.2	0.38 (±0.02)	1.26 (±0.04)	0.46 (±0.02)
E Sambo	0	-	-	-	-	-
Cheeca Rocks	4	41.2	57.3	0.53 (±0.02)	1.12 (±0.03)	0.58 (±0.02)
Alligator Reef	3	25.2	39.3	0.55 (±0.02)	1.05 (±0.04)	0.56 (±0.02)
Basin Hills	5	36.2	53.0	0.49 (±0.02)	1.14 (±0.02)	0.55 (±0.02)
Carysfort Reef	4	29.8	48.0	0.45 (±0.01)	1.24 (±0.02)	0.56 (±0.01)
Bache Shoals	5	34.3	56.6	0.45 (±0.01)	1.26 (±0.03)	0.55 (±0.01)
Fowey Rocks	3	17.7	18.7	0.46 (±0.02)	1.42 (±0.07)	0.64 (±0.03)

Table 2.1. Summary of growth parameters for *Siderastrea siderea* (top) and *Pseudodiploria strigosa* (bottom). Site-wide averages of colony size (estimated by core length), annual extension rate, density and calcification rate (±SE).

CHAPTER 3: ENVIRONMENTAL DRIVERS OF CORAL GROWTH ACROSS THE WESTERN CARIBBEAN SEA AND THE ATLANTIC COAST OF FLORIDA

Introduction

Often lauded as the nuclei of biodiversity in tropical oceans, coral reefs have drawn recent public attention not for their ecological wonder, but as early omens of the consequences of climate change for the natural world. With few exceptions, reef-building corals thrive in a narrow range of optimal temperatures and cannot tolerate extended periods in conditions outside of this range. Such events can cause critical dysfunction in the mutualism between corals and their algal endosymbionts, which in severe cases can lead to coral bleaching—the expulsion of endosymbionts from the coral tissue—and mortality (Baker, Glynn, & Riegl, 2008). Alas, as ocean heat content continues to rise, periodic warm phases of the El Niño-Southern Oscillation are pushing seawater temperatures above the upper limit of this range with increasing frequency and duration. As a result, global-scale coral bleaching events are becoming a recurrent phenomenon, with the most recent spanning the period from 2014-17 and leading to the mass mortality of more than 30% of corals on Australia's Great Barrier Reef (T. P. Hughes et al., 2018).

Throughout the Caribbean basin, similar large-scale die-offs have severely reduced live coral cover and shifted remaining reef communities to predominantly weedy or stress-adapted taxa, such as *Porites astreoides* or *Siderastrea spp*. (Gardner, Côté, Gill, Grant, & Watkinson, 2003; Green, Edmunds, & Carpenter, 2008; Ruzicka et al., 2013). For these depauperate reefs,

just as consequential as the acute impacts of bleaching and mortality are the chronic, nonlethal effects of climate change that can significantly influence the rate of community calcification and, in effect, the ecological role of coral reefs as productive ecosystem engineers.

Seawater temperature and carbonate chemistry have been shown to modulate coral calcification in critical ways. Experimental and field observations demonstrate that calcification generally follows a typical thermal response curve, wherein calcification increases linearly with average temperature up to a maximum rate, and once temperatures exceed a thermal optimum, it declines with further warming (Castillo et al., 2014; Lough & Barnes, 2000). Indeed, at several reef locations across the Caribbean, Indo-Pacific and Arabian Gulf, reports of declining coral growth rates suggest that average ocean temperatures have already surpassed optimum growth conditions for certain coral species (Cantin, Cohen, Karnauskas, Tarrant, & McCorkle, 2010; Castillo et al., 2012; De'ath et al., 2009). By comparison, the association between coral growth and seawater carbonate chemistry is not as well understood. In some instances, lower calcification rates have been correlated with reduced pH in experimental settings and across natural pH gradients (Albright et al., 2018). In others, calcification follows a more complex, nonlinear correlation or shows no association at all to seawater chemistry (Comeau, Carpenter, & Edmunds, 2013; Ries, Cohen, & McCorkle, 2010). A recent investigation of *Porites* corals from Palauan reefs found that aragonite saturation state is directly proportional to skeletal density (Mollica et al., 2018), but not to extension or calcification, an effect also demonstrated in *Orbicella* corals from the Florida Keys (Helmle et al., 2011).

Importantly, substantial variability exists among and within species regarding resilience to these climate change stressors (Okazaki et al., 2017). This has been attributed to a number of factors, including features of the local water quality regime (MacNeil et al., 2019), genetic

adaptation (Bay & Palumbi, 2014) and physiological acclimatization of individual colonies (Dixon, Liao, Bay, & Matz, 2018). In particular, growing evidence suggests that individuals from highly variable temperature regimes are better able to tolerate a wide range of conditions and therefore better suited to cope with climate change-associated warming (Palumbi et al., 2014). A series of experiments conducted in American Samoa illustrate a shared contribution of short-term acclimatization and longer-term genetic adaptation in attaining this added thermal tolerance, although the specific mechanisms are not fully understood (Bay & Palumbi, 2014; Palumbi et al., 2014). Recent transcriptomic research suggests the possibility of genetic 'frontloading', whereby corals that experience a highly fluctuating thermal environment maintain expression of stress tolerance genes in a constitutive state and are therefore prepared physiologically to endure thermal stress (Barshis et al., 2013). However, these patterns are found to depend on the frequency of variability experienced (i.e. seasonal vs. daily) (Kenkel & Matz, 2017).

Water quality is also frequently implicated in coral resilience and has been shown to moderate the influence of thermal stress via the attenuation of damaging UV radiation by suspended particulate matter (MacNeil et al., 2019; van Woesik & McCaffrey, 2017). In addition, some coral species have shown evidence of trophic plasticity, with the ability to switch from symbiotic autotrophy to heterotrophy when suspended organic matter is in high concentration (Anthony & Fabricius, 2000). On the contrary, poor water quality has also been found to degrade coral resistance to thermal stress (Vega Thurber et al., 2014) and reduce calcification rates by way of elevated inorganic nutrient concentrations (Fabricius, 2005). Some hypothesize that an enhancement of inorganic nitrogen, for example, releases symbiotic algae

from nutrient limitation, allowing them to proliferate, draw down available CO_2 and ultimately constrain calcium carbonate production (Marubini & Atkinson, 1999).

Numerous studies of long-term coral growth trajectories have highlighted recent downturns in rates of calcification or extension, often drawing connections to climate warming during the modern era (De'ath et al., 2009). Many others, however, find no such pattern and in some cases predict that warming may enhance coral growth rates in the short term (Cooper et al., 2012; Courtney et al., 2017). The multitude of confounding environmental and biological factors that influence coral calcification across broad geographic ranges likely underlies many of these contrasting findings. As a result, we are often left with an incomplete picture of the nature and extent to which climate change is already impacting coral reef growth, and how we can expect corals to respond under projected emissions scenarios.

Here, we address this shortcoming with a fully replicated and comprehensive sampling scheme of two coral species spanning three reef ecosystems and 16 degrees of latitude to characterize the principal environmental factors controlling coral growth rates in the western Caribbean and the Atlantic coast of Florida. Annual growth chronologies were generated for 195 coral cores collected across inner and outer reef sites within each reef system and were compared to concurrent annual records of temperature and water quality conditions at each site. The nested sampling design employed here thoroughly represents the wide scope of environmental conditions facing coral reefs in this region.

Materials and Methods

Study design

From 2009 to 2015, a total of 195 skeletal cores of *Siderastrea siderea* and *Pseudodiploria strigosa* were collected from three reef ecosystems spanning 16 degrees of latitude in the western Caribbean and the Atlantic coast of Florida—the Bocas del Toro Reef Complex in Panama (BTRC; 9.3° N), the Mesoamerican Barrier Reef System in Belize (MBRS; 16.7° N) and the Florida Keys Reef Tract (FKRT; 25.0° N). Within each region, four pairs of inner-outer reef sampling sites were identified encompassing the full geographic extent of each reef system. At every site (n = 24), five healthy colonies of each species were selected randomly for coring; although, in some cases less than five colonies of *S. siderea* and *P. strigosa* were sampled either because the dive team was unable to locate five colonies of sufficient size at certain sites or because coring efforts were halted due to inclement weather.

Skeletal cores were extracted from each coral colony using a hydraulic core drill and scanned using X-ray computed tomography to visualize annual density growth bands. Full details of core extraction and X-ray procedures and the methods employed to generate annual growth chronologies are outlined in Chapter 2, Materials and Methods – *Sclerochronology development*. Please refer to this section for a thorough description of the methodology and analysis. Note, the average core length and total sample size for each species in each of the three reef systems are provided in Table 3.1.

Environmental datasets

To assess environmental drivers of coral growth, a compilation of high-resolution sea surface temperature (SST), carbonate chemistry, Atlantic Multidecadal Oscillation (AMO) index

and water quality datasets were obtained for each of the 24 sampling sites. Daily measurements of SST were acquired from two satellite products made available by the Group for High Resolution Sea Surface Temperature, each maximizing either temporal scale or spatial resolution for downstream comparisons to coral growth rates. In particular, daily gridded 0.25° (~28 km) resolution SST measurements spanning 1982-2014 were extracted from the Level 4 Advanced Very High Resolution (AVHRR) Optimally Interpolated SST (OISST) dataset. In addition, daily gridded 0.01° (~1 km) resolution SST measurements from 2003-2014 were acquired from the Level 4 Multi-scale Ultra-high Resolution (MUR) SST dataset.

To characterize the carbonate chemistry at each site, satellite-derived measurements of pH and the saturation state of seawater with respect to aragonite were extracted from the monthly gridded 0.09° (~9 km) resolution Level 4 Ocean Acidification Product Suite produced by Coral Reef Watch and updated in 2014 by the ACCRETE team at the NOAA Atlantic Ocean and Meteorological Laboratory. Monthly measurements were obtained for the entire available record spanning 2014-2017. Note, however, that measurements were not available for the southern Caribbean basin at the time of this study, so only values for the FKRT and MBRS could be compared in downstream analyses.

Annual measurements of the AMO index were derived from the Kaplan Extended SST v2 dataset, and were calculated as the area-weighted SST average over the North Atlantic (0-70°N), which is then detrended using the global climatology. This data was acquired from the NOAA Earth System Research Laboratory (Enfield, Mestas-Nuñez, & Trimble, 2001).

Water quality was characterized indirectly based on two parameters representative of local terrestrial influence: water clarity and rainfall. First, water clarity at each site was measured using the satellite-based diffuse attenuation coefficient at 490 nm (K_d490), as this proxy has been

shown to accurately reflect water column turbidity across global oceans (Shi & Wang, 2010). Daily K_d490 data (Level 2) at 750 m resolution spanning 2012-2017 were collected from the Visible Infrared Imaging Radiometer Suite sensor aboard the Suomi NPP satellite and compiled by NOAA CoastWatch/OceanWatch. Prior to analysis, data were mapped to a custom map projection and a time series for each of the 24 sampling sites was extracted using the CoastWatch Utilities Tool. Data were then quality filtered by removing values with a QA score < 0.8 based on J. Wei, Lee, and Shang (2016). The QA score represents the accuracy with which a satellite spectral observation matches a sample from a pool of in situ reference spectra, with 0 representing no match and 1 representing a perfect match. Statistical outliers were also removed from the dataset so that prevailing long-term water clarity was represented.

Second, historical rainfall data were obtained from logs maintained by regional meteorological and aviation agencies. Annual rainfall records for the MBRS, FKRT and BTRC were acquired from the National Meteorological Service of Belize, from the Florida Climate Center managed by Florida State University and from the Smithsonian Tropical Research Institute, respectively. For the MBRS, data were obtained from the nearest weather station to each of the four inner-outer reef site pairs spanning the reef system; however, for the FKRT and BTRC, the nearest rainfall record was the same for all sampling sites.

Statistical Analysis

Principal component analysis (PCA) was used to characterize the composite temperature and water quality environment at each sampling site, incorporating ten statistics summarizing the temperature and thermal stress characteristics as well as the median K_d490 across the full available record. In this case, median was used to avoid positive bias from turbidity anomalies

during major storm or rainfall events. Temperature and thermal stress parameters included the annual mean, annual minimum, annual maximum, and annual range, as well as annually averaged weekly range to account for shorter term temperature fluctuations. Summer mean temperature was calculated as the average temperature for the months of July, August and September, as these three months encompass the summer maximum on the FKRT as well as the rising late summer peak in the tropical regions (Figure 3.1A). Note, this late summer peak on the MBRS and BTRC is generally warmer as the sun passes back across the tropical latitudes in approach of the autumnal equinox.

Following the methodology of Coral Reef Watch, the thermal stress environment was characterized by counting bleaching hotspots as days during which SST exceeded the highest climatological monthly mean for each site. Monthly climatologies were derived for each site based on the full SST record available (OISST: 1982-2014, MUR: 2003-2014). Bleaching hotspots > 1.0°C have been identified as sufficient to cause significant thermal stress to corals (Glynn & D'Croz, 1990), so we incorporated the total number of thermal stress events (bleaching hotspots > 1.0°C), the average duration of stress events (consecutive bleaching hotspots > 1.0°C) and the average number of days between subsequent stress events. Moreover, a joint metric combining the magnitude and cumulative history of thermal stress has been most directly correlated with coral bleaching susceptibility (Manzello et al., 2007), so to account for the severity of thermal stress, we calculated annual cumulative stress at each site as the cumulative sum of bleaching hotspots > 1.0°C. Thus, two bleaching hotspots of 2.0°C would yield a cumulative sum of 4.0°C. Note, all temperature parameters included in the PCA analysis were derived from the MUR SST dataset in order to take advantage of the high spatial resolution to

differentiate between all sampling sites and were averaged across the full available record (2003-2014). Region-specific summaries of each parameter can be found in Table S1.

Generalized additive models were used to assess long-term trajectories of coral extension rates through time, following the methodology outlined in Chapter 2, Materials and Methods – *Statistical analysis*. Briefly, growth chronologies for each reef system and species were fit with a model incorporating an adaptive smoothing spline of *Year* as a fixed effect predictor and each individual *Core* as a random effect. The smoothing basis ($k = 25$ for *S. siderea*; $k = 20$ for *P. strigosa*) was selected following the protocol recommended by Wood (2017), whereby k was increased progressively ($k = 5, 10, 15, 20, 25$) until the effective degrees of freedom stabilized at a value sufficiently lower than $k - 1$. This modeling procedure was implemented using the *mgcv* package in R (R Core Team, 2017; Wood, 2011). Importantly, extension rates were the focus of this study as density and calcification data were not available for 20 *S. siderea* cores from MBRS (> 10% of total sample size). To verify that extension rate is an accurate proxy of calcification rate in the sampled corals, we performed a simple linear regression between annual extension, density and calcification rates for both species. Correlation between extension and calcification yields an R^2 of 0.92 and 0.48 for *S. siderea* and *P. strigosa*, respectively, and between density and calcification yields an R^2 of <0.01 and 0.24 for *S. siderea* and *P. strigosa*, respectively (Figure S3.1).

To compare coral growth trajectories with putative environmental correlates, linear mixed effect (LME) models were implemented using the *nlme* package in R (Pinheiro, Bates, DebRoy, Sarkar, & R Core Team, 2012). Prior to modeling, all growth chronologies were truncated at 1982 for comparison to the OISST dataset, and annual extension values were log-transformed in order to satisfy the assumption of normality. An AIC-based forward stepwise

model selection approach was used in which preliminary models were established by incorporating *Year* as the primary predictor of annual extension and allowing slopes and intercepts to vary based on all combinations of categorical grouping variables (i.e., *Species*, *Region*, *Reef Zone*). Accounting for individual variation around the model prediction by including individual *Core* as a random effect always performed best and was therefore included in all subsequent models.

Environmental correlates were then added as predictors to this model sequentially to generate a new set of candidate models for comparison. Decisions to include specific predictor combinations were made deliberately and were informed by established knowledge of putative controls on coral growth rates. Thus, we focused our analyses on annual mean temperature (Lough & Barnes, 2000), annual and weekly temperature range (Kenkel, Almanza, & Matz, 2015), summer mean temperature (Castillo et al., 2012), annual cumulative thermal stress (Mendes & Woodley, 2002), AMO index (Helmle et al., 2011), turbidity (K_d490) and rainfall (Fabricius, 2005), as each of these factors has been shown to influence coral growth and/or resilience to ocean warming. Because only the SST, AMO and rainfall records overlap significantly with coral growth chronologies, median K_d490 was calculated at each site across the full record and used as a stationary variable. In addition, because seawater chemistry data were not available for the BTRC, we chose not to include pH or aragonite saturation state in the model.

Lastly, a set of level-1 residual correlation structures was incorporated to account for autocorrelation between annual extension measurements within each individual core. These correlation structures include all combinations of an autoregressive-moving average model (ARMA) of order (p,q), with each component (AR and MA) ranging from 0 to 2. For the full

table including all model structures that were tested with associated AIC and log-likelihood scores, please refer to Appendix 2.

Results

Environmental variation across the Western Caribbean Sea

Each of the three reef systems experiences a unique physical environment with respect to both temperature and water quality conditions. In particular, the Florida Keys Reef Tract (FKRT) and Bocas del Toro Reef Complex (BTRC) represent the two extremes for virtually all temperature statistics: the FKRT experiences the greatest annual maximum, annual range, weekly range and summer mean and Panama experiences the greatest annual mean, annual minimum and highest measure of all thermal stress indices. By comparison, the Belize Mesoamerican Barrier Reef System (MBRS) experiences intermediate conditions with respect to all temperature statistics (Figure 3.1; Table S3.1).

Within each reef system, inner and outer reef environments also experience significantly different temperature and thermal stress conditions, reflected as separation along the PC2 axis in Figure 3.1D. Weekly temperature range as well as the frequency, duration and annual accumulation of thermal stress are greater at inner reef sites. Note, the reef zone difference in weekly temperature range is particularly pronounced on the FKRT, while the difference in thermal stress is more pronounced on the MBRS and BTRC (Figure 3.1D; Table S3.1).

Turbidity (K_d490) is also consistently greater at inner reef sites, as is expected due to their proximity to terrestrial runoff and riverine outflow (Figure 3.1C). Interestingly, outer reef sites on the MBRS separate into two distinct site pairs based on water quality, with one pair

exhibiting the lowest turbidity of all sampling sites and the other exhibiting relatively high turbidity compared to all other outer reef sites (Figure 3.1C; Table 3.S1).

Lastly, seawater pH and aragonite saturation state (Ω_{arag}) exhibit contrasting trends between the FKRT and MBRS. Specifically, pH is slightly lower while Ω_{arag} is greater on the MBRS in comparison to the FKRT. These data suggest, however, that ambient conditions on both reef systems are super-saturated with respect to aragonite concentration ($\Omega_{arag} > 1$; Table 3.1).

Long-term trends in coral extension

Long-term trends in annual extension rates reveal that corals of both species are currently experiencing significant declines on both the BTRC and MBRS in comparison to past growth rates (Figure 3.2). On the BTRC, however, the onset of the downturn differs between the two species. *S. siderea* extension rates have been declining throughout nearly the entire 20th century, whereas growth of *P. strigosa* has only recently declined, albeit precipitously, beginning in 2005. On the MBRS, declines in extension appear to have initiated around the mid- to late-1990s for both species. Contrastingly, on the FKRT, corals experience decadal-scale fluctuations around baseline mean extension rates without evidence of consistent declines as is evident on the other reef systems (Figure 3.2).

It is important to point out that *P. strigosa* were largely absent from inner reef sites on the BTRC (n = 2), whereas colonies of *S. siderea* were ubiquitous across all three reef systems (Table 3.1). Consequently, the modeled growth trend for *P. strigosa* on the BTRC largely represents colonies from outer reef sites.

Environmental drivers of coral extension in the Western Caribbean Sea

Comparison among the full set of preliminary candidate models revealed that a fully interactive model allowing slopes and intercepts to vary based on *Species* and *Region* out-performed all other models substantially. Adding in environmental correlates, the best fit model based on AIC comparison included $K_d490 \cdot$ *Species*, *Summer Mean Temperatures (MBRS)*, *AMO (FKRT)*, *Cumulative Thermal Stress (BTRC)*, *Rainfall (BTRC)* and *Cumulative Thermal Stress · Rainfall (BTRC)* as fixed effect predictors, where the reef system in parentheses indicates where the effect is significant (Appendix 2).

Model coefficient estimates indicate that higher water column turbidity correlates with greater extension rates for *S. siderea*, but confers no significant effect for *P. strigosa* (Figure 3.3A). Additionally, summer mean temperatures are negatively associated with extension for both species; however, this effect is only significant on the MBRS. Likewise, a negative correlation between extension rates of both species and the AMO index is significant only on the FKRT. On the BTRC, *Annual cumulative stress* and *Rainfall* were found to have a positive effect on *P. strigosa* extension as independent predictors, but a negative interactive effect when they co-vary. The full model predictions reveal these effects to be particularly pronounced during and after a regional coral bleaching event in 2010. Unexpectedly, extension rates of *P. strigosa* actually peaked in 2010 when thermal stress was elevated and was significantly depressed in the years following when rainfall was anomalously low (Figure S3.2). None of the environmental parameters tested in the model were found to explain variations in *S. siderea* extension on the BTRC.

Discussion

Coral growth trajectories across the Western Caribbean are largely reflective of the widespread coral population declines during the modern era of climate change. On the Bocas del Toro Reef Complex (BTRC) in Panama and the Mesoamerican Barrier Reef System (MBRS) in Belize, corals of both species in this study are experiencing significant downturns in extension rates in comparison to their historic baseline. On the MBRS in particular, this decline appears to have begun in the mid- to late-1990s for both species, in close association with the first recorded global coral bleaching event in 1997-98. The impact of this event on coral reef communities throughout the Caribbean was catastrophic, with total recorded losses of living coral cover estimated at 5-10% regionally and reports of >25% coral mortality in some locations (Goreau, McClanahan, Hayes, & Strong, 2000). As seawater temperatures have continued to rise over the past two decades (Figure S3.3), these results suggest that *S. siderea* and *P. strigosa* on this reef system are experiencing extended consequences that have led to chronic reductions in growth.

In fact, on the MBRS, summer temperatures were found to exhibit a significant negative correlation with extension based on the best-fit LME model. This result is consistent with previous work from the southern MBRS based on a subset of the *S. siderea* cores analyzed here, which found that within the southernmost inner-outer reef transect, only outer reef corals experienced a significant growth reduction in association with increases in summer seawater temperature (Castillo et al., 2012). With a significantly increased sample size spanning the extent of the MBRS and the inclusion of an additional species, we find that corals across the reef system show similar evidence of sensitivity to rising summer temperatures. Moreover, this recent downturn in coral growth in association with summer temperatures is also consistent with reports

from the Red Sea and the Great Barrier Reef describing identical declining trajectories over the past two decades (Cantin et al., 2010; De'ath et al., 2009).

Surprisingly, however, this association is not significant for corals on the BTRC, despite experiencing the warmest conditions on average of any of the three reef systems (Table S3.1). Rather, the onset and time scale of declining growth trajectories differs substantially between species on the BTRC, where *S. siderea* have experienced a chronic deterioration over the course of the past century and *P. strigosa* have only recently exhibited a sharp and significant reduction in growth rates within the past decade. LME modeling suggests that this trend in *P. strigosa* growth can be attributed in part to the independent positive effects of cumulative thermal stress and local rainfall and the negative interaction of these two factors.

Cumulative thermal stress is well known to cause coral bleaching and mortality events; thus, its positive association with *P. strigosa* growth on the BTRC is certainly unexpected. One possible explanation stems from the calculation used to evaluate cumulative annual thermal stress. Similar to the degree heating week (DHW) metric established by NOAA CoralWatch, annual cumulative thermal stress was measured here as the total number of days per year where SST was at least 1°C greater than the maximum monthly mean (MMM) climatology multiplied by the magnitude of each day's SST deviation over the course of a year. Importantly, because the BTRC experiences relatively minimal seasonal SST variation (Figure 3.1B), the MMM for this region is cooler than that of other regions that experience warmer summers, and as a result, the thermal stress anomalies incorporated into this metric are also relatively cooler. Thus, it may be that the unusually warm temperatures experienced on the BTRC in 2010 in comparison to prevailing conditions still fell below the thermal optimum for *P. strigosa* growth and consequently led to a peak in the extension rate for this species.

Without corresponding data on the nutrient conditions in the region, it is difficult to parse the mechanism by which rainfall is positively associated with *P. strigosa* growth on the BTRC. Terrestrial runoff has been shown to significantly alter salinity and dissolved nutrient profiles as well as phytoplankton levels in the area (D'Croz, Rosario, & Gondola, 2005). During periods of heavy rainfall, river discharge originating from the southeastern portion of the adjacent Chiriquí Lagoon spreads across the reef complex, distributing elevated dissolved nutrient concentrations to both inner and outer reef areas (D'Croz et al., 2005). Corals have demonstrated mixed growth responses to experimental manipulation of various dissolved nutrients (e.g., nitrate, ammonium or phosphate), with some increasing their extension rate (Koop et al., 2001) and others decreasing or experiencing no change to their growth (Fabricius, 2005), often depending on the magnitude of nutrient enrichment. Here, we find evidence that *Pseudodiploria strigosa* may be one species that benefits from changes in the nutrient regime associated with rainfall on the BTRC.

The negative interactive effect of cumulative thermal stress and rainfall on *P. strigosa* growth is reflective of previous work showing that nutrient enrichment associated with terrestrial runoff can increase the prevalence and severity of coral bleaching (Vega Thurber et al., 2014; Wiedenmann et al., 2013; Wooldridge, 2009). Indeed, in this reef environment, *P. strigosa* seems to benefit from both anomalous warming events and high rainfall independently, but experiences a reduction in extension when these two conditions co-occur.

In comparison to the other two reef systems, the extension rates of both species on the FKRT appear to fluctuate regularly around the long-term average with no evidence of anomalous trends throughout the record. Based on the LME model, growth rates of both species show a significant negative correlation with the Atlantic Multidecadal Oscillation (AMO). The AMO

index represents a 20- to 40-year cycle in coupled ocean-atmosphere variability based on the temperature difference between the North Atlantic and global climatology. Cool and warm phases are characterized by a temperature difference of approximately 0.6°C and are generally associated with changes in precipitation and major storm intensity. Past research has shown that corals are able to track climatic cycles via isotopic signatures in their skeletal matrix (Hetzinger et al., 2008), and positive coral growth anomalies have been associated with the warm phase of the AMO (Kwiatkowski et al., 2013). Interestingly, however, we find that extension rates on the FKRT fluctuate out of phase with the AMO cycle, such that faster and slower growth is associated with the cool and warm phase of the AMO, respectively.

Since the full AMO record extends beyond 1982—the earliest year included in the LME model—a qualitative comparison between coral growth rates and AMO over the past century reveals that the synchronicity has reversed from the two parameters fluctuating in phase before 1980 to out of phase following 1980 (Figure S3.4). It is possible that the long-term warming trend on the FKRT of ~0.8°C since the late 1800s (Kuffner et al., 2015) has recently exceeded a thermal optimum for these two coral species, leading to declines in growth in association with the warm phase of the AMO but positive growth when the cool phase causes temperatures to fall below this thermal optimum.

The only environmental correlate found to influence growth rates consistently across all three reef systems was water column turbidity, which showed a positive association with growth for *S. siderea*. Although counterintuitive, high suspended particulate matter content has previously been shown to improve coral fitness through two primary mechanisms: through the attenuation of damaging UV radiation that exacerbates thermal stress (van Woesik & McCaffrey, 2017), and by providing a supplemental source of nutrition in addition to autotrophy via

symbiosis (Anthony, 2006; Anthony & Fabricius, 2000). To test the first hypothesis, an interactive effect between K_d490 and cumulative thermal stress was incorporated in a candidate model, but was not found to be significant for any region or species. Thus, it is more likely that the positive effect of turbidity on coral growth in this case can be attributed to the ability of *S. siderea* to take advantage of heterotrophic opportunity in more turbid coastal waters, whereas the lack of an effect in *P. strigosa* suggests that this species may not possess the same trophic plasticity.

Trophic plasticity has been identified as a possible mechanism buffering certain coral species from the worst effects of bleaching (A. D. Hughes & Grottoli, 2013). Some have proposed that corals that are well adapted to feeding are able to maintain sufficient respiratory rates during thermal stress to avoid a breakdown in the stability of symbiosis (Wooldridge, 2014). In this way, it is possible that the positive effect of turbidity on the extension rate of *S. siderea* is reflective not only of trophic plasticity, but also, by inference, of the overall resilience of this species to ocean warming. On the FKRT for example, in contrast to the widespread decline of most other hard coral species, the abundance of *S. siderea* has actually risen over the past two decades (Florida Fish and Wildlife Conservation Commission, 1996-2017), suggesting that this species exhibits higher than average tolerance to recent ocean warming and may come to dominate Caribbean reefs of the future.

The results of this study highlight the important interplay between local and global factors in driving coral growth rates. The detrimental effect of rising summer temperatures on growth within the MBRS, similar to other reef systems globally, highlights the pervasive threat of ocean warming to the ecological function of reefs as keystone habitat engineers. However, the absence of this correlation on the other two reef systems suggests that vulnerability to this threat

is highly dependent on the local environmental setting. Moreover, we find that AMO is closely associated with coral growth on the FKRT, while on the BTRC, growth of *P. strigosa* is associated with both the independent and interactive effects of cumulative thermal stress and rainfall. Lastly, turbidity maintains a positive effect on *S. siderea* growth rates across the W Caribbean and Atlantic coast of Florida but not on *P. strigosa*, indicating that these species likely differ in their ability to take advantage of heterotrophic opportunity. As managers and researchers continue to develop reef protection and recovery strategies in anticipation of future climate change scenarios, it remains imperative to take into account the local setting of the target reef environment in addressing coral resilience to these global threats.

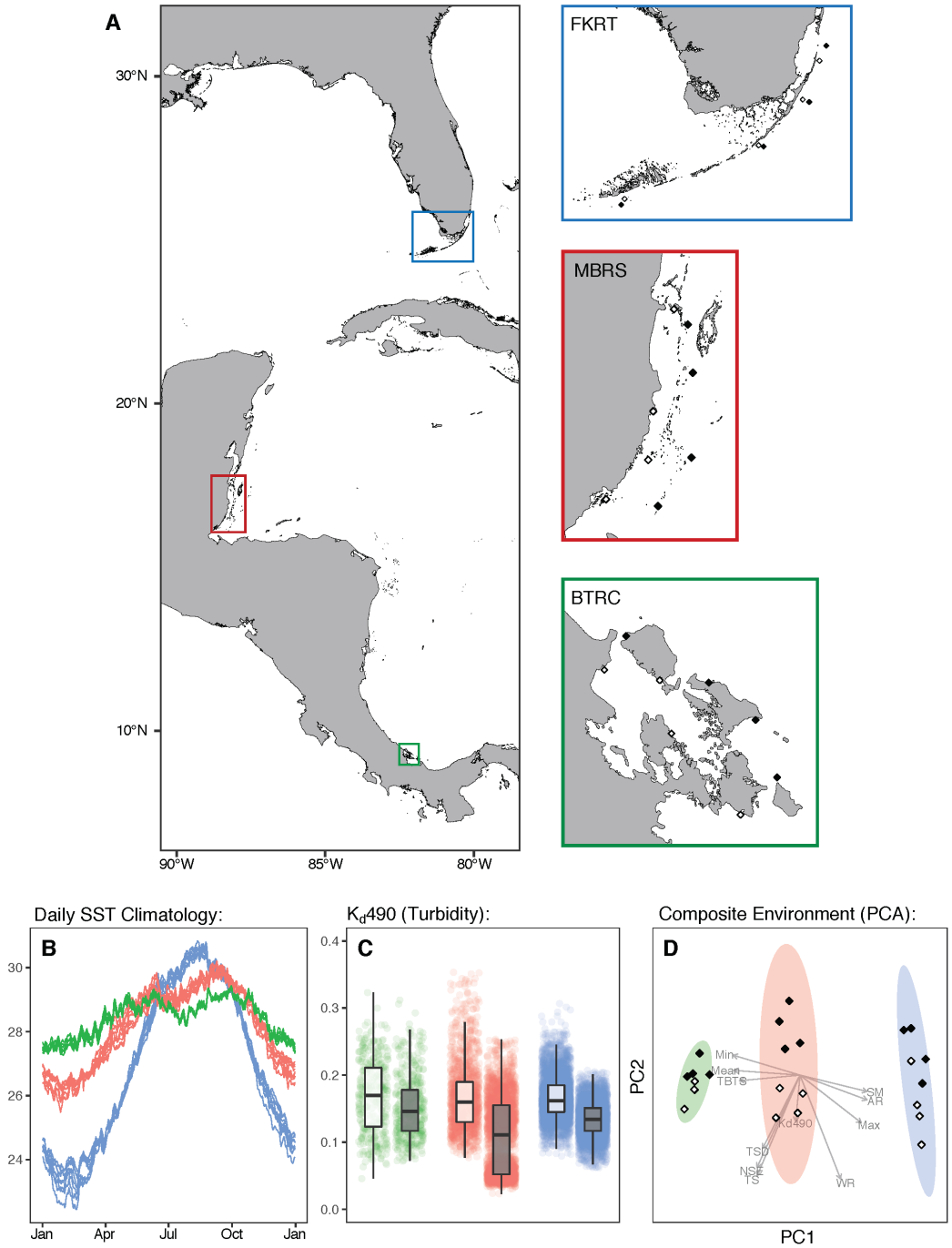

Figure 3.1. Sampling sites with temperature and water quality conditions across the Western Caribbean Sea. (A) Four pairs of inner-outer site pairs were identified spanning the three reef systems: Florida Keys Reef Tract (FKRT, blue), Belize Mesoamerican Barrier Reef System (MBRS, red) and Bocas del Toro Reef Complex (BTRC, green). Inner and outer reef sites are represented on the maps as open and closed diamonds respectively. Daily SST climatologies (B), K_d490 (turbidity; C) and multivariate environmental PCA (D) are depicted, with colors corresponding to regions and boxplots and point symbols corresponding to reef zone.

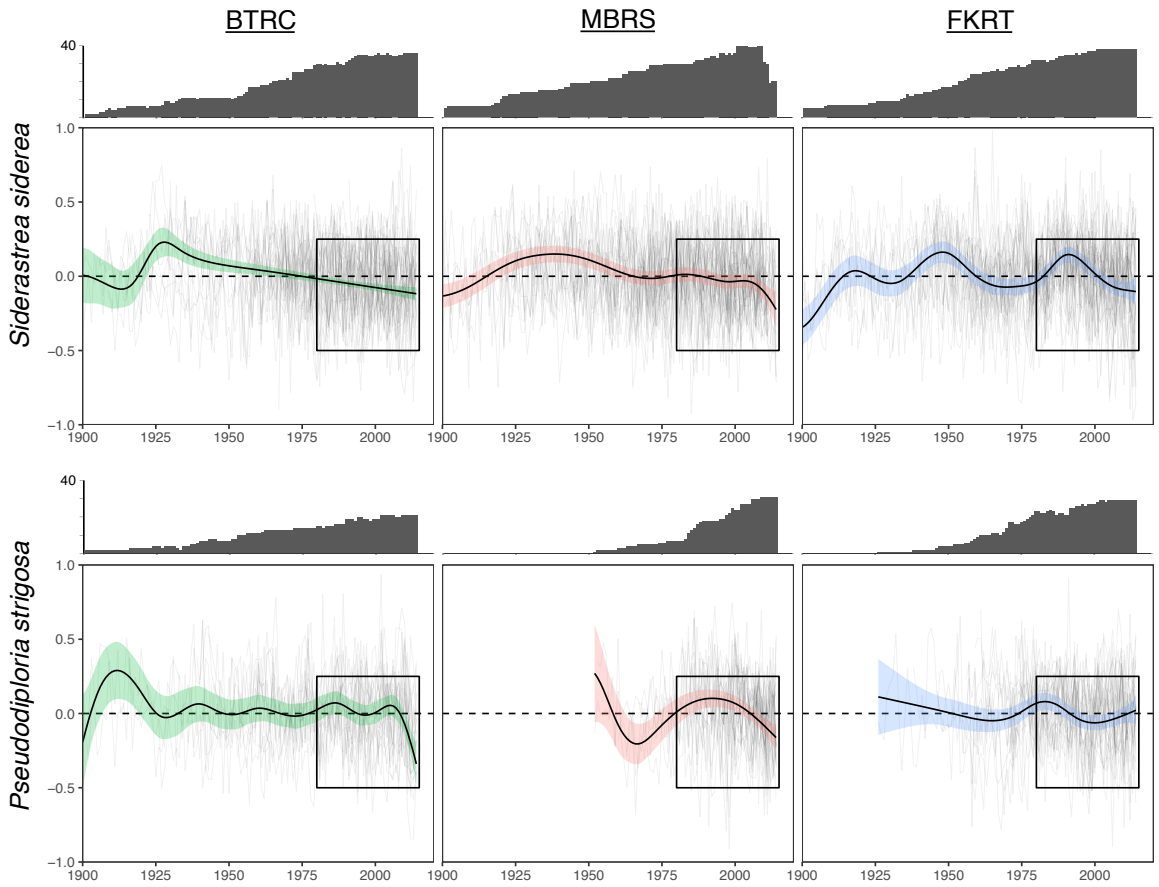

Figure 3.2. Long-term chronologies of coral extension rates. Plots are organized by species along the vertical axis and by region along the horizontal axis, with colors corresponding to region as in Figure 3.1. Generalized additive model predictions (±2 SE) overlay individual core chronologies of standardized annual extension (light gray). Bar charts along the top axis of each plot depict the number of cores represented for each year along the x-axis. Black boxes highlight the time period corresponding to the full length of OISST record (1983-2014), which was the focus of the linear mixed effect modeling.

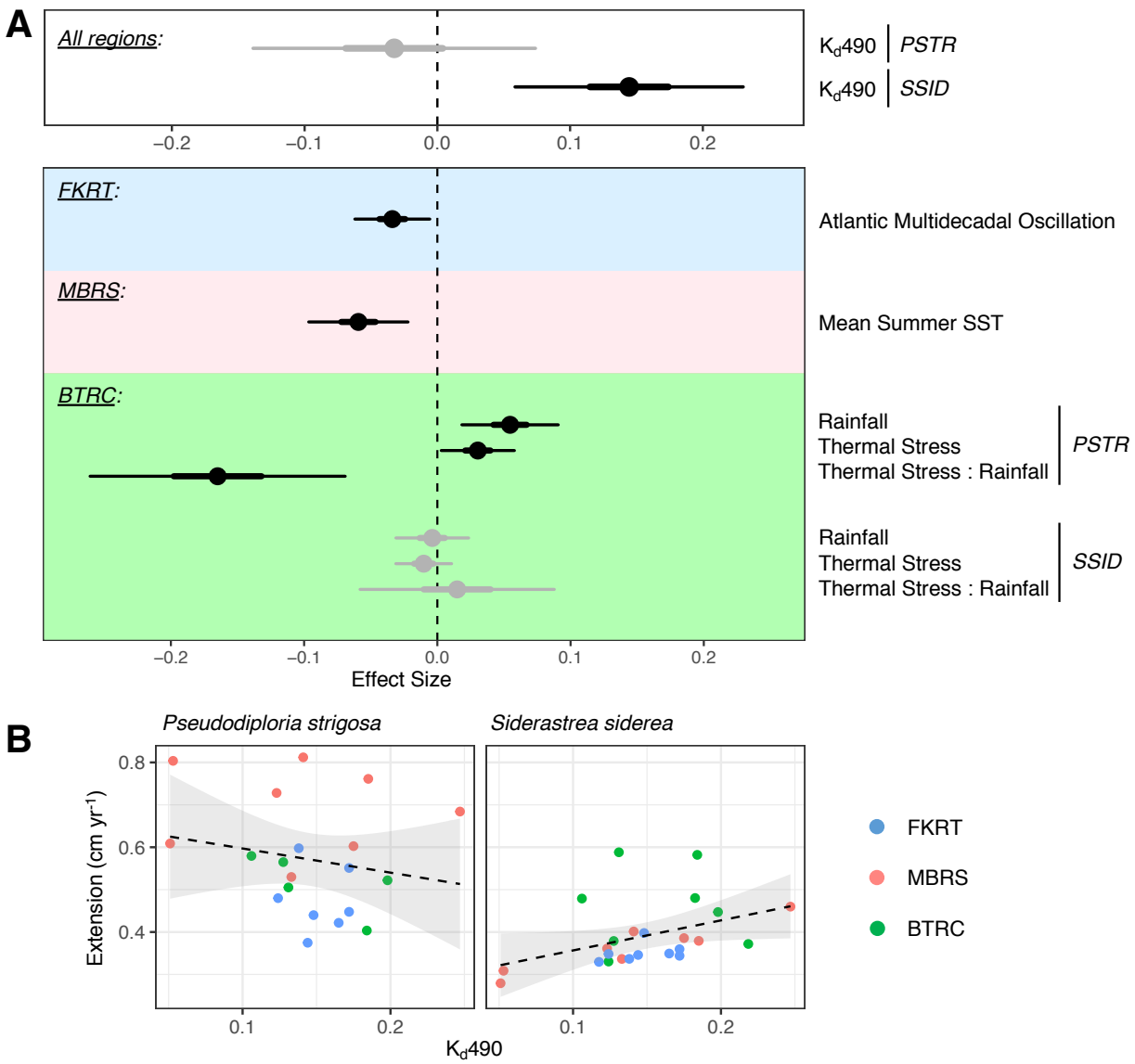

Figure 3.3. Linear mixed model coefficients for environmental drivers of coral growth. (A) Thick and thin bars represent 50% and 95% confidence intervals, respectively. Black and grey points statistically significant and non-significant effects. Correlates are separated by species and region of influence along the vertical axis, with *K_d490* influencing *S. siderea* in all regions, *Atlantic Multidecadal Oscillation* and *Mean Summer SST* influencing both species on the FKRT and MBRS, respectively, and the interaction of *Cumulative Thermal Stress · Weekly SST Range* influencing *P. strigosa* on the BTRC. (B) Effect of K_d490 on coral extension rates plotted as a linear regression and separated by species. Background colors in (A) and point colors in (B) correspond to reef systems, as in Figure 3.1.

Siderastrea siderea								
Region	**RZ**	**N**	**Size (cm)**	**Extension (cm yr^{-1})**	**Density (g $cm^{-3}yr^{-1}$)**	**Calcification (g $cm^{-2}yr^{-1}$)**	**pH (2014-17)**	**Ω_{arag} (2014-17)**
FKRT	ir	20	39.7	0.36 (±0.01)	1.39 (±0.01)	0.50 (±0.01)	8.08 (±0.01)	4.05 (±0.07)
	or	19	31.8	0.37 (±0.01)	1.42 (±0.01)	0.52 (±0.01)	8.08 (±0.01)	4.05 (±0.07)
MBRS	ir	14	40.2	0.38 (±0.01)	1.34 (±0.01)	0.65 (±0.01)	8.06 (±0.01)	4.14 (±0.02)
	or	23	43.4	0.34 (±0.01)	1.40 (±0.01)	0.56 (±0.01)	8.06 (±0.01)	4.17 (±0.02)
BTRC	ir	19	37.2	0.43 (±0.01)	1.35 (±0.01)	0.57 (±0.01)	-	
	or	20	50.8	0.50 (±0.01)	1.30 (±0.01)	0.65 (±0.01)	-	

Pseudodiploria strigosa								
Region	**RZ**	**N**	**Size (cm)**	**Extension (cm yr^{-1})**	**Density (g $cm^{-3}yr^{-1}$)**	**Calcification (g $cm^{-2}yr^{-1}$)**	**pH (2014-17)**	**Ω_{arag} (2014-17)**
FKRT	ir	19	32.7	0.47 (±0.01)	1.19 (±0.01)	0.54 (±0.01)	8.08 (±0.01)	4.05 (±0.07)
	or	12	25.2	0.49 (±0.01)	1.20 (±0.01)	0.57 (±0.01)	8.08 (±0.01)	4.05 (±0.07)
MBRS	ir	18	31.2	0.79 (±0.01)	0.94 (±0.01)	0.73 (±0.01)	8.06 (±0.01)	4.14 (±0.02)
	or	20	38.5	0.59 (±0.01)	1.16 (±0.01)	0.67 (±0.01)	8.06 (±0.01)	4.17 (±0.02)
BTRC	ir	2	20.9	0.58 (±0.03)	0.97 (±0.02)	0.56 (±0.03)	-	
	or	20	47.4	0.50 (±0.01)	0.74 (±0.01)	0.36 (±0.01)	-	

Table 3.1. Summary of growth parameters for regions and reef zones. Averages of colony size (estimated by core length), annual extension rate, density, calcification rate, seawater pH and aragonite saturation state (±SE) for each species, region and reef zone. Colors correspond to the three reef systems, as in Figure 3.1.

CHAPTER 4: POPULATION STRUCTURE AND CONNECTIVITY OF THE MOUNTAINOUS STAR CORAL, *ORBICELLA FAVEOLATA*, THROUGHOUT THE WIDER CARIBBEAN REGION[3]

Introduction

Over the past several decades, major physical, chemical and ecological changes to the marine environment have compromised the health and persistence of coral reefs globally (Andersson & Gledhill, 2013; Hoegh-Guldberg et al., 2007). In the wider Caribbean region specifically, large-scale surveys of live coral cover estimate losses on the order of 60% since the 1980s (Jackson et al., 2014). Particularly concerning is the disproportionate loss of critical framework species, such as the *Orbicella* species complex (*O. annularis*, *O. faveolata* and *O. franksi*), as their characteristic slow growth and long lifespans prevent rapid reef recovery following mortality (Gladfelter, Monahan, & Gladfelter, 1978). *Orbicella* spp. previously functioned as dominant reef-builders throughout the region; however, the abundance of this species complex has declined sharply (Bruckner & Bruckner, 2006; Edmunds, 2015), and it has largely been replaced by smaller "weedy" coral species with shorter generation times, such as *Agaricia* spp. and *Porites* spp. (Davies, Matz, & Vize, 2013; Green et al., 2008; Knowlton, 2001). This transition has led to reduced structural habitat complexity and as a result, lower diversity and abundance of reef-dependent fishes (Gratwicke & Speight, 2005; Risk, 1972) and invertebrates (Idjadi & Edmunds, 2006) on Caribbean reefs. In addition, it has been shown that

[3] This chapter previously appeared as an article in Ecology and Evolution. The original citation is as follows: Rippe, J.P., Matz, M.V., Green, E.A., Medina, M., Khawaja, N.Z., Pongwarin, T., Pinzón C., J.H., Castillo, K.D., and Davies, S.W. "Population structure and connectivity of the mountainous star coral, *Orbicella faveolata*, throughout the wider Caribbean basin." *Ecology and Evolution*, 7, no. 22 (Nov 2017): 9234-9246.

declines of *Orbicella* spp. have been exacerbated by persistent recruitment failure (T. P. Hughes & Tanner, 2000; van Woesik, Scott, & Aronson, 2014). These severe population declines coupled with a lack of recruitment led the National Marine Fisheries Service to classify the *Orbicella* species complex as threatened under the Endangered Species Act in 2014 (National Marine Fiseries Service, 2014).

Effective management of coral reefs relies on a sound understanding of the level to which spatially discrete populations are linked by dispersal. In its most basic sense, dispersal facilitates an influx of individuals to recipient reefs that can bolster population persistence demographically via immigration (Gaines, Gaylord, & Largier, 2003; Hastings & Botsford, 2003; Palumbi, 2003). Additionally, connectivity via larval dispersal also fosters the exchange of genetic variants, which acts to increase standing genetic variation (fuel for evolutionary adaptation) and facilitates the spread of advantageous alleles within and between reefs. In purple sea urchins (*Strongylocentrotus purpuratus*) for example, populations along the U.S. west coast were found to be genetically differentiated at certain loci due to adaptation to their local environment; yet, all alleles which confer an advantage in any one environment are spread at low frequencies almost everywhere else throughout the species range due to dispersal (Pespeni & Palumbi, 2013). As a result, connectivity primes populations to adapt to a range of environmental pressures across the extent of the species distribution. In this way, understanding the source-sink dynamics of larval supply and dispersal across a seascape provides insight into valuable reef areas for protection and can greatly enhance the effectiveness of marine conservation planning, especially in light of ongoing global change.

For corals and other sessile organisms, dispersal distance is primarily a function of pelagic larval duration (PLD), or the time required for a larva to become competent to settle

(Selkoe & Toonen, 2011; Shanks, 2009). PLD varies across species, fertilization strategy, larval development rate, and responsiveness to settlement cues (Graham, Baird, & Connolly, 2008; K. Miller & Mundy, 2003; Tebben et al., 2015; Underwood, Smith, Van Oppen, & Gilmour, 2009). *Orbicella faveolata* is a hermaphroditic broadcast-spawner that releases its gametes synchronously following the full moon in the warmest month of the year (Szmant, 1991; Vize, 2006). *Orbicella* spp. larvae are generally competent to settle five days post fertilization (dpf; although see Davies, Meyer, Guermond, and Matz (2014)) and most will attempt to settle within two weeks if the appropriate cue is received (Szmant & Meadows, 2006; Wellington & Fitt, 2003). However, if the appropriate cue is unavailable, larvae of *Orbicella franksi* have been shown to successfully settle up to 120 dpf in the laboratory, highlighting the long distance dispersal potential of this species complex (Davies, Strader, Kool, Kenkel, & Matz, 2017).

The once widely held paradigm that marine populations routinely exchange individuals across great distances has been challenged by mounting evidence that suggests local retention plays a much greater role in structuring populations at demographically relevant time scales than previously appreciated (Almany, Berumen, Thorrold, Planes, & Jones, 2007; Bode, Bode, & Armsworth, 2006; Cowen, Lwiza, Sponaugle, Paris, & Olson, 2000; Swearer et al., 2002). Over the last decade, the development of more sophisticated genetic analyses and biophysical models has allowed researchers to better predict where along the dispersal continuum from "open" to "closed" marine populations lie (Cowen & Sponaugle, 2009). To date, our understanding of *O. faveolata* population structure is limited to three regional studies within the Caribbean seascape, of which two observed genetic homogeneity between populations along the Florida Reef Tract (Baums, Johnson, Devlin-Durante, & Miller, 2010) and between populations in Puerto Rico, the Yucatan, and lower Florida Keys (Severance & Karl, 2006). More recently however, Porto-

Hannes et al. (2015) observed significant genetic structure within the Mesoamerican Barrier Reef System. These divergent findings illustrate that larval dispersal across the Caribbean may be influenced by multiple complex processes, which leads to uncertainty about the degree of population connectivity unless the entire basin is considered.

Here, we explore the patterns of *O. faveolata* population connectivity across the geographic extent of the wider Caribbean region using nine polymorphic microsatellite loci (Davies, Rahman, et al., 2013; Severance, Szmant, & Karl, 2004). In a study across a similar spatial scale, *O. annularis* (sister species to *O. faveolata*) was shown to differentiate into three genetic neighborhoods comprising the eastern, western and central regions of the Caribbean (Foster et al., 2012). Using a combination of empirical genetic data with a biophysical projection model, Foster et al. (2012) refine the location of a previously described genetic break between populations in the eastern and western portions of the basin (Baums, Paris, & Cherubin, 2006; Vollmer & Palumbi, 2007) to the area between the British Virgin Islands to the east and Dominica to the west. It remains to be seen, however, if *O. faveolata* follow the same patterns of genetic structure.

With the findings of this investigation, we specifically seek to achieve three primary goals: (1) quantifying the extent to which populations of *O. faveolata* are open or closed to long distance gene flow across the wider Caribbean, (2) evaluating the uniformity of a previously established genetic break between eastern and western populations across taxa, and (3) identifying unique patterns of substructure within the broader framework of *O. faveolata* population genetics in the region. This study contributes to a growing understanding of the dispersal capabilities of marine invertebrates in the wider Caribbean. In doing so, it helps to further inform regional conservation strategies for an endangered foundation coral species and

provides a foundation for future investigations into the mechanisms that underlie the observed patterns of population genetics.

Materials and Methods

Sample Collection

Between 2012-15, a total of 416 tissue samples (~2 cm^2) of the mountainous star coral, *Orbicella faveolata*, were collected from 10 sites that span the extent of the wider Caribbean seascape (Figure 4.1A, Table 4.1). At several locations, samples were collected from a group of neighboring reefs. To account for the large spatial scale of interest in this study, these samples were pooled as single populations for all analyses performed (Table 4.1; see Appendix 3 for further justification regarding pooling). All samples were collected between 5-15 m depth with the exception of those from the Flower Garden Banks (FGB), which were collected at 20-25 m depth.

At all locations except the lower Florida Keys (Sugarloaf Key), fragments of tissue were excised from adult colonies using a hammer and chisel and were placed in individual plastic bags filled with seawater. Tissue samples collected at Sugarloaf Key were siphoned from the coral surface using a plastic syringe to minimize physical damage, in compliance with permit requirements. The filter paper containing each tissue sample was placed in a labeled plastic bag filled with a 96% ethanol (EtOH) solution. At all sites, colonies of *O. faveolata* were identified visually based on the morphological criteria outlined in Weil and Knowton (1994). Care was taken to avoid sampling connected colonies and those within 5 m of each other in order to minimize the possibility of sampling clones.

All samples were then transported in an insulated cooler to the laboratory for preservation. Samples from the Bahamas, Barbados, Belize, Florida Keys, and USVI were transferred to DMSO Buffer (20% dimethyl sulfoxide and 0.25 ethylene diaminetetaacetic acid (EDTA) in NaCl-saturated water), while those from the FGB were transferred to 96% EtOH. All of the above were stored at -20°C. Samples from Curaçao, Mexico, Panama and Puerto Rico were flash frozen in liquid nitrogen and stored at -80°C.

Note, to maintain consistent terminology throughout the manuscript, the terms *sampling site*, *site* and *population* will be used interchangeably to refer to the 10 sampling sites discussed above and outlined in Table 4.1, while the term *region* will refer to four specific groups of these sampling sites that are identified statistically, as described below and in Table 4.2.

DNA Extraction and Sequencing

In preparation for DNA isolation, tissue was removed from storage solution, submerged in digest buffer (100 mM NaCl, 10 mM Tris-Cl pH 8.0, 25 mM EDTA pH 8.0, 0.5 % SDS, 0.1 mgml−1 Proteinase K, and 1 μgml−1 RNaseA) and was heated to 42°C for 1 hour. DNA was then isolated following a standard phenol-chloroform extraction protocol (Davies, Rahman, et al., 2013). A panel of nine microsatellite loci was amplified using 10 μL multiplex polymerase chain reactions following Davies, Rahman, et al. (2013). PCR products were visualized on agarose gels to verify amplification, and molecular weights were assessed using an ABI 3130XL capillary sequencer with an ROX-labeled size standard. Alleles were scored and genotypes were assigned based on amplicon size using GeneMarker 1.70. If loci amplifications of an individual failed within multiplex reactions, additional PCRs were attempted to assemble the most complete dataset possible.

Statistical Analysis

Before further analysis, the probability of identity (P_{ID}), or the probability that two independently sampled individuals within a population share an identical multilocus genotype by chance, was calculated using GenAlEx v6.502 (Peakall & Smouse, 2006) and was found to be ≤2.6E–08 for all populations. Hence, any identical genotypes found in the dataset were presumed to be clones and were removed (n = 39). Clone mates were only found within the same geographic site. Additionally, samples with data missing for more than three loci were removed, leaving 369 unique genets for downstream analysis.

FSTAT v2.9.3 (Goudet, 1995, 2001) was used to calculate allelic richness and to test for linkage disequilibrium (LD) between all pairs of loci in each sampled population (7200 permutations). Allelic richness is a particularly robust measure of gene diversity, as it incorporates a rarefaction procedure to standardize estimates to the smallest common sample size (n = 11). Genepop v4.5.1 (Raymond & Rousset, 1995; Rousset, 2008) was used to calculate observed and expected proportions of heterozygotes and to perform single-locus tests of conformity to Hardy-Weinberg (HW) equilibrium using Fishers' exact test based on Markov chain iterations (10,000 dememorization steps, 500 batches of 10,000 iterations). To address deviations from HW proportions, the frequency of null alleles was estimated in FreeNA (Chapuis & Estoup, 2007) using the EM algorithm of Dempster, Laird, and Rubin (1977). Additionally, to determine whether populations differ significantly in allelic richness and heterozygosity, a randomized block ANOVA and Tukey's honest significant difference (HSD) test were performed in R using the sampling sites as treatment levels and locus as a covariate.

Global F_{ST} was calculated in FSTAT v2.9.3 with 95% confidence intervals constructed by bootstrapping over all loci. To investigate the hierarchical partitioning of diversity within and

among sampling sites and regions, an analysis of molecular variance (AMOVA) procedure was implemented in GenAlEx v6.502 using an infinite allele model and 9999 random permutations. The demarcation of four discrete regions across the sampling range was guided by the apparent clustering of populations based on pairwise estimates of differentiation, which were also calculated via AMOVA. Pairwise F_{ST} was calculated to enable comparisons to past research; however, Hedrick's G''_{ST} statistic is also reported, as it incorporates standardized estimates for total and within-population expected heterozygosity developed by Nei and Chesser (1983) in order to correct for small sample sizes, as well as an adjustment when a small number of populations are sampled (Meirmans & Hedrick, 2011). Thus, while the overall patterns remain largely unchanged between the two estimates, given the sampling scheme in this study, pairwise G''_{ST} values more accurately represent genetic differentiation and were therefore used to visualize population structure via Principal Coordinates Analysis (PCoA) and to test for the presence of isolation by distance. Both estimates were calculated using GenAlEx v6.502.

Isolation by distance was assessed by calculating the correlation between $G''_{ST}/(1 - G''_{ST})$ and the natural logarithm of over-water distance using a Mantel test in R (9999 permutations), as recommended by Rousset (1997). Over-water distance was approximated in Google Earth as the shortest path between two sites without crossing land.

A Bayesian model-based clustering method was used to infer the number of genetically distinct populations and assign individuals proportionally to inferred populations. This analysis was implemented in STRUCTURE v2.3.4 (Falush, Stephens, & Pritchard, 2003, 2007; Pritchard, Stephens, & Donnelly, 2000). Ten independent replicate runs were performed for each K from 1 to 10 using a burn-in period of 300,000 followed by 1,000,000 MCMC repetitions, where K represents the number of genetic populations. Mean membership coefficients (q) are calculated

for each individual, which describe the likelihood that an individual belongs to each of the inferred populations. The clustering algorithm was assisted using the 10 sampling sites as a prior (Hubisz, Falush, Stephens, & Pritchard, 2009) and allele frequencies were assumed to be correlated between populations. The most likely number of genetic clusters was then determined using the *ad hoc* statistic ΔK based on the posterior probability of the data following the methods of Evanno, Regnaut, and Goudet (2005), as implemented in STRUCTURE Harvester (Earl & vonHoldt, 2012). Simulation results were compiled in CLUMPP v1.1.2 (Jakobsson & Rosenberg, 2007) and visualized using distruct v1.1 (Rosenberg, 2004).

Lastly, Simpson's index (E) was calculated for each sampling site to describe qualitatively the evenness of representation from each of the inferred genetic clusters:

$$E = \frac{D}{D_{max}} = \frac{1/\sum_{i=1}^{n} p_i^2}{n}$$

where D represents Simpson's diversity index, p_i represents the mean probability of assignment to each inferred cluster (1-5), and n is the total number of clusters. This index ranges from $1/D_{max}$ (in this case, 0.20) to 1, which would indicate an equal proportion of all clusters.

Results

Genetic Diversity

Genetic diversity as measured by expected heterozygosity and mean allelic richness was moderately high in all populations, with values ranging from 0.582-0.694 and 5.433-6.940, respectively (Table 4.1). Allelic richness was greatest in Belize and the Flower Garden Banks (FGB) and lowest in Mexico, although none of the differences between populations were statistically significant (randomized block ANOVA, $P = 0.113$). Similarly, while ANOVA results provide evidence that heterozygosity may differ between populations (randomized block

ANOVA, $P = 0.025$), the more statistically stringent Tukey's HSD test revealed no significant pairwise differences between populations. Thus, there is not sufficient evidence to conclude that heterozygosity in any population was greater or less than that of any other.

Twenty-two of 90 locus-by-population tests revealed evidence of heterozygote deficiency after sequential Bonferroni correction, of which 18 were associated with four particular microsatellite loci: Mfav5_CGA, Mfav4_TTTG, Mfav6_CA, and Mfav8_CAA (Table S4.1). This pattern of locus-specific heterozygote deficiency is often interpreted as a symptom of null alleles and in many studies has been used as grounds for removing affected loci from analysis. However, we find the frequency and influence of null alleles in our dataset to be low and insignificant (max $\hat{r} = 0.22$; Table S4.2), suggesting that the observed heterozygote deficit may instead reflect underlying biological patterns. Hence, all loci were retained for subsequent analysis. Refer to the Supplemental Information for greater detail regarding our treatment and assessment of null alleles for this dataset.

Significant linkage disequilibrium (LD) was observed in ~10% (33 of 360) of locus pair comparisons after sequential Bonferroni adjustment. No locus pairs were significantly associated across more than three sampling sites, suggesting that the observed disequilibrium is likely not a result of physical linkage of the markers (Table S4.3). Interestingly, 31 of the 33 significant tests of association occurred in samples from Florida, Mexico and Curaçao, which also accounted for ~82% (32 of 39) of the clonal individuals removed from the dataset prior to analysis (Table S4.4).

Population Structure via F-statistics

Global F_{ST} was low but significantly different from zero (F_{ST} = 0.038; 95% confidence interval: 0.024 to 0.061). Pairwise F_{ST} and G''_{ST} estimates between localities ranged from 0.009 to 0.065 and 0.013 to 0.290, respectively (Figure 4.1B, Table S4.5). Only 7 of 17 comparisons involving the Bahamas or US Virgin Islands were statistically significant after sequential Bonferroni correction, likely due to the small sample sizes from these sites (n=11 at each location); however, all other comparisons except Panama-FGB were significant.

A principal coordinates analysis based on pairwise G''_{ST} values reveals four distinct clusters segregated along Principal Coordinate (PC) 1, which explains 62.59% of the variation in these data (Figure 4.2). Most notably, the population in Carrie Bow Cay, Belize was distantly isolated from all other populations and was most highly differentiated from its closest geographic neighbor in Puerto Morelos, Mexico. The US Virgin Islands, Puerto Rico, Curaçao and Mexico group along PC1, but diverge considerably along PC2, which explains 22.75% of variation. The remaining groupings are composed of the Bahamas, Florida and the Flower Garden Banks, and Barbados and Panama, respectively. An AMOVA detected low, but significant differentiation between these four regions and among populations within these regions, explaining 1.83% and 2.91% of the total variance in allelic frequencies, respectively ($P < 0.001$; Table 4.2).

Overall, we found no evidence that genetic differentiation between sites ($G''_{ST}/1 - G''_{ST}$) was correlated with pairwise over-water distance (Mantel's r = 0.0563, $P = 0.3493$; Figure 4.3). However, if we remove Belize from analysis as an outlier based on observed genetic isolation, a positive trend emerges that approaches significance at the $\alpha = 0.05$ level (Mantel's r = 0.2705, $P = 0.0604$; Figure 4.3). This suggests that geographic distance is not the principal structuring

force across the study range, but may be a weak, underlying mechanism of genetic isolation existing within a complex system of oceanographic and biological factors.

Population Structure via Clustering Analysis

Based on the *ad hoc* statistic ΔK (Evanno *et al.* 2005), the optimal solution for STRUCTURE analysis exhibited five distinct genetic clusters throughout the sampling range (Brown, Tan, Light Blue, Teal, Dark Blue colors in Figure 4.4; Figure S4.2). All except the Dark Blue cluster were dominant (>50%) in at least one of the sampling sites; however, only three of the 10 populations (Belize, Mexico and Puerto Rico) could be assigned unambiguously to one cluster. Rather, the inferred pattern of population structure reflected considerable mixing across the seascape consistent with the low global F_{ST} observed. The FGB, in particular, exhibited a markedly even distribution of individuals assigning to each of the five genetic clusters. Of the 10 sampling sites, Simpson's evenness was highest in the FGB (E = 0.746) and lowest in Mexico, Belize and Puerto Rico (E = 0.312, 0.338 and 0.343, respectively). All other populations exhibited intermediate values within this range (Table 4.1).

Basin-wide patterns of genetic differentiation based on STRUCTURE results generally mirrored those revealed by pairwise estimates of F_{ST} and G''_{ST}. Specifically, three main observations were revealed:

(1) The Brown cluster occurred predominantly and almost exclusively in the eastern Caribbean populations, with the exception of Barbados.

(2) The FGB and Florida Keys populations seemed to reflect a similar mixture of individuals of the Tan, Light Blue and Teal clusters. In particular, the Light Blue cluster was restricted primarily to these two populations.

(3) Despite a physical separation of only 470 km, populations from Belize and Mexico shared virtually no similarity in their clustering assignments. Each was >75% associated with the Teal (Belize) and Tan (Mexico) cluster with <3% of each population associating with the dominant cluster of the other population, highlighting the structure across these two populations.

Discussion

East-West Genetic Barrier

Overall, our results illustrate that populations of *Orbicella faveolata* are relatively well mixed across the wider Caribbean (F_{ST} = 0.038), although within this broad setting, we find complex patterns of substructure arising at both local and regional scales. Our analysis indicates that eastern populations diverge considerably from populations to the west, which reflects patterns of connectivity previously described for *Acropora palmata* (Baums et al., 2005; Baums et al., 2006), *Acropora cervicornis* (Galindo, Olson, & Palumbi, 2006) and *Orbicella* (previously: *Montastraea*) *annularis* (Foster et al., 2012). Notably, this finding contrasts with that of Severance and Karl (2006), who found significant divergence between populations of *O. annularis* in Puerto Rico, Mexico and Florida, but not between populations of *O. faveolata*.

Moreover, our clustering results reveal a significant level of gene flow between Curaçao and Mexico, suggesting that the southern extent of this genetic break may be more pervious to dispersal than previously acknowledged (Baums et al., 2006; Foster et al., 2012). Oceanographic models demonstrate that westward larval dispersal from Puerto Rico in the north is physically impeded by complex oceanographic patterns associated with the Mona Passage (Baums et al., 2006; Cowen, Paris, & Srinivasan, 2006), but the mechanisms that would constitute a barrier at

the southern extent of the basin are not as clear. Throughout the seascape, surface transport is dominated by the strong flow of the Caribbean Current, which enters the basin through the southern Lesser Antilles in the east and travels west-northwest towards the Yucatan Peninsula (Alvera-Azcárate, Barth, & Weisberg, 2009; P. Richardson, 2005). The swiftest portion of this current creates a nearly direct corridor along the Venezuelan coast that passes near Curaçao en route to Mexico, reaching mean velocities of 80-120 cm/s (P. Richardson, 2005). With larval competency lasting up to 30 days, as has been shown for *O. faveolata* (Szmant & Miller, 2006), these current speeds are more than sufficient to maintain significant connectivity between Curaçao and Mexico, particularly on the evolutionary timescale addressed by F_{ST} and STRUCTURE analyses.

We also find that Barbados does not conform to a simple east-west dichotomy. Rather, it exhibits greater genetic similarity to populations in the western Caribbean than to nearby localities in the east. A similar pattern of local segregation has been seen previously in soft corals (Andras, Rypien, & Harvell, 2013) and reef fish (Paris & Cowen, 2004) and has been attributed primarily to the local flow environment. Larvae of the bicolor damselfish, *Stegastes partitus*, exhibit unusually high retention rates around Barbados due to their ability to migrate vertically within the water column and take advantage of a persistent onshore current at depth (Cowen & Castro, 1994; Paris & Cowen, 2004; Paris, Cowen, Lwiza, Wang, & Olson, 2002). While the poor swimming proficiency of most marine invertebrate larvae likely limits their ability to actively adjust their position in the water column to the same extent as reef fish, we suggest that a similar oceanographic mechanism may be at work to locally retain larvae of *O. faveolata* in Barbados. Yet, while this may help explain the observed genetic isolation from nearby localities in the eastern Caribbean, the apparent connectivity between Barbados and western sites such as

Panama, Belize and the FGB, suggests that the processes governing larval dispersal from Barbados are complex and likely function at multiple spatial and temporal scales.

Evidence of Larval Retention in Southern Mesoamerican Barrier Reef

Perhaps our most striking finding is the relatively strong population differentiation between Carrie Bow Cay, Belize and Puerto Morelos, Mexico (F_{ST} = 0.063), two sites within the Mesoamerican Barrier Reef System (MBRS) separated by only 470 km. With the use of five microsatellites, Porto-Hannes et al. (2015) did not detect significant differentiation between *O. faveolata* populations near these two sites. However, we were able to distinguish significant structure at this small spatial scale, likely due to the additional four microsatellite markers utilized.

We hypothesize that certain features of the prevailing oceanographic patterns in this area may underlie the strong local differentiation observed here as well as the overall genetic isolation of the Belize population from the rest of the wider Caribbean. Notably, the MBRS is characterized by two divergent flow regimes originating where the Caribbean Current encounters the Yucatan Peninsula (Tang, Sheng, Hatcher, & Sale, 2006). To the north, the Caribbean Current veers into the Yucatan Channel maintaining high northward current velocities as it travels into the Gulf of Mexico. Contrastingly, the southern extent of the MBRS is characterized by the preponderance of sub-mesoscale eddies (~10-100 km), which are shed from the Caribbean Current and comprise a persistent cyclonic gyre covering much of the Gulf of Honduras (Carrillo, Johns, Smith, Lamkin, & Largier, 2015; Lindo-Atichati, Curcic, Paris, & Buston, 2016; Paris, Chérubin, & Cowen, 2007; Tang et al., 2006). Using a nested grid ocean circulation model, Tang et al. (2006) illustrate that during the month of August, when *O. faveolata* are

known to spawn, this recirculation cell severely constrains the dispersal of simulated larvae released from Glovers Reef Atoll (just offshore from Carrie Bow Cay) to inshore regions of the southern Belize shelf. This provides compelling support for a genetic break between Carrie Bow Cay and Puerto Morelos. However, further research is needed to determine whether such a barrier to dispersal could persist over the timescale required to generate the level of population divergence observed here.

Downstream Populations as Genetic Sinks

A strong signal of connectivity between populations in Mexico, the Florida Keys and the Bahamas is consistent with previous findings of virtually no genetic structure across this range in *A. palmata* (Baums et al., 2005) and *O. faveolata* (Severance & Karl, 2006). Interestingly, Severance and Karl (2006) find that this pattern contrasts with that of *O. annularis*, a sister species within the *Orbicella* complex, which exhibits significant population divergence across the same range (*Rho* = 0.02-0.23). The authors propose that such a stark difference between two closely related taxa may have arisen through the accumulation of chance differences in recruitment success across years. Additionally, such contrasting patterns could result from genetic introgression or the unintended inclusion of sibling species in their analysis. To be sure, future work is needed to elucidate these species-specific dynamics.

A particularly unique aspect of the present study is the incorporation of the FGB in our analysis of Caribbean-wide population genetics. Located in the northwestern reaches of the Gulf of Mexico, the FGB is distantly separated from other reefs in the basin and is only occasionally accessible to dispersing larvae via northbound eddies shed from the Loop Current (Lugo-Fernández, Deslarzes, Price, Boland, & Morin, 2001). Yet, despite its remote location, we find

that its genetic signature represents a nearly even mixture of genets originating from populations across the whole Caribbean basin, a pattern that can be characteristic of a genetic sink (Andras et al., 2013). Additionally, very low population differentiation between FGB and the Florida Keys (F_{ST} = 0.009) suggests relatively strong connectivity between these two sites. The net direction of larval transport between the sites remains unknown; however, a recently developed biophysical model demonstrates a mechanism by which larvae of *O. franksi* are able to disperse from FGB to reefs in the Florida Keys and Bahamas (Davies et al., 2017). Thus, while the FGB may be interpreted as a possible genetic sink relative to populations across the Caribbean basin, it may also provide some larval subsidy to reef areas that are downstream of the prevailing Loop and Caribbean Currents. It is worth pointing out that the reefs of the FGB remain among the healthiest in the wider Caribbean (Aronson, Precht, Murdoch, & Robbart, 2005; Zimmer et al., 2010) and stand in stark contrast to the deteriorating reefs of the Florida Keys (Ruzicka et al., 2010). Significant gene flow between these two populations may become crucial to the long-term recovery of the Florida Keys Reef Tract.

Heterozygote Deficiency Putatively due to Introgressive Hybridization

The discovery of locus-specific heterozygote deficiency in our dataset is not uncommon among studies of marine populations and is most often attributed to some combination of the following factors: the occurrence of null alleles, the Wahlund effect, inbreeding, and/or selection against heterozygotes (sexual or otherwise) (Allendorf, Luikart, & Aitken, 2013). The observed deficiency cannot be attributed exclusively to any one factor with certainty; however, several can be ruled out for this study. For instance, we show that the estimated frequency of null alleles within this dataset is relatively low and that their effect on patterns of population differentiation

is negligible. Additionally, the Wahlund effect describes the reduction in heterozygosity that is observed when multiple genetically differentiated populations are inadvertently collected as one sample (Dharmarajan, Beatty, & Rhodes, 2013; Wahlund, 1928). This is expected to occur when there are a number of highly differentiated populations; yet, given the overall genetic similarity of the individuals in this study (F_{ST} = 0.038), a significant Wahlund effect is relatively unlikely. Furthermore, while it is possible that inbreeding may play a role, it would be expected to affect all loci relatively equally (Gaffney, Scott, Koehn, & Diehl, 1990; Slate et al., 2004; Waples, 2014), which is not seen in the sampled populations studied here.

Rather, in this case, we hypothesize that the observed disagreement with Hardy-Weinberg expectations is most likely due to genetic introgression and/or the inadvertent sampling of sibling species within the *Orbicella* complex. All but one of the microsatellite markers used in this study (Mfav8_CAA) have been shown to amplify in other *Orbicella* species with ≥80% success (Davies, Rahman, et al., 2013; Severance et al., 2004). Additionally, the three *Orbicella* species occur in sympatry throughout their range with overlapping distributions across depth and have shown a capacity for interspecific hybridization, particularly near the northern extent of their distribution (Budd & Pandolfi, 2004; Fukami et al., 2004; Knowlton, Mate, Guzman, Rowan, & Jara, 1997; Szmant, Weil, Miller, & Colon, 1997). Thus, while great care was taken to identify and sample colonies of *O. faveolata*, it can be quite difficult in some locations to visually distinguish this species from its close relatives in the *Orbicella* complex and especially from hybridized "intermediate" morphologies, as has been documented in the Florida Keys and Bahamas (Budd & Pandolfi, 2004; Fukami et al., 2004; Manica & Carter, 2000; Szmant et al., 1997). A deficit in heterozygotes will arise when two differentiated populations (or in this case, species) interbreed to some extent, but mate preferentially and with greater success

within their own population (Roques, Sévigny, & Bernatchez, 2001). This has been shown to occur within the *Orbicella* species complex, whereby interspecific fertilization was achieved in experimental crosses between *O. faveolata* and its sibling species, but at rates significantly lower than what is observed between conspecifics (Szmant et al., 1997).

Introgressive hybridization may also account for the significant tests of linkage disequilibrium, which are seen predominantly in Florida, Mexico and Curaçao, through the introduction of foreign alleles into the sampled gene pools. Even without strong linkage between alleles within their parent population, the joint introduction of novel alleles into a hybrid would imitate linkage to an observer. It is important to note that the association between loosely linked loci would decay rapidly at a rate equal to the recombination rate, and therefore must be a result of hybridization within the last few generations (Goodman, Barton, Swanson, Abernethy, & Pemberton, 1999). However, it is possible that this signal of linkage disequilibrium would persist through time if F_1 and F_2 hybrids are less fit than the parental types, either in viability or fecundity. Such a scenario, described by Barton and Hewitt (1985) as the Tension Zone model, would maintain a stable, but marginal population of first- or second-generation hybrids.

Interestingly, the same populations with the highest observed linkage disequilibrium (Florida Keys, Mexico and Curaçao) also account for the large majority of (~82%) of clonal individuals removed from the dataset prior to analysis. The uneven distribution of these patterns may reflect underlying ecological circumstances at these locations. However, to confirm the true extent and dynamics of hybridization and a possible association with asexual reproduction, a more comprehensive investigation of allele frequencies within these populations that includes all possible parental genotypes is required.

Conclusion

The results of this study advance the current understanding of population connectivity throughout the wider Caribbean and offer insight into local and regional patterns of genetic structure for the important reef-building coral *O. faveolata*. Within the context of strong overall connectivity across the seascape, we find further support for a genetic break between eastern and western populations as has been observed for other coral species. We discover evidence for strong differentiation between neighboring populations within the MBRS and also find evidence that the FGB may function as a genetic sink for the Caribbean basin.

From a management perspective, it is essential to bear in mind that the findings and interpretations presented here describe patterns of population connectivity that have arisen over an evolutionary timescale (thousands of generations). Accordingly, we can use these data to infer the extent to which genetic material is shared between populations, which can have important implications for overall genetic variation and potential for adaptation. However, estimates of genetic divergence alone provide little information on demographic connectivity, that is, whether or not the per generation rate of migration between populations is large enough to significantly affect population growth. Understanding both the genetic and demographic connectivity among populations is critical to the management of *O. faveolata*, and we therefore encourage the use of the genetic patterns discussed here to inform future investigations into the magnitude of larval dispersal throughout the wider Caribbean seascape.

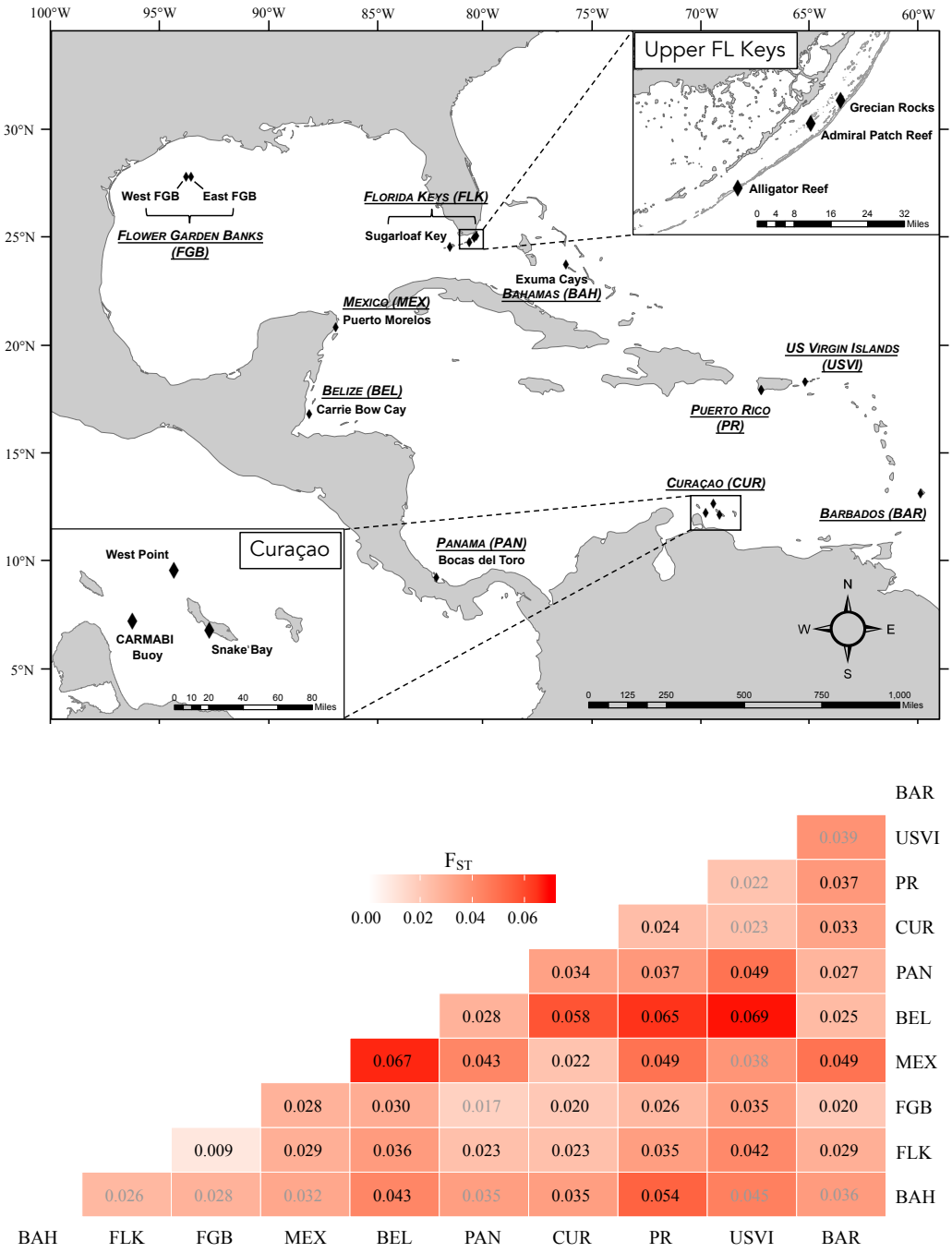

Figure 4.1. (A) Map of sampling sites. Individuals from neighboring reefs within each sampling site were grouped as single populations for all analyses performed. **(B) Heat map of pairwise F_{ST} estimates between all sampling sites**. Darker shades of red correspond to higher estimates of population differentiation via pairwise F_{ST}. All bolded values are significant at the $\alpha = 0.05$ level following sequential Bonferroni correction. Site abbreviations are as in Table 4.1 and are organized along the axes by relative geographic location in the basin.

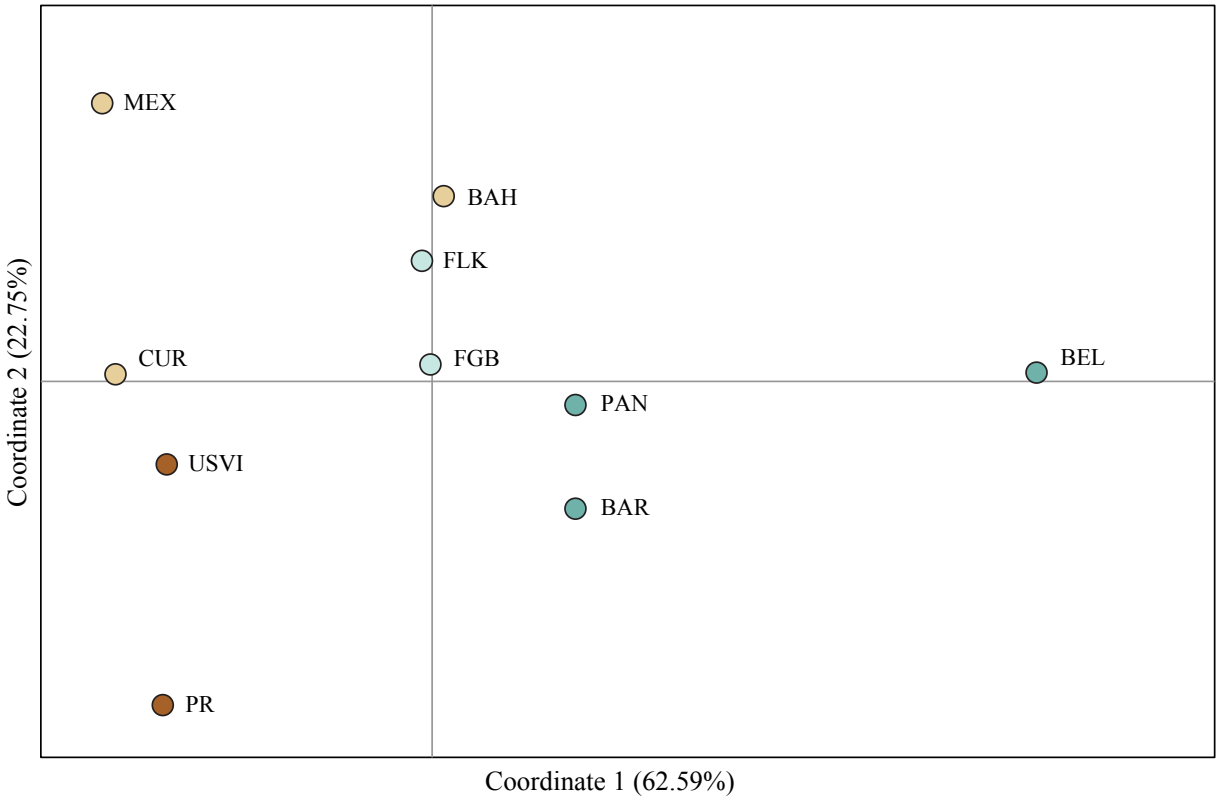

Figure 4.2. Principal Coordinates Analysis (PCoA) via pairwise estimates of G''_{ST}. The distance separating points in ordinate space along each axis corresponds to genetic divergence as estimated via pairwise G''_{ST}. Percentages indicate the proportion of variation in the data explained by each axis. Marker colors denote the dominant genetic cluster within each population as inferred by STRUCTURE analysis. Site abbreviations are as in Table 4.1.

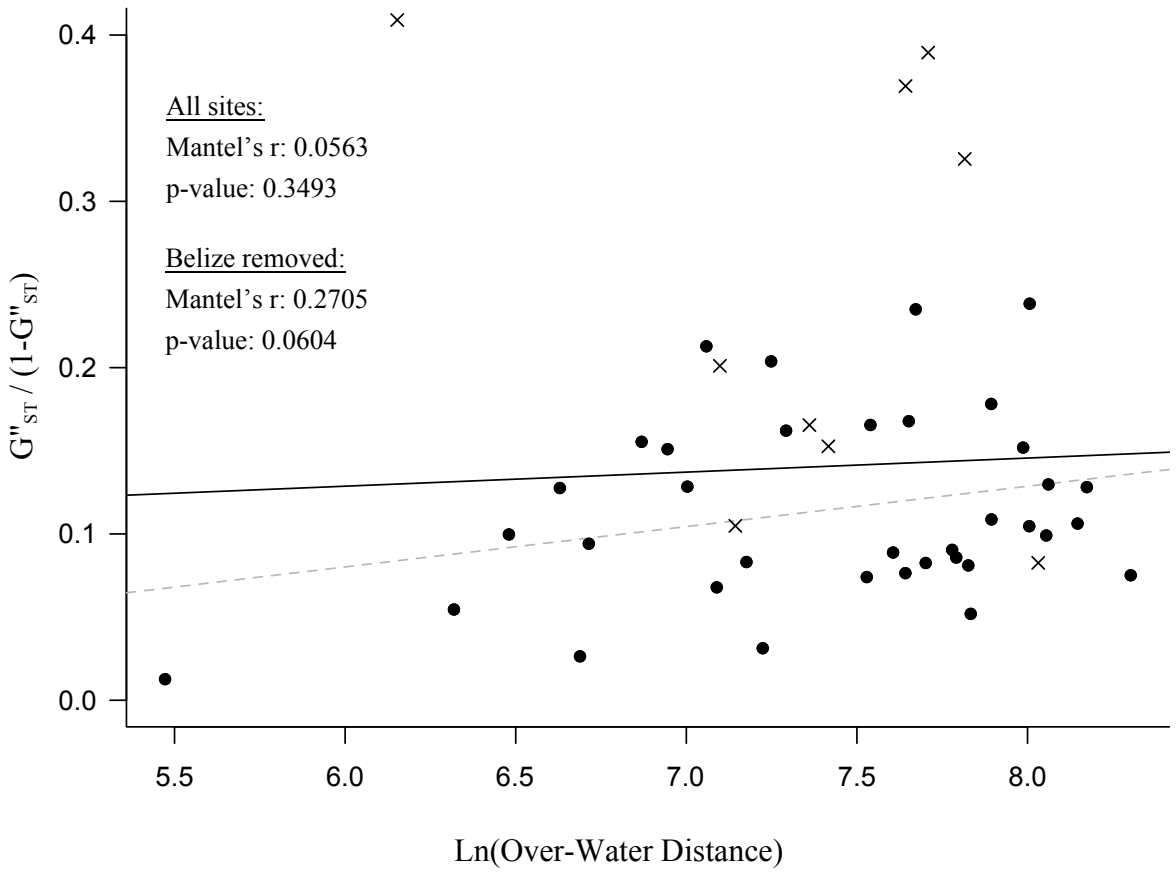

Figure 4.3. Isolation by distance observed for *O. faveolata*. Pairwise genetic differentiation $[G''_{ST}/(1 - G''_{ST})]$ as a function of the natural logarithm of over-water distance between populations. Correlations are plotted for pairwise estimates between all populations (solid line) and excluding Belize (dashed line). × indicates a pairwise estimate involving Belize.

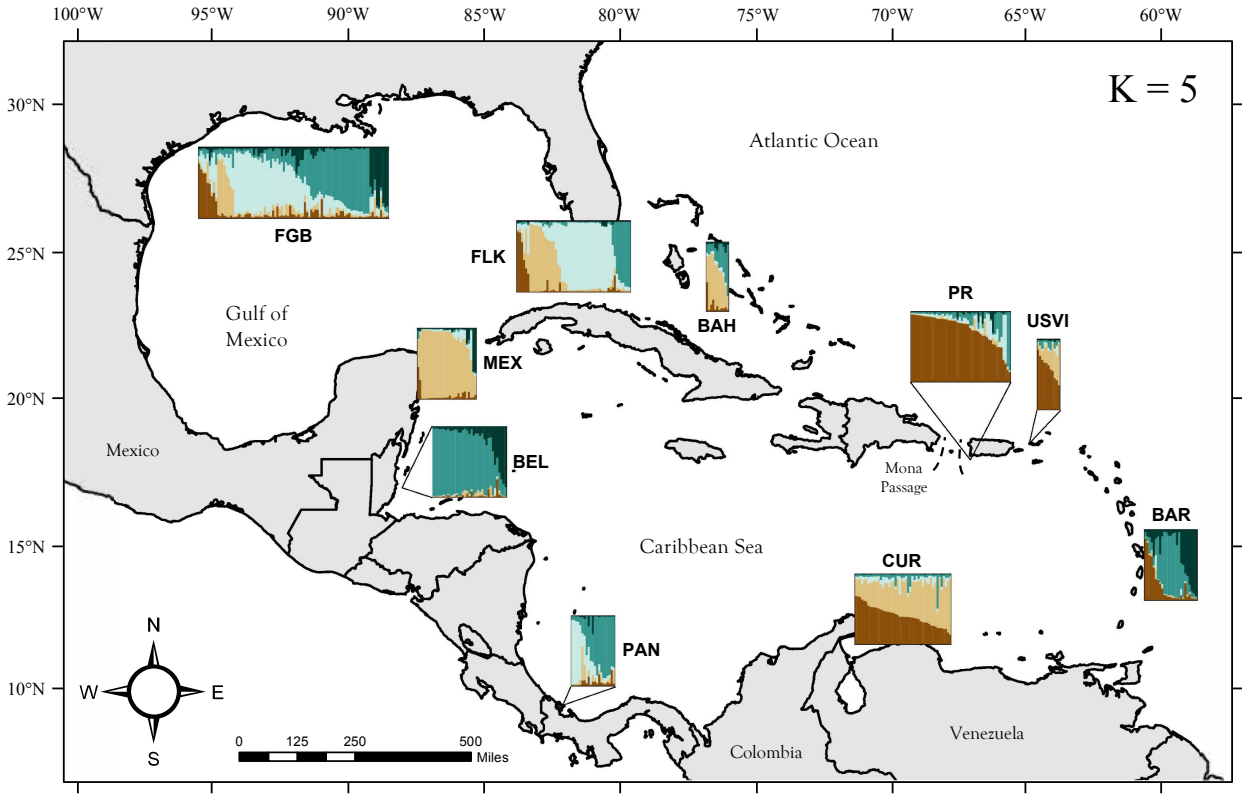

Figure 4.4. STRUCTURE population assignments for *O. faveolata* across the wider Caribbean region. Thin vertical columns in each population block represent individual samples and their associated probability of assignment to K = 5 color-coded genetic clusters (Brown, Tan, Light Blue, Teal, and Dark Blue). Individual columns are of uniform width; thus, the size of population blocks is proportional to the number of samples representing each population. Site abbreviations are as in Table 4.1.

Sampling Site	Reef Locations	Lat	Long	N	N_A	N_{PA}	AR	H_O	H_E	*E*
Bahamas **(BAH)**	*Exuma Cays*	23.783	-76.118	11 (1)	6.67	0	6.380	0.505	0.633	0.532
Barbados **(BAR)**		13.100	-59.634	25 (1)	9.00	0.78	6.623	0.419	0.665	0.598
Belize **(BEL)**	*Carrie Bow Cay*	16.802	-88.077	35 (1)	11.56	1.56	6.940	0.491	0.660	0.338
Curacao **(CUR)**	*Snake Bay*	12.125	-68.973	46 (8)	10.33	0.78	6.175	0.551	0.647	0.518
	West Point	12.637	-69.270							
	CARMABI Buoy	12.210	-69.619							
Flower Garden Banks **(FGB)**	*East*	27.900	-93.583	90 (1)	14.00	1.89	6.932	0.486	0.694	0.746
	West	27.883	-93.817							
Florida Keys **(FLK)**	*Alligator Reef*	24.842	-80.624	54 (13)	10.56	1.22	6.390	0.538	0.689	0.568
	Grecian Rocks	25.119	-80.302							
	Admiral Patch	25.045	-80.395							
	Sugarloaf Key	24.591	-81.536							
Mexico **(MEX)**	*Puerto Morelos*	20.877	-86.858	28 (11)	7.67	0.22	5.433	0.476	0.620	0.312
Panama **(PAN)**	*Bocas del Toro*	9.200	-82.150	21 (1)	8.89	0.33	6.636	0.582	0.687	0.531
Puerto Rico **(PR)**	*Media Luna*	17.935	-67.034	48 (1)	9.22	0.44	5.943	0.392	0.608	0.343
	Turromote	17.935	-67.019							
US Virgin Islands **(USVI)**	*Flat Cay West*	18.318	-64.991	11 (1)	6.22	0.22	6.008	0.461	0.582	0.447
	Botany Bay	18.358	-65.033							

Table 4.1. Sampling sites and estimates of genetic diversity. *N*: number of unique multilocus genets (number of clonal individuals listed in parentheses), N_A: number of alleles, N_{PA}: number of private alleles, *AR*: allelic richness, calculated as the population mean of locus-specific allelic richness, H_O: observed heterozygosity, H_E: expected heterozygosity, *E*: Simpson's evenness index.

Model	Source of Variation	d.f.	Sum of squares	Variance components	Variation (%)	Fixation indices
4 regions	Among regions	3	60.122	0.058	1.83	$F_{CT} = 0.018$*
(PCoA-derived)	Among sampling sites within regions	6	55.196	0.093	2.91	$F_{SC} = 0.030$*
	Among individuals within sampling sites	728	2214.052	3.041	95.26	$F_{ST} = 0.047$*
	Total	737	2329.37	3.193	100	
10 sampling sites	Among sampling sites	9	115.318	0.138	4.35	
	Among individuals within sampling sites	728	2214.052	3.041	95.65	$F_{ST} = 0.043$*
	Total	737	2329.37	3.179	100	

Table 4.2. Analysis of molecular variance (AMOVA) among and within sampling sites and regions. The four regions identified by principal coordinate analysis include: (1) PR, USVI, CUR, and MEX, (2) FGB, FLK, and BAH, (3) BAR and PAN, and (4) BEL. Fixation indices denote the variation among regions (F_{CT}), among sampling sites within each region (F_{SC}) and among individuals within sampling sites (F_{ST}). An * denotes significance at the $\alpha = 0.05$ level based on 9999 random permutations.

APPENDIX 1: SUPPLEMENTAL DESCRIPTIONS AND FIGURES – CHAPTER 2

Model selection diagnostics – Linear mixed effects

Before fitting all models, the variable *Year* is centered on a value at which the random slopes and intercepts are least correlated. In general, centering enhances model interpretability and improves numerical stability by making it more likely that the optimization algorithm converges to the correct solution. The estimate of the slope is unchanged by centering, but the intercept now estimates the mean value of the response variable at the centering constant, rather than year 0 in the un-centered model.

(1) Extension

```
M1: lm(ext ~ 1)
M2: lme(ext ~ 1, random=~1|Core)
M3: lm(ext ~ I(Year-2000))
M4: lme(ext ~ I(Year-2000), random=~1|Core)
M5: lme(ext ~ I(Year-2000), random=~I(Year-2000)|Core)
```

	Model	AIC
M1:	Ordinary Regression:Intercept	-1194.910
M2:	Random Intercepts:Intercept	-1192.910
M3:	Ordinary Regression:Year	-1194.401
M4:	Random Intercepts:Year	-1192.401
M5:	**Random Slopes and Intercepts**	**-1324.014**

Having determined that the random slopes and random intercepts model best explains the data, we then interrogate the model further including *reefZone* as a fixed effect.

```
M6: lme(ext ~ I(Year-2000) + reefZone, random=~I(Year-2000)|Core))
M7: lme(ext ~ I(Year-2000) + reefZone:I(Year-2000), random=~I(Year-
     2000)|Core))
M8: lme(ext ~ I(Year-2000) + reefZone + reefZone:I(Year-2000),
     random=~I(Year-2000)|Core))
```

	Model	AIC
M5:	**Common slope and intercept (no reef zone)**	**-1324.014**
M6:	Intercepts vary by reef zone	-1322.006
M7:	Slopes vary by reef zone	-1322.269
M8:	Intercepts and slopes vary by reef zone	-1320.732

Comparison of AIC scores again suggests that a simple model with random variation around a common slope and intercept (without reef zone included as a predictor) provides the best fit to the data; although, differences between AIC scores is marginal. Thus, we find no evidence from this procedure that long-term trends in skeletal extension differ between inner and outer reef coral colonies. We reach the same conclusion for density and calcification trends based on the model results below.

(2) Density

```
M1: lm(ext ~ 1)
M2: lme(ext ~ 1, random=~1|Core)
```

```
M3: lm(ext ~ I(Year-2002))
M4: lme(ext ~ I(Year-2002), random=~1|Core)
M5: lme(ext ~ I(Year-2002), random=~I(Year-2002)|Core)
M6: lme(ext ~ I(Year-2002) + reefZone, random=~I(Year-2000)|Core))
M7: lme(ext ~ I(Year-2002) + reefZone:I(Year-2002), random=~I(Year-
     2002)|Core))
M8: lme(ext ~ I(Year-2002) + reefZone + reefZone:I(Year-2002),
     random=~I(Year-2002)|Core))
```

Model	AIC
M1: Ordinary Regression:Intercept	-7343.141
M2: Random Intercepts:Intercept	-7341.141
M3: Ordinary Regression:Year	-7434.535
M4: Random Intercepts:Year	-7432.535
M5: Random Slopes and Intercepts (no reef zone)	**-8131.934**
M6: Intercepts vary by reef zone	-8131.278
M7: Slopes vary by reef zone	-8129.950
M8: Intercepts and slopes vary by reef zone	-8130.048

(2) Calcification

```
M1: lm(ext ~ 1)
M2: lme(ext ~ 1, random=~1|Core)
M3: lm(ext ~ I(Year-2002))
M4: lme(ext ~ I(Year-2002), random=~1|Core)
M5: lme(ext ~ I(Year-2002), random=~I(Year-2002)|Core)
M6: lme(ext ~ I(Year-2002) + reefZone, random=~I(Year-2000)|Core))
M7: lme(ext ~ I(Year-2002) + reefZone:I(Year-2002), random=~I(Year-
     2002)|Core))
M8: lme(ext ~ I(Year-2002) + reefZone + reefZone:I(Year-2002),
     random=~I(Year-2002)|Core))
```

Model	AIC
M1: Ordinary Regression:Intercept	-1279.258
M2: Random Intercepts:Intercept	-1277.258
M3: Ordinary Regression:Year	-1286.741
M4: Random Intercepts:Year	-1284.741
M5: Random Slopes and Intercepts (no reef zone)	**-1394.983**
M6: Intercepts vary by reef zone	-1393.202
M7: Slopes vary by reef zone	-1393.272
M8: Intercepts and slopes vary by reef zone	-1393.990

Lastly, in order to generate the final model results presented in Figure 2.2A, a set of level-1 correlation structures was considered to account for autocorrelation between annual growth measurements within each individual core. These correlation structures include all possible combinations of an autoregressive-moving average model (ARMA) of order (*p*,*q*), with each component (AR and MA) ranging from 0 to 2.

For the purposes of trend comparison and visualization in Figure 2.2A, this procedure was performed on the model including *reefZone* as a predictor of slope (Model 7 above). Results of model comparisons are below. Note, for all growth parameters, models including a correlation structure vastly out-performed the model including only random slopes and intercepts.

(1) Extension

Correlation structure	AIC
AR(1)	-1703.671
AR(2)	-1788.767
ARMA(1,1)	-1817.484
ARMA(1,2)	-1814.032
ARMA(2,1)	**-1819.445**
MA(1)	-1565.454
MA(2)	-1701.003
ARMA(2,2)	-1818.906
none	-1322.269

(2) Density

Correlation structure	AIC
AR(1)	-11623.33
AR(2)	-11687.24
ARMA(1,1)	**-11689.67**
ARMA(1,2)	-11687.69
ARMA(2,1)	-11687.69
MA(1)	-10038.80
MA(2)	-10967.08
ARMA(2,2)	-11689.26
none	-8129.95

(3) Calcification

Correlation structure	AIC
AR(1)	-1748.765
AR(2)	-1827.532
ARMA(1,1)	**-1850.351**
ARMA(1,2)	-1846.738
ARMA(2,1)	-1849.136
MA(1)	-1628.170
MA(2)	-1749.438
ARMA(2,2)	-1848.075
none	-1393.272

For reference, below are the AIC scores for all candidate models including *Reef Zone*, *Transect* (i.e., inner-outer reef site pairs), and *Site* as fixed effect variables. With respect to model comparison, low ΔAIC scores for top models suggest that inclusion of grouping variables does not significantly improve model fit for any of the three growth parameters (Burnham and Anderson, 2004).

(1) Extension

	K	AIC	ΔAIC	AICWt	Cum.Wt	LL
rsri	6	-1324.01	0	0.42	0.42	668.01
rz-sl	7	-1322.27	1.75	0.18	0.6	668.13
rz-int	7	-1322.01	2.01	0.15	0.75	668
rz-sl.int	8	-1320.73	3.28	0.08	0.83	668.37
tran-int	9	-1320.63	3.39	0.08	0.91	669.31
tran-sl.int	12	-1319.61	4.4	0.05	0.96	671.8

tran-sl	9	-1318.49	5.52	0.03	0.98	668.25
site-int	13	-1317.24	6.78	0.01	1	671.62
site-sl	13	-1312.75	11.26	0	1	669.38
site-sl.int	20	-1309.98	14.03	0	1	674.99

(2) Density

	K	AIC	ΔAIC	AICWt	Cum.Wt	LL
tran-sl	9	-8133.09	0	0.26	0.26	4075.54
tran-int	9	-8132.25	0.84	0.17	0.43	4075.13
rsri	6	-8131.93	1.15	0.15	0.58	4071.97
rz-int	7	-8131.28	1.81	0.11	0.69	4072.64
tran-sl.int	12	-8131.21	1.87	0.1	0.79	4077.61
site-int	13	-8130.6	2.48	0.08	0.87	4078.3
rz-sl.int	8	-8130.05	3.04	0.06	0.92	4073.02
rz-sl	7	-8129.95	3.14	0.05	0.98	4071.98
site-sl	13	-8127.94	5.15	0.02	1	4076.97
site-sl.int	20	-8123.47	9.61	0	1	4081.74

(3) Calcification

	K	AIC	Delta_AIC	AICWt	Cum.Wt	LL
rsri	6	-1394.98	0	0.38	0.38	703.49
rz-sl.int	8	-1393.99	0.99	0.23	0.61	705
rz-sl	7	-1393.27	1.71	0.16	0.77	703.64
rz-int	7	-1393.2	1.78	0.16	0.93	703.6
tran-int	9	-1390	4.98	0.03	0.96	704
tran-sl	9	-1389.51	5.47	0.02	0.99	703.75
tran-sl.int	12	-1388	6.98	0.01	1	706
site-int	13	-1384.24	10.75	0	1	705.12
site-sl	13	-1383.02	11.96	0	1	704.51
site-sl.int	20	-1377.54	17.44	0	1	708.77

Model abbreviations are as follows:

`rsri`
Random slopes, random intercepts

`rz-sl, tran-sl, site-sl`
Slopes varying by reef zone, transect, and site, respectively

`rz-int, tran-int, site-int`
Intercepts varying by reef zone, transect, and site, respectively

`rz-sl.int, tran-sl.int, site-sl.int`
Slopes and intercepts varying by reef zone, transect, and site, respectively

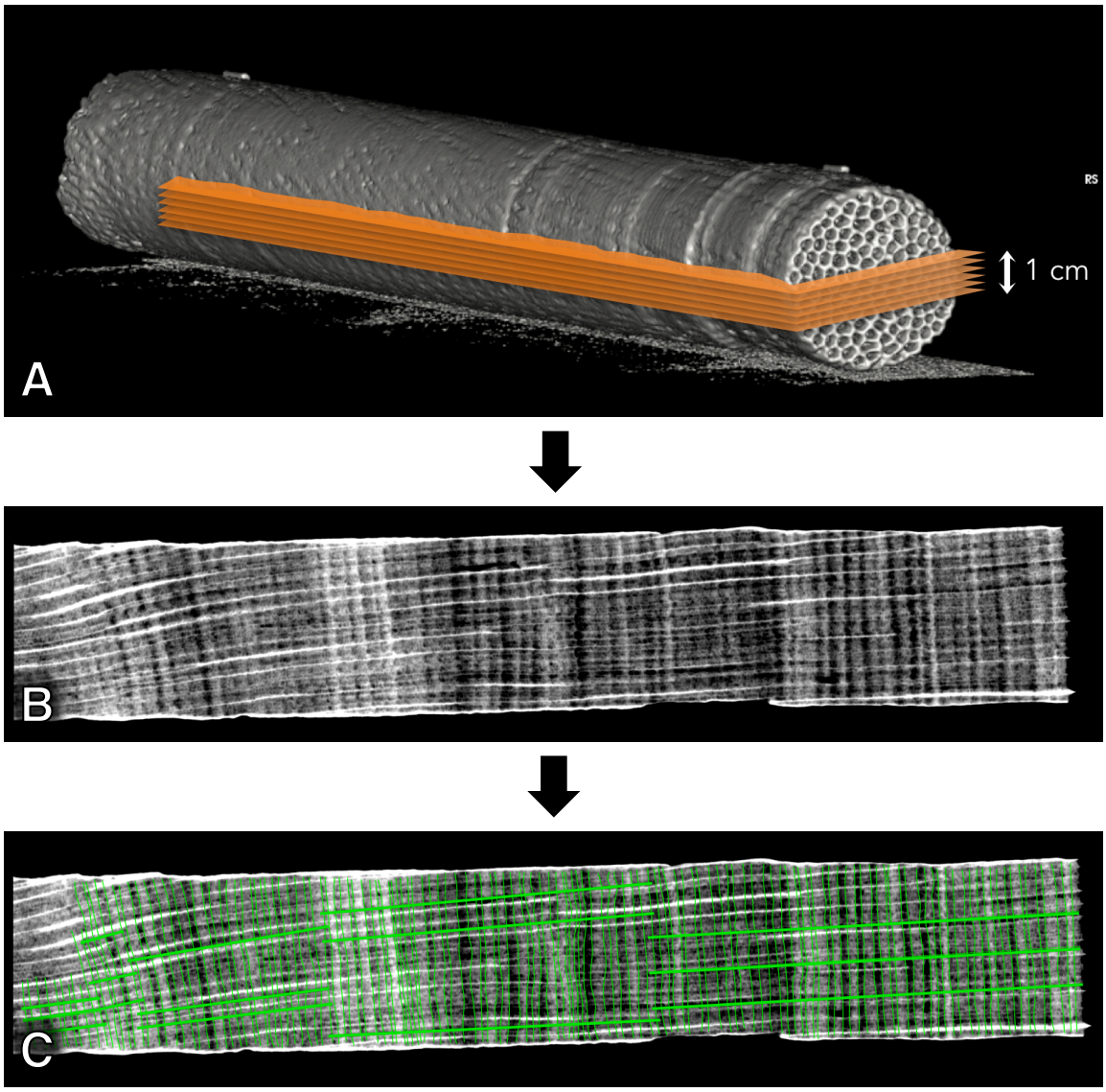

Figure S2.1. Step-by-step core analysis procedure in Horos image viewing software. (A) A digital slab of 1 cm thickness is oriented lengthwise through the middle of the coral core. **(B, C)** Band boundaries are manually drawn on to the two-dimensional image reconstruction. Three sets of linear transects are drawn along the length of the core and are averaged together to provide annual measurements of skeletal extension, density and calcification.

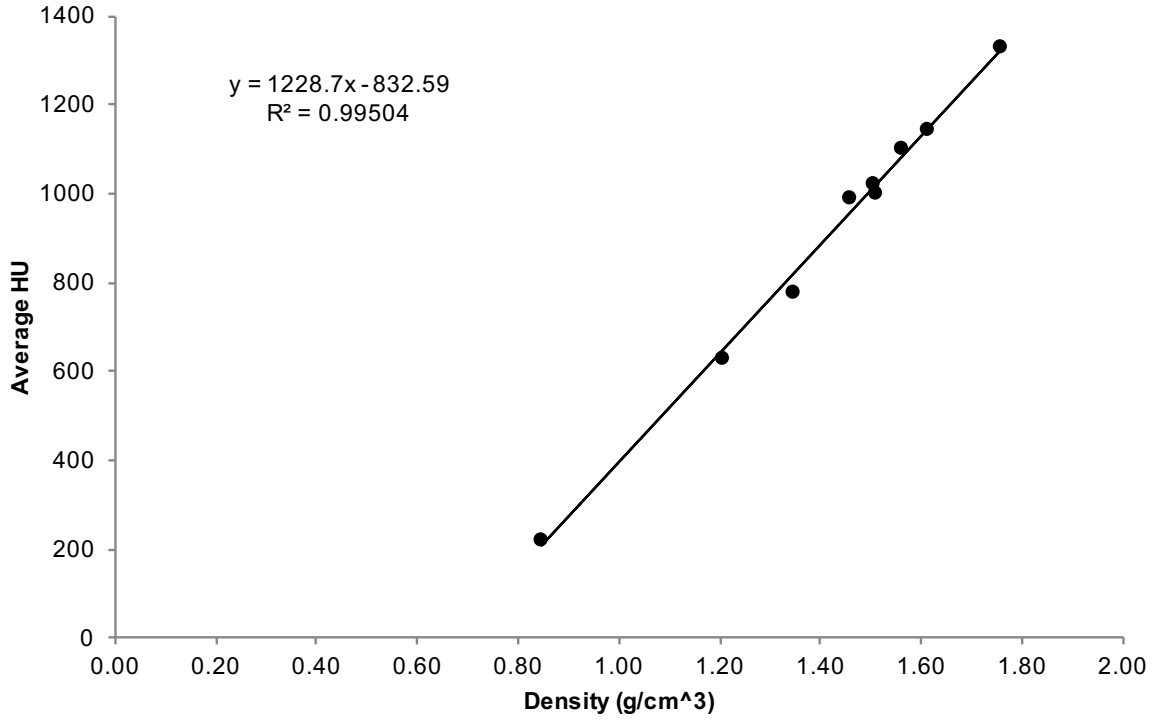

Figure S2.2. Density calibration curve. CT Hounsfield units are converted to real-world density based on the measurements of nine coral standards of known density. Calibration curves were generated for each CT scanning session.

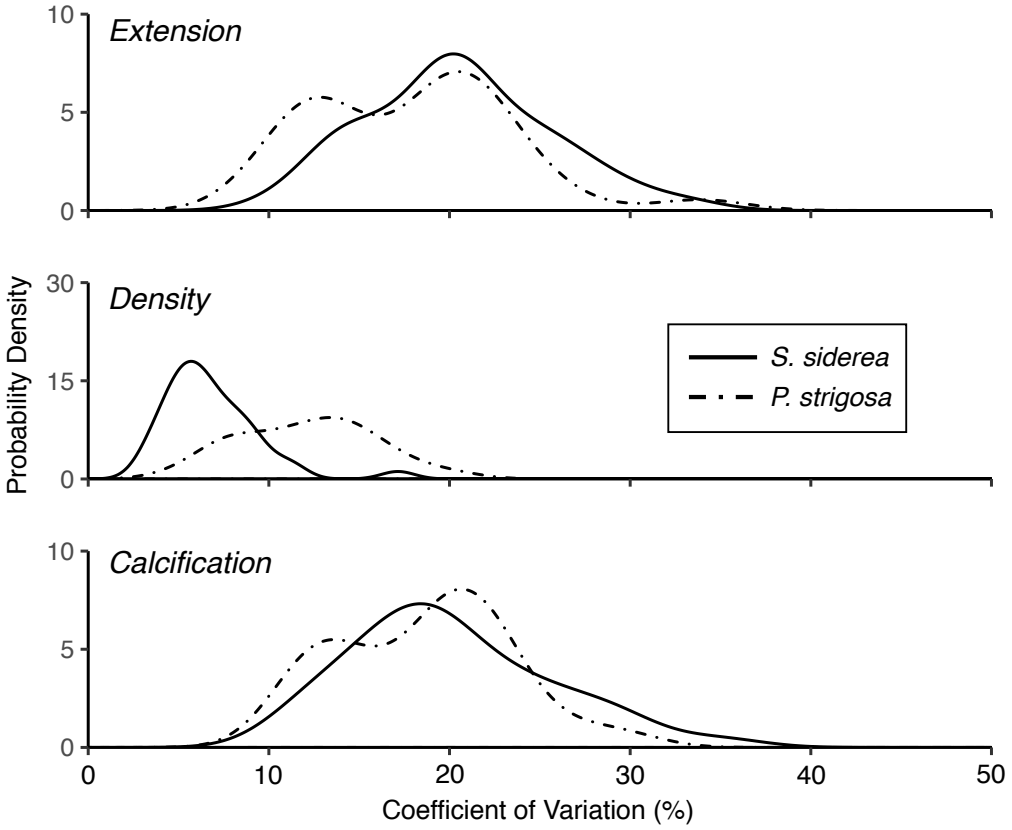

Figure S2.3. Interannual variation in extension, density and calcification within each core. Coefficient of variation is represented along the x-axis, and the solid and dashed lines depict the probability density plots for *S. siderea* and *P. strigosa* cores, respectively.

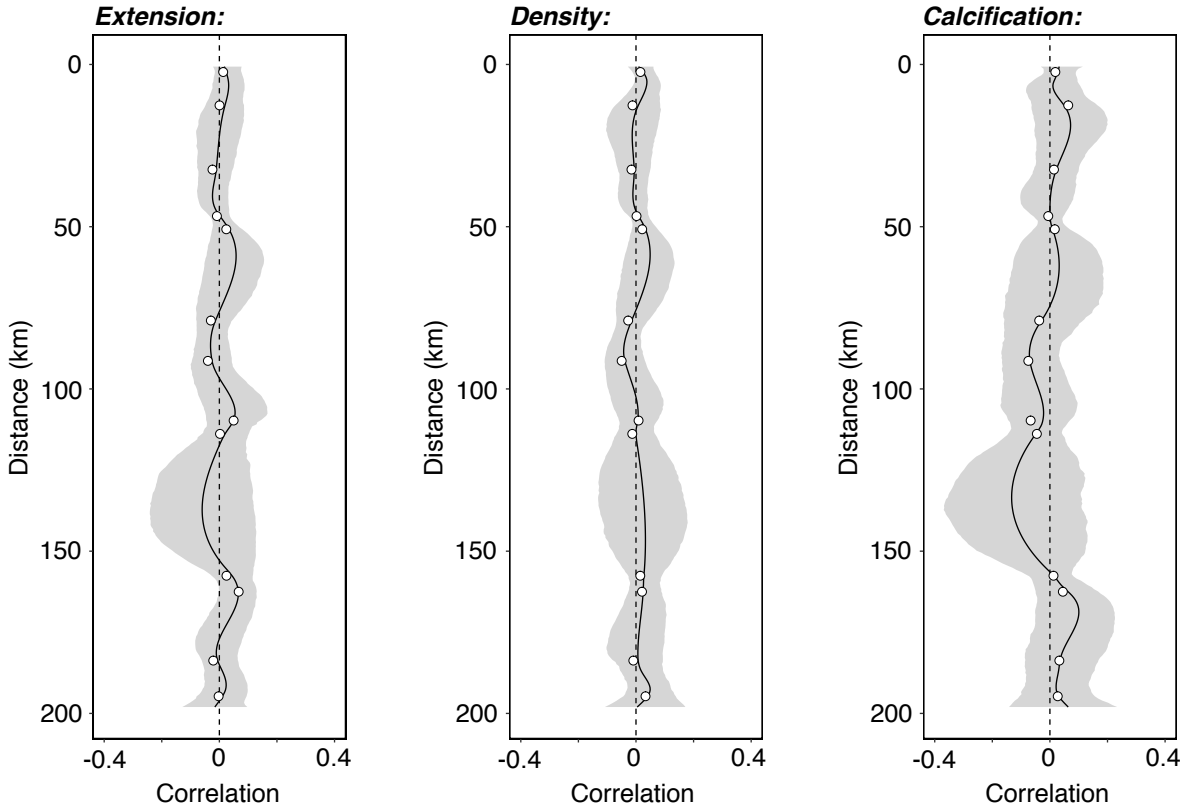

Figure S2.4. Spatial autocorrelation profiles for extension, density and calcification. All growth parameters during the period 1985-2014 were tested for spatial autocorrelation among all cores (*S. siderea* and *P. strigosa*). Open circles represent non-significant Mantel correlation values for 13 uniformly-spaced distance classes within the dataset, determined by permutation test (n = 1000). A non-parametric spatial correlation spline is plotted with a 95% confidence interval determined by bootstrapping (n = 1000). Standardized growth measurements were used to account for differences in mean growth between species and colonies.

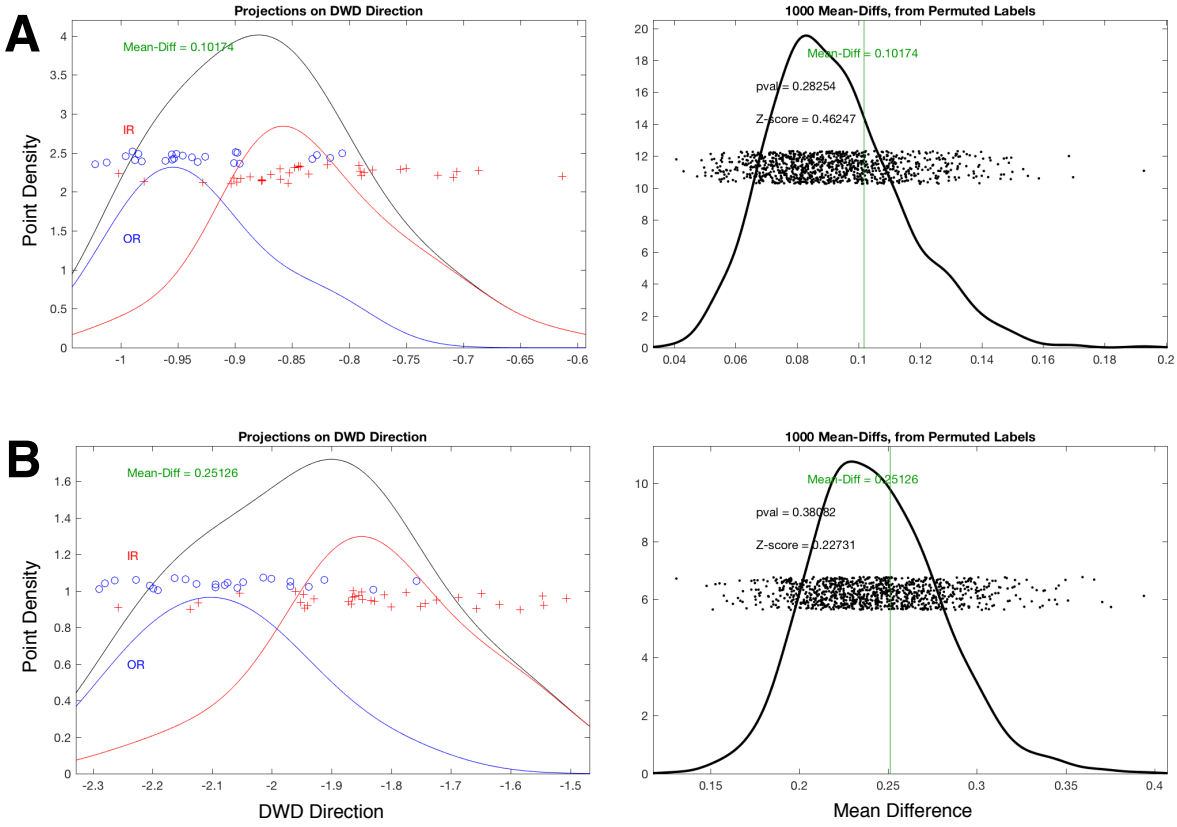

Figure S2.5. DWD and DiProPerm results for density (A) and calcification (B).

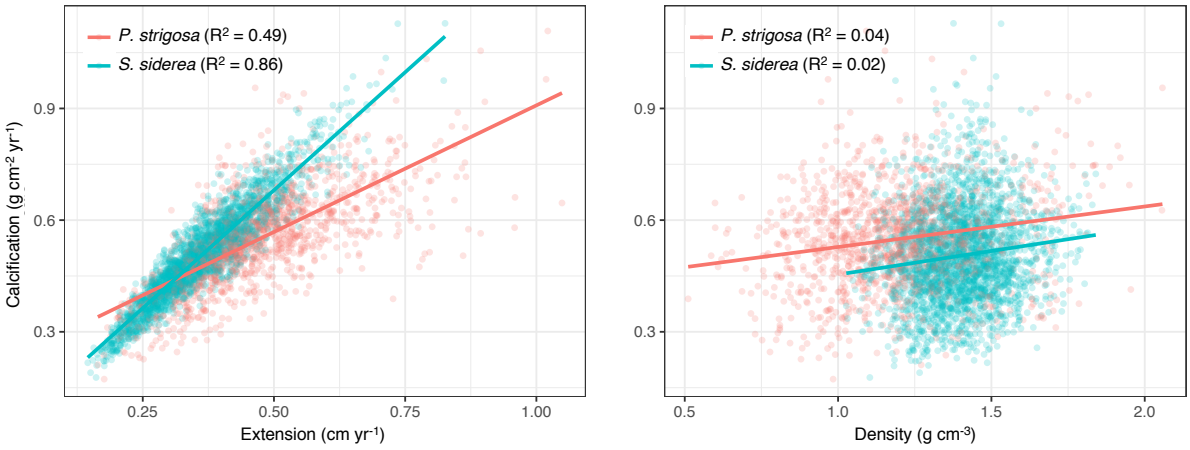

Figure S2.6. Linear regressions between calcification, extension and density for both species, *S. siderea* (blue) and *P. strigosa* (red).

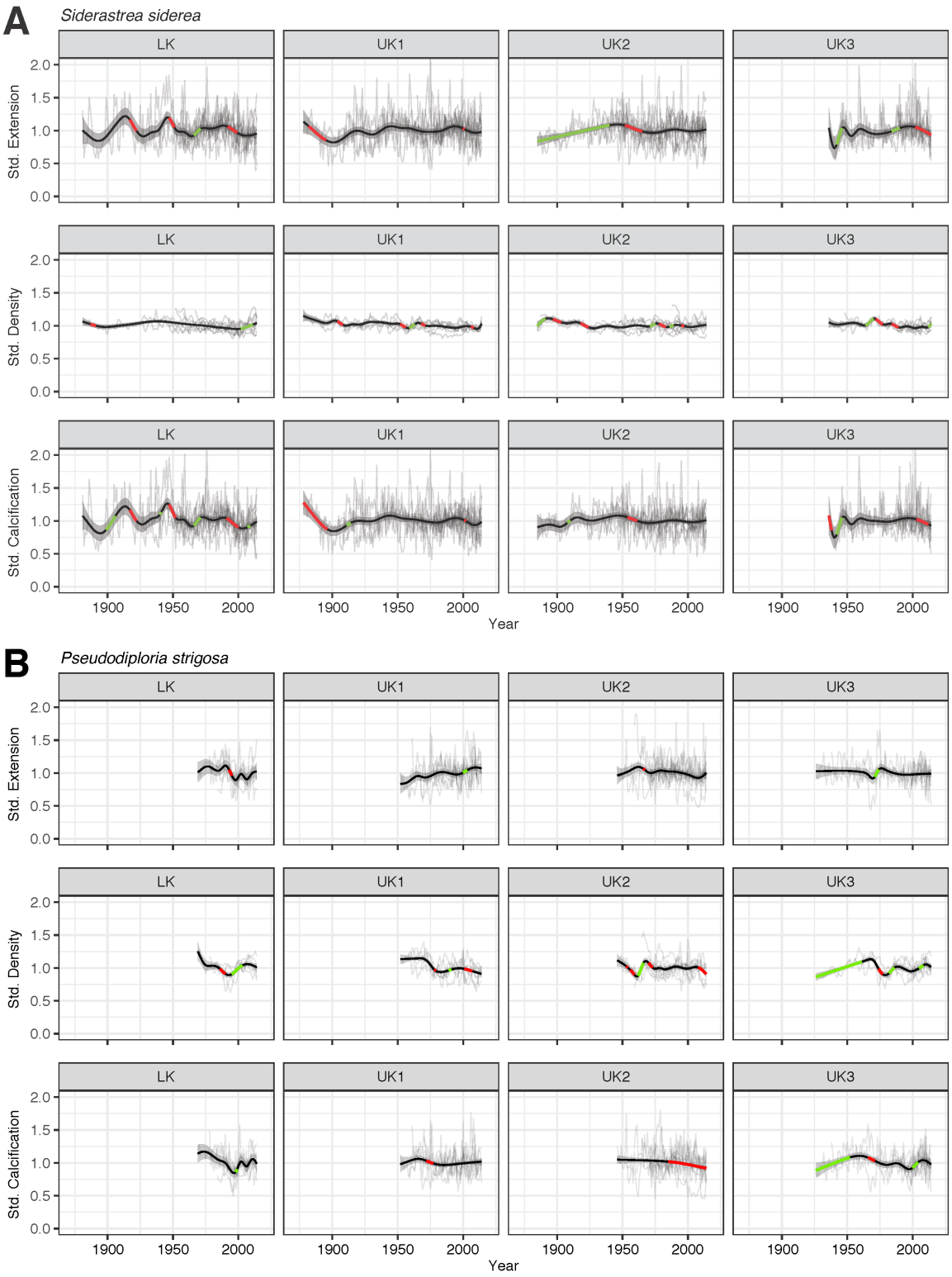

Figure S2.7. Generalized additive model results for all growth parameters organized by inner-outer reef transect and species.

Region	Reef Zone	Site Name	Latitude	Longitude	Max Depth (m)
LK	IR	W Washerwoman	24.535 N	-81.622 W	4.9
	OR	E Sambo	24.496 N	-81.649 W	6.7
UK1	IR	Cheeca Rocks	24.904 N	-80.610 W	7.3
	OR	Alligator Reef	24.895 N	-80.573 W	4.6
UK2	IR	Basin Hill Shoal	25.218 N	-80.276 W	4.4
	OR	Carysfort Reef	25.201 N	-80.227 W	4.6
UK3	IR	Bache Shoals	25.485 N	-80.149 W	3.7
	OR	Fowey Rocks	25.588 N	-80.097 W	4.3

Table S2.1. Geographic coordinates and maximum depth at each sampling site.

S. siderea	# Years	*P. strigosa*	# Years
yircr12s	125	yircr14p	55
yircr13s	106	yircr15p	57
yircr16s	137	yircr17p	54
yircr18s	107	yircr20p	63
yircr19s	59	yirbh36p	69
yirbh34s	92	yirbh40p	56
yirbh35s	27	yirbh41p	50
yirbh37s	79	yirbh42p	44
yirbh38s	128	yirbh43p	46
yirbh39s	130	yirww47p	46
yirww48s	48	yirww50p	31
yirww49s	61	yirww52p	21
yirww51s	80	yirww53p	37
yirww54s	57	yirww55p	36
yirww56s	36	yirbs66p	89
yirbs65s	17	yirbs70p	59
yirbs67s	79	yirbs71p	39
yirbs69s	41	yirbs72p	77
yirbs74s	73	yirbs73p	19
yores01s	63	yorar04p	38
yores02s	134	yorar07p	45
yores03s	58	yorar08p	35
yores44s	89	yorcf23p	44
yores46s	70	yorcf31p	68
yorar05s	50	yorcf32p	36
yorar06s	61	yorcf33p	44
yorar09s	37	yorfr57p	19
yorar10s	34	yorfr60p	14
yorcf21s	68	yorfr64p	23
yorcf26s	53		
yorcf27s	46		
yorcf28s	81		
yorcf30s	57		
yorfr58s	38		
yorfr59s	21		
yorfr61s	16		
yorfr62s	30		
yorfr63s	67		

Table S2.2. Chronological length of each coral core.

APPENDIX 2: SUPPLEMENTAL DESCRIPTIONS AND FIGURES – CHAPTER 3

```
Linear mixed-effects model fit by maximum likelihood
 Data: lme.data.center
        AIC      BIC   logLik
  -31.53909 140.9009 41.76954

Random effects:
 Formula: ~centerYear | coreID
 Structure: General positive-definite, Log-Cholesky parametrization
            StdDev      Corr
(Intercept) 0.239229902 (Intr)
centerYear  0.008030608 0.055
Residual    0.220739353

                                                     Value  Std.Error   DF    t-value p-value
(Intercept)                                     -0.3936651 0.04650859 5401  -8.464354  0.0000
centerYear                                      -0.0060750 0.00197713 5401  -3.072650  0.0021
spps                                            -0.6804839 0.06068621  187 -11.213155  0.0000
regionw                                         -0.3628022 0.07297264  187  -4.971756  0.0000
regiony                                         -0.4127698 0.06694500  187  -6.165805  0.0000
centerYear:spps                                  0.0036448 0.00249915 5401   1.458400  0.1448
centerYear:regionw                               0.0021231 0.00286162 5401   0.741923  0.4582
centerYear:regiony                               0.0059546 0.00269467 5401   2.209778  0.0272
spps:regionw                                     0.5642422 0.09295692  187   6.069932  0.0000
spps:regiony                                     0.4145698 0.08716571  187   4.756111  0.0000
summer.mean.all:belize                          -0.0451791 0.01936608 5401  -2.332898  0.0197
AMO:FL                                          -0.0324515 0.01424964 5401  -2.277357  0.0228
sppp:kd_490                                     -0.0289838 0.05502164  187  -0.526772  0.5990
spps:kd_490                                      0.1499961 0.04430751  187   3.385343  0.0009
centerYear:spps:regionw                         -0.0017975 0.00359544 5401  -0.499927  0.6171
centerYear:spps:regiony                         -0.0052501 0.00339949 5401  -1.544387  0.1226
sppp:Rain.mm:panama                              0.0594242 0.01776431 5401   3.345146  0.0008
spps:Rain.mm:panama                             -0.0048712 0.01339029 5401  -0.363785  0.7160
sppp:annual.cumulative.stress.all:panama         0.0338157 0.01467864 5401   2.303738  0.0213
spps:annual.cumulative.stress.all:panama        -0.0088405 0.01118053 5401  -0.790703  0.4292
sppp:annual.cumulative.stress.all:Rain.mm:panama -0.1565945 0.04908660 5401  -3.190169  0.0014
spps:annual.cumulative.stress.all:Rain.mm:panama  0.0383374 0.03728633 5401   1.028189  0.3039
 Correlation:

Standardized Within-Group Residuals:
        Min          Q1         Med          Q3         Max
-4.26525450 -0.58261314  0.02628053  0.58461972  4.79706685

Number of Observations: 5610
Number of Groups: 195
```

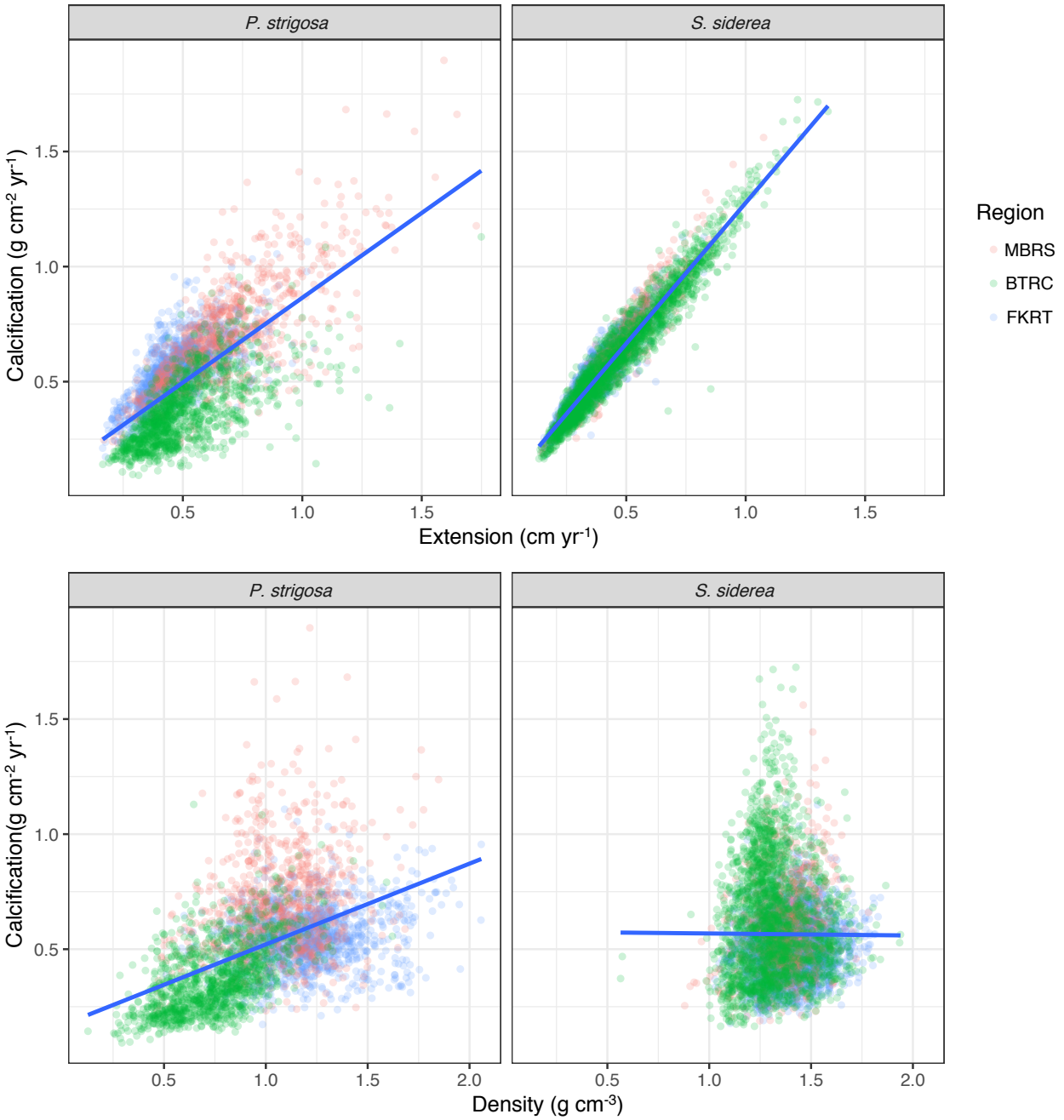

Figure S3.1. Linear regressions between calcification, extension and density for both species, *S. siderea* and *P. strigosa*.

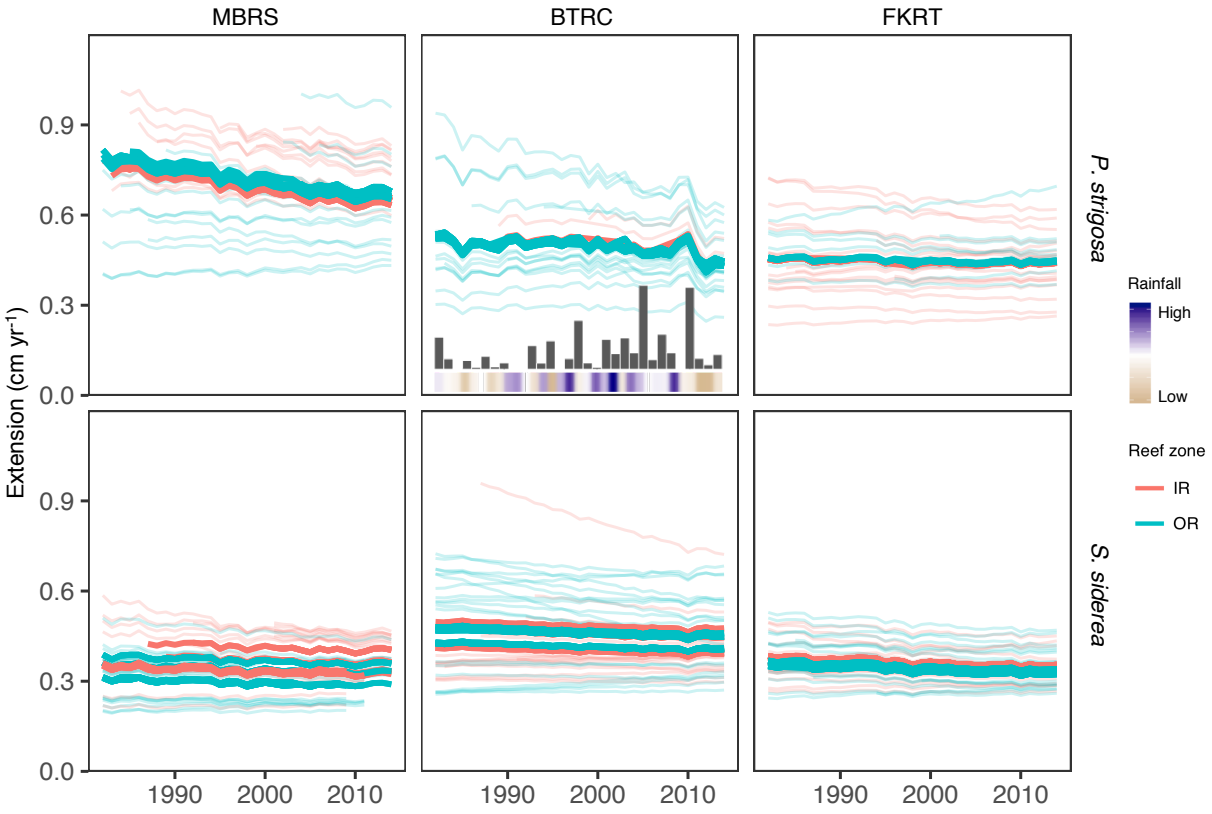

Figure S3.2. Predictions of coral extension rates across all regions and species based on the final linear mixed effect model. A bar plot and color chart depicting annual cumulative stress and rainfall, respectively, are included as an inset in the middle panel, as the interaction of these parameters was shown to significantly influence *P. strigosa* growth on the BTRC.

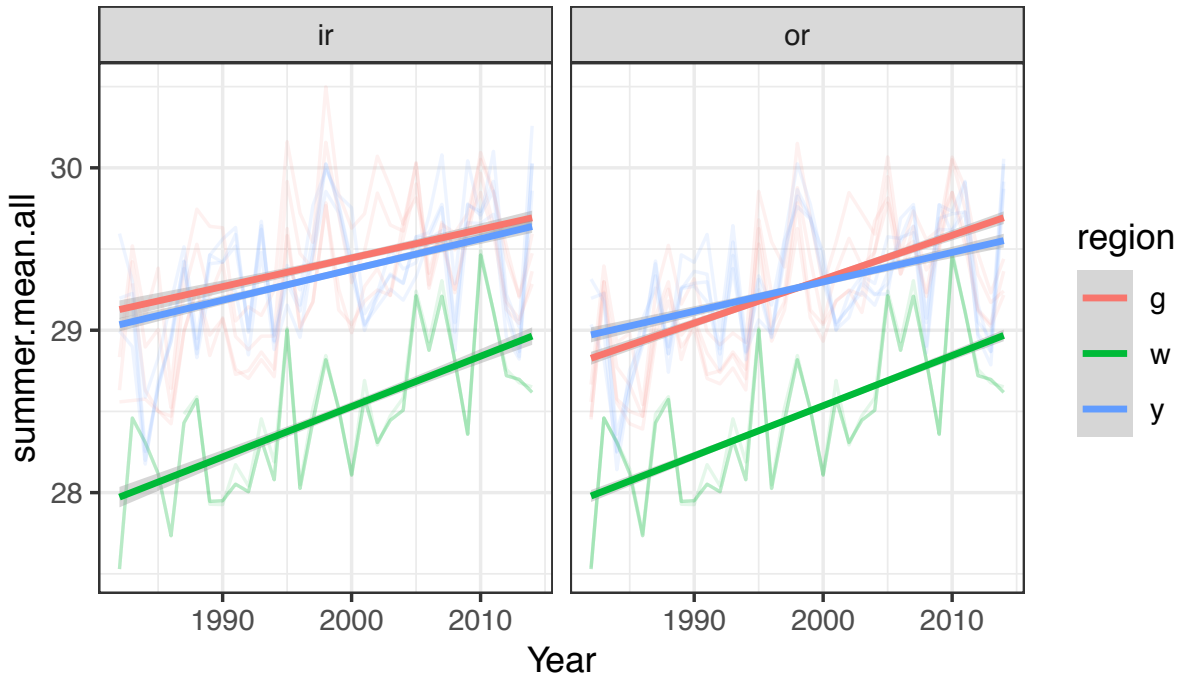

Figure S3.3. Summer mean temperatures for each reef system separated by reef zone. Colors are as in Figure 3.1.

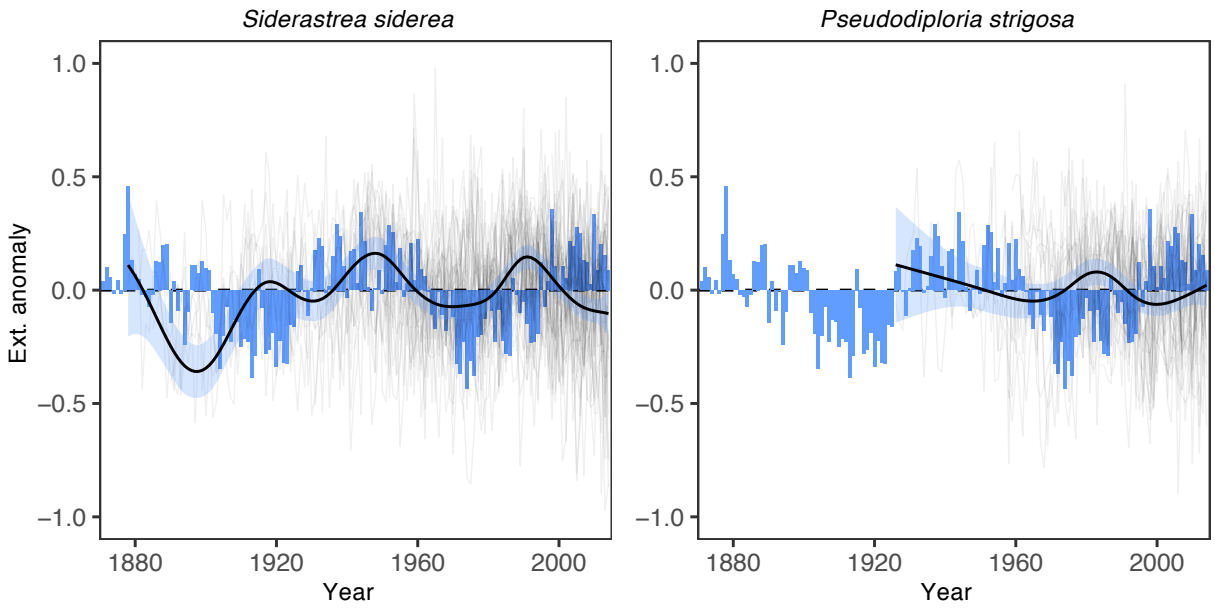

Figure S3.4. Extension anomalies of each species overlying the Atlantic Multidecadal Oscillation index from 1870 to 2014.

Region	RZ	Annual Mean	Annual Max	Annual Min	Annual Range	Weekly Range	Summer Mean	Days 24-30ºC
Florida	ir	26.83 ± 0.01	31.30 ± 0.02	21.74 ± 0.04	9.56 ± 0.05	1.01 ± 0.00	30.04 ± 0.02	243.16 ± 1.70
	or	26.87 ± 0.01	31.07 ± 0.02	22.13 ± 0.04	8.94 ± 0.05	0.88 ± 0.00	29.89 ± 0.02	265.90 ± 2.09
Belize	ir	28.15 ± 0.01	31.04 ± 0.02	24.90 ± 0.03	6.14 ± 0.03	0.92 ± 0.00	29.54 ± 0.01	331.80 ± 0.83
	or	28.08 ± 0.01	30.70 ± 0.02	25.47 ± 0.02	5.23 ± 0.03	0.80 ± 0.00	29.36 ± 0.01	346.60 ± 0.58
Panama	ir	28.44 ± 0.01	30.46 ± 0.02	26.38 ± 0.04	4.08 ± 0.04	0.86 ± 0.01	28.85 ± 0.02	355.56 ± 0.55
	or	28.36 ± 0.01	30.36 ± 0.01	26.31 ± 0.02	4.05 ± 0.03	0.83 ± 0.00	28.80 ± 0.01	358.68 ± 0.31

Region	RZ	Annual Cumulative Stress	# Stress Events	Stress Duration	Days Between Stress	pH (2014-17)	Ω_{arag} (2014-17)	K_d490 (2012-17)
Florida	ir	3.66 ± 0.31	1.20 ± 0.08	2.11 ± 0.05	9.24 ± 0.54	8.08 ± 0.00	4.05 ± 0.02	0.17 ± 0.04
	or	1.03 ± 0.12	0.60 ± 0.06	1.36 ± 0.03	4.99 ± 0.10	8.08 ± 0.00	4.05 ± 0.02	0.13 ± 0.03
Belize	ir	5.37 ± 0.27	1.58 ± 0.07	2.64 ± 0.06	31.66 ± 1.40	8.06 ± 0.00	4.14 ± 0.00	0.17 ± 0.06
	or	1.50 ± 0.13	0.62 ± 0.05	2.04 ± 0.06	22.70 ± 1.43	8.06 ± 0.00	4.17 ± 0.00	0.11 ± 0.10
Panama	ir	7.21 ± 0.52	2.29 ± 0.13	2.59 ± 0.08	46.93 ± 2.53	-	-	0.17 ± 0.09
	or	5.26 ± 0.29	1.68 ± 0.07	2.35 ± 0.06	58.64 ± 2.39	-	-	0.15 ± 0.06

Table S3.1. Summary of temperature, turbidity and carbonate chemistry parameters separated by reef zone within each reef system. With the exception of pH and Ω_{arag}, all other parameters were considered as possible predictors of coral extension rates within the linear mixed effect modeling approach.

APPENDIX 3: SUPPLEMENTAL DESCRIPTIONS AND FIGURES – CHAPTER 4

Pooling populations within sampling sites

The primary interest of this investigation was in large-scale patterns of population structure across the wider Caribbean, and therefore we pooled all sampling locations from each reef system into a single population to avoid overcomplicating regional patterns. For the samples collected from immediately adjacent reefs (i.e., two in Puerto Rico and two in USVI), this is unlikely to create a problem. However, within certain reef systems, the sampling locations were considerably far apart (i.e., Florida Keys, Curaçao and FGB).

In regard to the Florida Keys, only six samples were collected from each of the upper Keys sites, while 49 were collected from the Lower Keys site. We were not comfortable assuming that six samples would accurately represent the true allele frequencies at those locations, so we elected to group all the Florida Keys samples into a single population. Similarly, the 46 samples from Curaçao were almost evenly split between the three collection sites, leaving 14-16 samples per site. Again, rather than base allele frequency distributions on small neighboring populations, we pooled these sites into a larger population representing the entire Curaçao reef system.

The two populations from the Flower Garden Banks, however, had sufficiently large sample sizes (n = 39, 51) and are uniquely separated by 13 miles of open ocean (60-150 m depth). Thus, we ran analyses both with and without pooling the sites and found that the populations on the banks were quite similar genetically. The pairwise F_{ST} between the two populations was 0.012 and non-significant after Bonferroni correction, which was the lowest value for any pairwise comparison in that analysis. Due to the geographic proximity of the two sites, the genetic similarity warranted pooling them into a larger population for the basin-wide study.

Analysis of Null Alleles

In developing the microsatellites used in this study, Davies, Rahman, et al. (2013) found evidence for null alleles at three of the four loci associated with substantial heterozygote deficit, suggesting that the observed pattern may be due to the presence of null alleles. Re-analysis with the expanded dataset of this study corroborates this finding, in that the highest frequencies of null alleles estimated using the EM algorithm of Dempster et al. (1977) were found in the same four loci. It is important to note, however, that all estimates were relatively low (max $\hat{r}$ = 0.22; Table S2). Chapuis and Estoup (2007) demonstrate through simulations that a null allele rate of approximately 20% has a negligible effect on estimates of population structure.

To assess the effect of null alleles on our analyses, pairwise F_{ST} values between sites were adjusted using the excluding null allele (ENA) method executed in FreeNA, as recommended by Chapuis and Estoup (2007). A Mantel test between uncorrected and ENA-corrected pairwise F_{ST} (9999 permutations) showed these values to be very similar and strongly correlated (mean difference: 0.0001, r = 0.985, p-value = 0.0001; Figure S4.1), indicating that the presence of null alleles does not significantly alter downstream analyses. For this reason, and due to the relatively low frequency of null alleles, we elected to retain all nine microsatellite loci in our analysis.

Site	N	maMS8_CAA			Mfav5_CGA			Mfav7_CAT			Mfav3_ATG			Mfav4_TTTG		
		A_e	HWE	F_{IS}	A_e	HWE	F_{IS}	A_e	HWE	F_{IS}	A_e	HWE	F_{IS}	A_e	HWE	F_{IS}
BAH	11	1.984	0.044	0.661	5.902	0.017	0.278	7.806	0.281	0.005	1.635	0.047	0.341	3.315	0.002	0.515
BAR	25	2.390	0.003	0.331	5.343	**<0.0001**	0.272	9.584	**<0.0001**	0.311	1.409	0.482	0.056	5.097	**<0.0001**	0.650
BEL	35	1.517	0.316	0.092	8.249	0.031	0.072	9.714	0.243	0.064	1.492	0.002	0.320	6.033	**<0.0001**	0.539
CUR	46	1.758	0.568	0.003	7.985	0.002	0.141	8.123	0.187	0.019	1.495	0.479	0.027	4.707	**<0.0001**	0.265
FGB	90	2.668	0.030	0.064	7.831	**<0.0001**	0.297	9.627	**<0.0001**	0.139	1.488	0.020	0.226	4.360	**<0.0001**	0.547
FLK	54	2.187	0.990	-0.288	4.369	**<0.0001**	0.455	10.600	0.200	0.030	1.709	0.093	0.116	4.330	0.017	0.286
MEX	28	1.788	0.788	-0.117	4.612	0.001	0.377	6.247	0.003	0.252	1.905	0.769	-0.034	3.500	0.008	0.267
PAN	21	2.571	0.392	0.011	7.875	0.008	0.259	8.018	0.242	-0.009	2.478	0.266	0.146	3.852	0.441	0.060
PR	48	1.670	0.036	0.282	5.210	**<0.0001**	0.534	7.875	0.015	0.248	1.309	0.188	0.109	4.299	0.008	0.315
USVI	11	1.582	1.000	-0.191	4.102	0.079	0.322	6.205	0.006	0.286	1.095	N/A	N/A	2.881	0.226	0.211
ALL POPS	369	2.011		0.042	6.148		0.307	8.380		0.123	1.601		0.141	4.237		0.398

Site	N	Mfav6_CA			Mfav9_CAAT			Mfav30_TTTTG			Mfav8_CAA		
		A_e	HWE	F_{IS}	A_e	HWE	F_{IS}	A_e	HWE	F_{IS}	A_e	HWE	F_{IS}
BAH	11	3.143	0.146	0.245	6.722	0.723	-0.020	1.000	N/A	N/A	8.067	0.054	0.216
BAR	25	4.056	**<0.0001**	0.734	4.167	0.517	0.020	1.235	0.127	0.361	10.105	**<0.0001**	0.507
BEL	35	2.872	0.001	0.528	6.731	**<0.0001**	0.209	1.387	0.275	0.092	8.313	**<0.0001**	0.393
CUR	46	3.586	0.001	0.406	4.760	0.123	0.020	1.142	1.000	-0.041	8.498	**<0.0001**	0.296
FGB	90	3.654	**<0.0001**	0.571	7.112	**<0.0001**	0.255	1.385	0.001	0.206	9.356	**<0.0001**	0.336
FLK	54	3.358	**<0.0001**	0.753	6.139	0.107	0.146	1.626	0.114	0.191	8.090	0.001	0.226
MEX	28	3.621	**<0.0001**	0.857	3.431	0.144	0.261	1.114	1.000	-0.025	4.893	0.230	-0.052
PAN	21	3.173	0.002	0.463	4.820	0.542	0.003	1.156	1.000	-0.035	7.737	**<0.0001**	0.472
PR	48	1.920	0.002	0.450	5.813	0.211	0.040	1.199	0.035	0.206	11.765	**<0.0001**	0.752
USVI	11	3.507	0.005	0.527	7.333	0.703	-0.005	1.105	N/A	N/A	7.407	0.004	0.464
ALL POPS	369	3.289		0.580	5.703		0.141	1.235		0.170	8.423		0.349

Table S4.1. Single locus estimates of heterozygote deficiency. *N*: number of unique multilocus genets, A_e: effective number of alleles, *HWE*: *P* value of Fishers' exact test for heterozygote deficit based on 10,000 dememorization steps with 500 batches of 10,000 random permutations, F_{IS}: inbreeding coefficient. All values shaded in grey are significant at the $\alpha = 0.05$ level following sequential Bonferroni correction. Site abbreviations are as in Table 4.1.

	BAH	BAR	BEL	CUR	FGB	FLK	MEX	PAN	PR	USVI	**MEAN (%)**
maMS8	0.211	0.128	0.011	0	0.048	0	0	0.009	0.104	0	**5.1**
Mfav5	0.086	0.123	0.036	0.066	0.136	0.198	0.149	0.088	0.238	0.091	**12.1**
Mfav7	0.000	0.141	0.006	0.008	0.072	0.010	0.109	0.025	0.091	0.105	**5.7**
Mfav3	0.118	0.076	0.140	0	0.077	0.028	0	0	0	0	**4.4**
Mfav4	0.207	0.287	0.234	0.132	0.229	0.110	0.101	0	0.124	0.027	**14.5**
Mfav6	0.061	0.316	0.191	0.168	0.252	0.316	0.359	0.178	0.145	0.208	**21.9**
Mfav9	0	0	0.092	0.030	0.112	0.041	0.059	0	0.011	0	**3.5**
Mfav30	N/A	0.090	0.035	0	0.097	0.031	0	0	0.065	0	**3.5**
Mfav8	0.074	0.235	0.175	0.132	0.170	0.096	0.007	0.222	0.357	0.189	**16.6**

Table S4.2. Single locus estimates of null allele frequency based on EM algorithm of Dempster et al. (1977). Site abbreviations are as in Table 4.1.

	BAH	BAR	BEL	CUR	FGB	FLK	MEX	PAN	PR	USVI
maMS8 x Mfav5	0.3076	0.1590	0.1739	0.0897	0.0054	**0.0001**	0.0017	0.0136	0.3961	0.0185
maMS8 x Mfav7	0.5236	0.1739	0.1450	0.4942	0.0008	**0.0001**	**0.0001**	0.0349	0.7889	0.1368
maMS8 x Mfav3	0.6931	0.0114	0.0443	0.0450	0.2296	0.0432	0.0003	0.2615	0.9689	0.0894
maMS8 x Mfav4	0.9699	0.2150	0.4768	0.0763	0.0010	0.0483	0.0007	0.0068	0.2682	1
maMS8 x Mfav6	0.4518	0.5918	0.0933	0.3385	0.9758	0.0285	0.0008	0.1883	0.3194	0.1824
maMS8 x Mfav9	1	0.3106	0.2158	0.0772	0.3936	0.0121	0.0006	0.0539	0.1094	0.3782
maMS8 x Mfav30	N/A	0.0422	0.0535	0.2226	0.5926	0.0003	0.7303	1	0.0901	1
maMS8 x Mfav8	1	0.4582	0.1775	0.4586	0.0371	**0.0001**	0.9253	0.0199	0.6850	0.1403
Mfav5 x Mfav7	1	0.1501	0.0019	**0.0001**	0.0011	**0.0001**	**0.0001**	0.0003	0.0483	0.0078
Mfav5 x Mfav3	1	0.1356	0.1290	0.0174	0.0790	0.0113	**0.0001**	0.2643	0.1944	0.4564
Mfav5 x Mfav4	1	0.2171	0.0315	0.0031	0.0328	**0.0001**	**0.0001**	0.0014	0.1710	0.6700
Mfav5 x Mfav6	1	1	1	0.0275	0.5063	0.1000	0.0419	0.6168	0.5236	1
Mfav5 x Mfav9	1	0.4626	0.0044	**0.0001**	0.1669	**0.0001**	**0.0001**	0.0004	0.3949	0.1279
Mfav5 x Mfav30	N/A	0.5347	0.0489	0.4679	0.0732	0.0004	0.0054	0.5251	0.3583	0.1833
Mfav5 x Mfav8	1	1	1	0.0176	0.0444	**0.0001**	0.0147	**0.0001**	0.1426	0.0075
Mfav7 x Mfav3	0.6614	0.7394	0.3771	0.5422	0.0124	**0.0001**	**0.0001**	0.1439	0.4304	0.6357
Mfav7 x Mfav4	1	1	0.0758	0.1008	0.0288	**0.0001**	**0.0001**	0.0028	0.7278	0.2397
Mfav7 x Mfav6	1	0.4319	1	**0.0001**	0.2981	0.0003	**0.0001**	0.3719	0.9025	1
Mfav7 x Mfav9	1	1	0.0128	0.0225	**0.0001**	**0.0001**	**0.0001**	0.0014	0.0935	0.0338
Mfav7 x Mfav30	N/A	0.6500	0.5531	0.0426	0.0642	**0.0001**	0.0149	0.6839	0.8646	0.3732
Mfav7 x Mfav8	1	1	1	0.4614	0.0006	**0.0001**	0.0076	0.0004	1	0.0008
Mfav3 x Mfav4	0.4814	0.3700	0.6274	0.0033	0.9282	**0.0001**	**0.0001**	0.1032	0.5804	1
Mfav3 x Mfav6	0.6003	0.5396	0.2535	0.1806	0.0931	0.0132	0.0058	0.6638	0.1408	0.3656
Mfav3 x Mfav9	0.3686	0.7719	0.1857	0.3271	0.1456	0.0085	0.0003	0.1810	0.3514	0.8219
Mfav3 x Mfav30	N/A	0.1086	0.0113	0.8699	0.1911	0.4382	0.0025	0.7028	0.6363	1
Mfav3 x Mfav8	0.3846	0.8429	0.1232	0.0185	0.0028	0.0028	0.2876	0.2213	0.8610	0.6399
Mfav4 x Mfav6	0.1068	0.5471	0.4965	0.2779	0.6719	0.0010	0.0907	0.2981	0.1171	0.5183
Mfav4 x Mfav9	1	0.0569	0.0861	0.0221	0.1229	**0.0001**	0.0006	0.0800	0.3028	0.1289
Mfav4 x Mfav30	N/A	0.3960	0.0808	0.3819	0.3581	0.0593	0.0014	0.3969	0.1274	0.8364
Mfav4 x Mfav8	1	1	0.7122	0.0939	0.0135	**0.0001**	0.0731	0.0106	0.1028	0.2469
Mfav6 x Mfav9	1	0.2600	0.1272	0.0022	0.3954	**0.0001**	0.0022	0.0026	0.7213	1
Mfav6 x Mfav30	N/A	0.0560	0.6714	0.1828	0.0529	0.8219	0.8738	0.6186	0.0544	1
Mfav6 x Mfav8	1	0.4796	0.1006	0.1524	0.0076	0.0171	0.1565	0.8806	0.7408	1
Mfav9 x Mfav30	N/A	0.9015	0.5138	0.2567	0.1415	0.0569	0.0629	0.7933	0.1547	0.6551
Mfav9 x Mfav8	0.0190	1	0.0878	0.0706	0.0004	**0.0001**	0.1188	0.0049	0.4867	0.0415
Mfav30 x Mfav8	N/A	0.1117	0.6328	0.7640	0.5956	**0.0001**	0.1279	0.2282	0.6257	0.5896

Table S4.3. Tests of linkage disequilibrium between pairs of loci. *P* values for significance tests are based on 7200 random permutations. All values shaded in grey are significant at the α = 0.05 level following sequential Bonferroni correction. Site abbreviations are as in Table 4.1.

Site	N	Genotypes			Individuals	
		Unique	Clonal	%	Clonal	%
BAH	12	11	1	9.1	1	8.3
BAR	26	25	1	4.0	1	3.8
BEL	36	35	1	2.9	1	2.8
CUR	54	46	8	17.4	8	14.8
FGB	91	90	1	1.1	1	1.1
FLK	67	54	7	13.0	13	19.4
MEX	39	28	8	28.6	11	28.2
PAN	22	21	1	4.8	1	4.5
PR	49	48	1	2.1	1	2.0
USVI	12	11	1	9.1	1	8.3
TOTAL	408	369	30	8.1	39	9.6

Table S4.4. Number and proportion of clonal genotypes and individuals. *N*: total number of sampled colonies. Site abbreviations are as in Table 4.1.

										USVI
									0.013	PR
								0.142	**0.144**	PAN
							0.169	**0.190**	0.083	MEX
						0.113	**0.082**	**0.151**	**0.132**	FLK
					0.030	**0.114**	**0.049**	**0.115**	**0.096**	FGB
				0.090	**0.098**	**0.071**	**0.139**	**0.091**	0.026	CUR
			0.270	**0.142**	**0.167**	**0.290**	**0.095**	**0.280**	**0.246**	BEL
		0.076	**0.131**	**0.070**	**0.114**	**0.193**	**0.075**	**0.134**	0.086	BAR
	0.076	**0.132**	**0.095**	0.069	0.052	0.064	0.079	**0.175**	0.077	BAH
BAH	BAR	BEL	CUR	FGB	FLK	MEX	PAN	PR	USVI	

Table S4.5. Pairwise estimates of G''_{ST} between all populations. All values shaded in grey are significant at the $\alpha = 0.05$ level following sequential Bonferroni correction. Site abbreviations are as in Table 4.1.

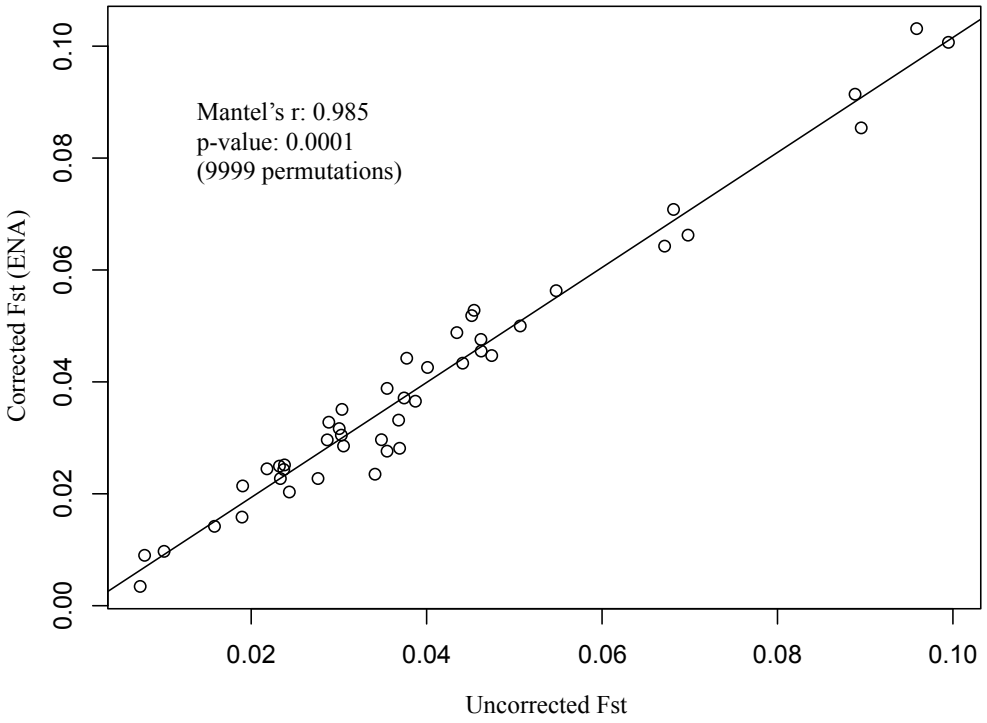

Figure S4.1. Correlation between uncorrected pairwise estimates of F_{ST} and pairwise estimates corrected by excluding null alleles.

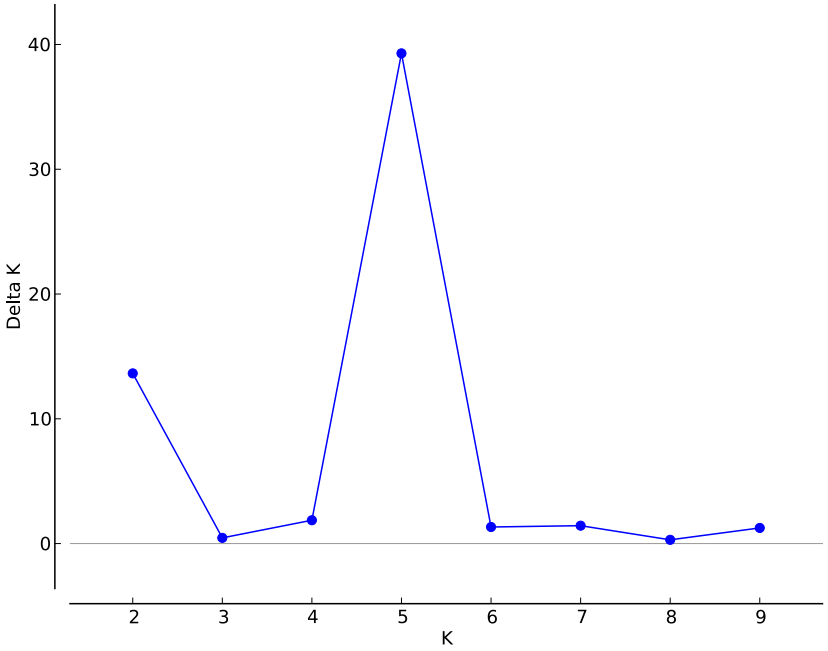

Figure S4.2. Estimation of the optimum number of genetic clusters (K) from STRUCTURE analysis based on the ad hoc statistic, ΔK (Evanno et al., 2005).
ΔK = mean(| L″(K) |) / sd(L(K)).

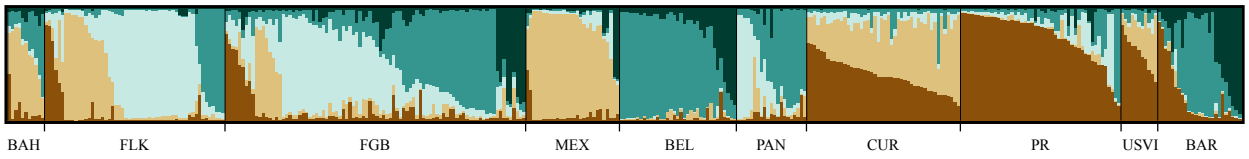

Figure S4.3. STRUCTURE population assignments displayed side-by-side. As in Figure 4.4, thin vertical columns in each population block represent individual samples and their associated probability of assignment to K = 5 color-coded genetic clusters (Brown, Tan, Light Blue, Teal, and Dark Blue). Site abbreviations are as in Table 4.1 and are organized along the axes by relative geographic location in the basin.

REFERENCES

Albright, R., Takeshita, Y., Koweek, D. A., Ninokawa, A., Wolfe, K., Rivlin, T., . . . Caldeira, K. (2018). Carbon dioxide addition to coral reef waters suppresses net community calcification. *Nature, 555*(7697), 516.

Allendorf, F. W., Luikart, G., & Aitken, S. N. (2013). *Conservation and the Genetics of Populations, Second Edition*. Chichester, West Sussex, United Kingdom: Wiley-Blackwell.

Almany, G. R., Berumen, M. L., Thorrold, S. R., Planes, S., & Jones, G. P. (2007). Local replenishment of coral reef fish populations in a marine reserve. *Science, 316*(5825), 742-744.

Alvera-Azcárate, A., Barth, A., & Weisberg, R. H. (2009). The surface circulation of the Caribbean Sea and the Gulf of Mexico as inferred from satellite altimetry. *Journal of Physical Oceanography, 39*(3), 640-657.

An, H., Marron, J., Schwartz, T. A., Renner, J. B., Liu, F., Lynch, J. A., . . . Nelson, A. E. (2016). Novel statistical methodology reveals that hip shape is associated with incident radiographic hip osteoarthritis among African American women. *Osteoarthritis and Cartilage, 24*(4), 640-646.

Andersson, A. J., & Gledhill, D. (2013). Ocean acidification and coral reefs: effects on breakdown, dissolution, and net ecosystem calcification. *Annual Review of Marine Science, 5*, 321-348.

Andras, J. P., Rypien, K. L., & Harvell, C. D. (2013). Range-wide population genetic structure of the Caribbean sea fan coral, Gorgonia ventalina. *Molecular Ecology, 22*(1), 56-73.

Anthony, K. R. (2006). Enhanced energy status of corals on coastal, high-turbidity reefs. *Marine Ecology Progress Series, 319*, 111-116.

Anthony, K. R., & Fabricius, K. E. (2000). Shifting roles of heterotrophy and autotrophy in coral energetics under varying turbidity. *Journal of Experimental Marine Biology and Ecology, 252*(2), 221-253.

Aronson, R. B., & Precht, W. F. (2001). White-band disease and the changing face of Caribbean coral reefs *The Ecology and Etiology of Newly Emerging Marine Diseases* (Porter, J.W. ed., Vol. 159, pp. 25-38). Dordrecht: Springer.

Aronson, R. B., Precht, W. F., Murdoch, T. J., & Robbart, M. L. (2005). Long-term persistence of coral assemblages on the Flower Garden Banks, northwestern Gulf of Mexico: implications for science and management. *Gulf of Mexico Science, 23*(1), 84-94.

Aronson, R. B., Precht, W. F., Toscano, M., & Koltes, K. (2002). The 1998 bleaching event and its aftermath on a coral reef in Belize. *Marine Biology, 141*(3), 435-447.

Australian Institute of Marine Science. (2016). The facts on Great Barrier Reef coral mortality [Press release]. Retrieved from https://www.aims.gov.au/.

Baker, A. C., Glynn, P. W., & Riegl, B. (2008). Climate change and coral reef bleaching: An ecological assessment of long-term impacts, recovery trends and future outlook. *Estuarine, Coastal and Shelf Science, 80*(4), 435-471.

Barkley, H. C., Cohen, A. L., Golbuu, Y., Starczak, V. R., DeCarlo, T. M., & Shamberger, K. E. (2015). Changes in coral reef communities across a natural gradient in seawater pH. *Science Advances, 1*(5), e1500328.

Barnes, D., & Lough, J. (1993). On the nature and causes of density banding in massive coral skeletons. *Journal of Experimental Marine Biology and Ecology, 167*(1), 91-108.

Barnes, D., & Lough, J. (1996). Coral skeletons: storage and recovery of environmental information. *Global Change Biology, 2*(6), 569-582.

Barshis, D. J., Ladner, J. T., Oliver, T. A., Seneca, F. O., Traylor-Knowles, N., & Palumbi, S. R. (2013). Genomic basis for coral resilience to climate change. *Proceedings of the National Academy of Sciences, 110*(4), 1387-1392.

Barton, N. H., & Hewitt, G. M. (1985). Analysis of hybrid zones. *Annual review of Ecology and Systematics, 16*(1), 113-148.

Baumann, J. H., Ries, J. B., Rippe, J. P., Courtney, T. A., Aichelman, H. E., Westfield, I. T., & Castillo, K. D. (2018). Nearshore corals on the Mesoamerican Barrier Reef System on pace to cease growing as soon as year 2110. *bioRxiv*. doi:10.1101/298158

Baumann, J. H., Townsend, J. E., Courtney, T. A., Aichelman, H. E., Davies, S. W., Lima, F. P., & Castillo, K. D. (2016). Temperature Regimes Impact Coral Assemblages along Environmental Gradients on Lagoonal Reefs in Belize. *PloS one, 11*(9), e0162098.

Baums, I. B., Johnson, M., Devlin-Durante, M., & Miller, M. (2010). Host population genetic structure and zooxanthellae diversity of two reef-building coral species along the Florida Reef Tract and wider Caribbean. *Coral Reefs, 29*(4), 835-842.

Baums, I. B., Miller, M. W., & Hellberg, M. E. (2005). Regionally isolated populations of an imperiled Caribbean coral, Acropora palmata. *Molecular Ecology, 14*(5), 1377-1390.

Baums, I. B., Paris, C. B., & Cherubin, L. (2006). A bio-oceanographic filter to larval dispersal in a reef-building coral. Limnol Oceanogr. *Limnology and Oceanography, 51*(5), 1969-1981.

Bay, R. A., & Palumbi, S. R. (2014). Multilocus adaptation associated with heat resistance in reef-building corals. *Current Biology, 24*(24), 2952-2956.

Bennion, H., Simpson, G. L., & Goldsmith, B. J. (2015). Assessing degradation and recovery pathways in lakes impacted by eutrophication using the sediment record. *Frontiers in Ecology and Evolution, 3*, 94.

Bjornstad, O. N. (2009). ncf: Spatial Nonparametric Covariance Functions. R package version 1.1-3. https://cran.r-project.org/package=ncf.

Bode, M., Bode, L., & Armsworth, P. R. (2006). Larval dispersal reveals regional sources and sinks in the Great Barrier Reef. *Marine Ecology Progress Series, 308*, 17-25.

Boyer, J. N., Fourqurean, J. W., & Jones, R. D. (1999). Seasonal and long-term trends in the water quality of Florida Bay (1989–1997). *Estuaries, 22*(2), 417-430.

Brandt, M. E., & McManus, J. W. (2009). Disease incidence is related to bleaching extent in reef-building corals. *Ecology, 90*(10), 2859-2867.

Briceño, H. O., & Boyer, J. N. (2014). *2014 Annual Report of the Water Quality Monitoring Project for the Water Quality Protection Program of the Florida Keys National Marine Sanctuary*. Retrieved from Florida International University:

Bruckner, A., & Bruckner, R. (2006). The recent decline of Montastraea annularis (complex) coral populations in western Curaçao: a cause for concern? *Revista de Biología Tropical, 54*, 45-58.

Bruno, J. F., Selig, E. R., Casey, K. S., Page, C. A., Willis, B. L., Harvell, C. D., . . . Melendy, A. M. (2007). Thermal stress and coral cover as drivers of coral disease outbreaks. *PLoS biology, 5*(6), e124.

Budd, A. F., & Pandolfi, J. M. (2004). Overlapping species boundaries and hybridization within the Montastraea "annularis" reef coral complex in the Pleistocene of the Bahama Islands. *Paleobiology, 30*(03), 396-425.

Cantin, N. E., Cohen, A. L., Karnauskas, K. B., Tarrant, A. M., & McCorkle, D. C. (2010). Ocean warming slows coral growth in the central Red Sea. *Science, 329*(5989), 322-325.

Carilli, J. E., Donner, S. D., & Hartmann, A. C. (2012). Historical temperature variability affects coral response to heat stress. *PloS one, 7*(3), e34418.

Carilli, J. E., Norris, R. D., Black, B., Walsh, S. M., & McField, M. (2010). Century-scale records of coral growth rates indicate that local stressors reduce coral thermal tolerance threshold. *Global Change Biology, 16*(4), 1247-1257.

Carricart-Ganivet, J. P., & Merino, M. (2001). Growth responses of the reef-building coral Montastraea annularis along a gradient of continental influence in the southern Gulf of Mexico. *Bulletin of Marine Science, 68*(1), 133-146.

Carricart-Ganivet, J. P., Vásquez-Bedoya, L., Cabanillas-Terán, N., & Blanchon, P. (2013). Gender-related differences in the apparent timing of skeletal density bands in the reef-building coral Siderastrea siderea. *Coral Reefs, 32*(3), 769-777.

Carrillo, L., Johns, E., Smith, R., Lamkin, J., & Largier, J. (2015). Pathways and Hydrography in the Mesoamerican Barrier Reef System Part 1: Circulation. *Continental Shelf Research, 109*, 164-176.

Castillo, K. D., Ries, J. B., Bruno, J. F., & Westfield, I. T. (2014). The reef-building coral *Siderastrea siderea* exhibits parabolic responses to ocean acidification and warming. *Proceedings of the Royal Society of London B: Biological Sciences, 281*(1797), 20141856.

Castillo, K. D., Ries, J. B., & Weiss, J. M. (2011). Declining coral skeletal extension for forereef colonies of *Siderastrea siderea* on the Mesoamerican Barrier Reef System, Southern Belize. *PloS one, 6*(2), e14615.

Castillo, K. D., Ries, J. B., Weiss, J. M., & Lima, F. P. (2012). Decline of forereef corals in response to recent warming linked to history of thermal exposure. *Nature Climate Change, 2*(10), 756.

Causey, B. (2001). *Lessons learned from the intensification of coral bleaching from 1980–2000 in the Florida Keys, USA.* Paper presented at the Proceedings of the Workshop on Mitigating Coral Bleaching Impact through MPA Design. Honolulu, Hawaii.

Chapuis, M.-P., & Estoup, A. (2007). Microsatellite null alleles and estimation of population differentiation. *Molecular biology and evolution, 24*(3), 621-631.

Chollett, I., Müller-Karger, F. E., Heron, S. F., Skirving, W., & Mumby, P. J. (2012). Seasonal and spatial heterogeneity of recent sea surface temperature trends in the Caribbean Sea and southeast Gulf of Mexico. *Marine Pollution Bulletin, 64*(5), 956-965.

Chollett, I., Mumby, P. J., Müller-Karger, F. E., & Hu, C. (2012). Physical environments of the Caribbean Sea. *Limnology and Oceanography, 57*(4), 1233-1244.

Colella, M., Ruzicka, R., Kidney, J., Morrison, J., & Brinkhuis, V. (2012). Cold-water event of January 2010 results in catastrophic benthic mortality on patch reefs in the Florida Keys. *Coral Reefs, 31*(2), 621-632.

Comeau, S., Carpenter, R., & Edmunds, P. (2013). Coral reef calcifiers buffer their response to ocean acidification using both bicarbonate and carbonate. *Proceedings of the Royal Society B: Biological Sciences, 280*(1753), 20122374.

Cooper, T. F., De'ath, G., Fabricius, K. E., & Lough, J. M. (2008). Declining coral calcification in massive *Porites* in two nearshore regions of the northern Great Barrier Reef. *Global Change Biology, 14*(3), 529-538.

Cooper, T. F., O'Leary, R. A., & Lough, J. M. (2012). Growth of Western Australian corals in the Anthropocene. *Science, 335*(6068), 593-596.

Courtney, T. A., Lebrato, M., Bates, N. R., Collins, A., de Putron, S. J., Garley, R., . . . Sabine, C. L. (2017). Environmental controls on modern scleractinian coral and reef-scale calcification. *Science Advances, 3*(11), e1701356.

Cowen, R. K., & Castro, L. R. (1994). Relation of coral reef fish larval distributions to island scale circulation around Barbados, West Indies. *Bulletin of Marine Science, 54*(1), 228-244.

Cowen, R. K., Lwiza, K. M., Sponaugle, S., Paris, C. B., & Olson, D. B. (2000). Connectivity of marine populations: open or closed? *Science, 287*(5454), 857-859.

Cowen, R. K., Paris, C. B., & Srinivasan, A. (2006). Scaling of connectivity in marine populations. *Science, 311*(5760), 522-527.

Cowen, R. K., & Sponaugle, S. (2009). Larval dispersal and marine population connectivity. *Marine Science, 1*.

Crook, E. D., Cohen, A. L., Rebolledo-Vieyra, M., Hernandez, L., & Paytan, A. (2013). Reduced calcification and lack of acclimatization by coral colonies growing in areas of persistent natural acidification. *Proceedings of the National Academy of Sciences, 110*(27), 11044-11049.

D'Croz, L., Rosario, J. B. d., & Gondola, P. (2005). The effect of fresh water runoff on the distribution of dissolved inorganic nutrients and plankton in the Bocas del Toro Archipelago, Caribbean Panama. *Caribbean Journal of Science*.

Davies, S. W., Matz, M. V., & Vize, P. D. (2013). Ecological complexity of coral recruitment processes: effects of invertebrate herbivores on coral recruitment and growth depends upon substratum properties and coral species. *PloS one, 8*(9), e72830.

Davies, S. W., Meyer, E., Guermond, S. M., & Matz, M. V. (2014). A cross-ocean comparison of responses to settlement cues in reef-building corals. *PeerJ, 2*, e333.

Davies, S. W., Rahman, M., Meyer, E., Green, E. A., Buschiazzo, E., Medina, M., & Matz, M. V. (2013). Novel polymorphic microsatellite markers for population genetics of the endangered Caribbean star coral, Montastraea faveolata. *Marine Biodiversity, 43*(2), 167-172.

Davies, S. W., Strader, M. E., Kool, J. T., Kenkel, C. D., & Matz, M. V. (2017). Modeled differences of coral life-history traits influence the refugium potential of a remote Caribbean reef. *Coral Reefs, 36*(3), 913-925.

De'ath, G., & Fabricius, K. (2010). Water quality as a regional driver of coral biodiversity and macroalgae on the Great Barrier Reef. *Ecological Applications, 20*(3), 840-850.

De'ath, G., Lough, J. M., & Fabricius, K. E. (2009). Declining coral calcification on the Great Barrier Reef. *Science, 323*(5910), 116-119.

DeCarlo, T. M., Cohen, A. L., Barkley, H. C., Cobban, Q., Young, C., Shamberger, K. E., . . . Golbuu, Y. (2015). Coral macrobioerosion is accelerated by ocean acidification and nutrients. *Geology, 43*(1), 7-10.

Dempster, A. P., Laird, N. M., & Rubin, D. B. (1977). Maximum likelihood from incomplete data via the EM algorithm. *Journal of the Royal Statistical Society. Series B (Methodological)*, 1-38.

Dharmarajan, G., Beatty, W. S., & Rhodes, O. E. (2013). Heterozygote deficiencies caused by a Wahlund effect: dispelling unfounded expectations. *The Journal of Wildlife Management, 77*(2), 226-234.

Dixon, G., Liao, Y., Bay, L. K., & Matz, M. V. (2018). Role of gene body methylation in acclimatization and adaptation in a basal metazoan. *Proceedings of the National Academy of Sciences, 115*(52), 13342-13346.

Dunn, J. G., Sammarco, P. W., & LaFleur Jr, G. (2012). Effects of phosphate on growth and skeletal density in the scleractinian coral Acropora muricata: A controlled experimental approach. *Journal of Experimental Marine Biology and Ecology, 411*, 34-44.

Dustan, P. (1977). Vitality of reef coral populations off Key Largo, Florida: recruitment and mortality. *Environmental Geology, 2*(1), 51-58.

Earl, D. A., & vonHoldt, B. M. (2012). STRUCTURE HARVESTER: a website and program for visualizing STRUCTURE output and implementing the Evanno method. *Conservation genetics resources, 4*(2), 359-361.

Edinger, E. N., Limmon, G. V., Jompa, J., Widjatmoko, W., Heikoop, J. M., & Risk, M. J. (2000). Normal coral growth rates on dying reefs: are coral growth rates good indicators of reef health? *Marine Pollution Bulletin, 40*(5), 404-425.

Edmunds, P. (2015). A quarter-century demographic analysis of the Caribbean coral, Orbicella annularis, and projections of population size over the next century. *Limnology and Oceanography, 60*(3), 840-855.

Enfield, D. B., Mestas-Nuñez, A. M., & Trimble, P. J. (2001). The Atlantic Multidecadal Oscillation and its relation to rainfall and river flows in the continental US. *Geophysical Research Letters, 28*(10), 2077-2080.

Evanno, G., Regnaut, S., & Goudet, J. (2005). Detecting the number of clusters of individuals using the software STRUCTURE: a simulation study. *Molecular Ecology, 14*(8), 2611-2620.

Eyre, B. D., Cyronak, T., Drupp, P., De Carlo, E. H., Sachs, J. P., & Andersson, A. J. (2018). Coral reefs will transition to net dissolving before end of century. *Science, 359*(6378), 908-911.

Fabricius, K. E. (2005). Effects of terrestrial runoff on the ecology of corals and coral reefs: review and synthesis. *Marine Pollution Bulletin, 50*(2), 125-146.

Fabricius, K. E., Langdon, C., Uthicke, S., Humphrey, C., Noonan, S., De'ath, G., . . . Lough, J. M. (2011). Losers and winners in coral reefs acclimatized to elevated carbon dioxide concentrations. *Nature Climate Change, 1*(3), 165.

Falush, D., Stephens, M., & Pritchard, J. K. (2003). Inference of population structure using multilocus genotype data: linked loci and correlated allele frequencies. *Genetics, 164*(4), 1567-1587.

Falush, D., Stephens, M., & Pritchard, J. K. (2007). Inference of population structure using multilocus genotype data: dominant markers and null alleles. *Molecular Ecology Notes, 7*(4), 574-578.

Florida Department of Environmental Protection. *Florida Reef Tract Coral Disease Outbreak: Regional Coordination Call #3 - September 29, 2016.* Retrieved from https://floridadep.gov/fco/coral/content/florida-reef-tract-coral-disease-outbreak

Florida Fish and Wildlife Conservation Commission. (1996-2017). *Coral Reef Evaluation and Monitoring Project*.

Florida Fish and Wildlife Conservation Commission. (2016). *Coral Reef Evaluation and Monitoring Project: Executive Summary 2016*.

Florida Reef Resilience Program. *DRM Annual Survey Data.* Retrieved from: http://www.frrp.org/data/

Foster, N. L., Paris, C. B., Kool, J. T., Baums, I. B., Stevens, J. R., Sanchez, J. A., . . . Day, O. (2012). Connectivity of Caribbean coral populations: complementary insights from empirical and modelled gene flow. *Molecular Ecology, 21*(5), 1143-1157.

Friedman, J., Hastie, T., & Tibshirani, R. (2010). Regularization paths for generalized linear models via coordinate descent. *Journal of statistical software, 33*(1), 1.

Fukami, H., Budd, A. F., Levitan, D. R., Jara, J., Kersanach, R., & Knowlton, N. (2004). Geographic differences in species boundaries among members of the Montastraea annularis complex based on molecular and morphological markers. *Evolution, 58*(2), 324-337.

Gaffney, P. M., Scott, T. M., Koehn, R., & Diehl, W. (1990). Interrelationships of heterozygosity, growth rate and heterozygote deficiencies in the coot clam, Mulinia lateralis. *Genetics, 124*(3), 687-699.

Gaines, S. D., Gaylord, B., & Largier, J. L. (2003). Avoiding current oversights in marine reserve design. *Ecological Applications*, S32-S46.

Galindo, H. M., Olson, D. B., & Palumbi, S. R. (2006). Seascape genetics: a coupled oceanographic-genetic model predicts population structure of Caribbean corals. *Current Biology, 16*(16), 1622-1626.

Gardner, T. A., Côté, I. M., Gill, J. A., Grant, A., & Watkinson, A. R. (2003). Long-term region-wide declines in Caribbean corals. *Science, 301*(5635), 958-960.

Gil-Agudelo, D. L., Smith, G. W., Garzón-Ferreira, J., Weil, E., & Petersen, D. (2004). Dark spots disease and yellow band disease, two poorly known coral diseases with high incidence in Caribbean reefs *Coral Health and Disease* (pp. 337-349): Springer.

Gintert, B. E., Manzello, D. P., Enochs, I. C., Kolodziej, G., Carlton, R., Gleason, A. C., & Gracias, N. (2018). Marked annual coral bleaching resilience of an inshore patch reef in the Florida Keys: A nugget of hope, aberrance, or last man standing? *Coral Reefs*, 1-15.

Gladfelter, E. H., Monahan, R. K., & Gladfelter, W. B. (1978). Growth rates of five reef-building corals in the northeastern Caribbean. *Bulletin of Marine Science, 28*(4), 728-734.

Glynn, P., & D'Croz, L. (1990). Experimental evidence for high temperature stress as the cause of El Nino-coincident coral mortality. *Coral Reefs, 8*(4), 181-191.

Goeman, J. J. (2010). L1 penalized estimation in the Cox proportional hazards model. *Biometrical Journal, 52*(1), 70-84.

Goodman, S. J., Barton, N. H., Swanson, G., Abernethy, K., & Pemberton, J. M. (1999). Introgression through rare hybridization: a genetic study of a hybrid zone between red and sika deer (genus Cervus) in Argyll, Scotland. *Genetics, 152*(1), 355-371.

Goreau, T., Cervino, J., Goreau, M., Hayes, R., Hayes, M., Richardson, L., . . . Garzon-Ferrera, J. (1998). Rapid spread of diseases in Caribbean coral reefs. *Revista de Biología Tropical, 46*(5), 157-171.

Goreau, T., McClanahan, T., Hayes, R., & Strong, A. (2000). Conservation of coral reefs after the 1998 global bleaching event. *Conservation Biology, 14*(1), 5-15.

Goudet, J. (1995). FSTAT (version 1.2): a computer program to calculate F-statistics. *Journal of Heredity, 86*(6), 485-486.

Goudet, J. (2001). FSTAT, a program to estimate and test gene diversities and fixation indices (version 2.9. 3).

Graham, E., Baird, A., & Connolly, S. (2008). Survival dynamics of scleractinian coral larvae and implications for dispersal. *Coral Reefs, 27*(3), 529-539.

Gratwicke, B., & Speight, M. R. (2005). Effects of habitat complexity on Caribbean marine fish assemblages. *Marine Ecology Progress Series, 292*, 301-310.

Green, D. H., Edmunds, P. J., & Carpenter, R. C. (2008). Increasing relative abundance of Porites astreoides on Caribbean reefs mediated by an overall decline in coral cover. *Marine Ecology Progress Series, 359*, 1-10.

Grottoli, A. G., Rodrigues, L. J., & Palardy, J. E. (2006). Heterotrophic plasticity and resilience in bleached corals. *Nature, 440*(7088), 1186.

Haslun, J. A., Hauff-Salas, B., Strychar, K. B., Ostrom, N. E., & Cervino, J. M. (2018). Biotic stress contributes to seawater temperature induced stress in a site-specific manner for Porites astreoides. *Marine Biology, 165*(10), 160.

Hastings, A., & Botsford, L. W. (2003). Comparing designs of marine reserves for fisheries and for biodiversity. *Ecological Applications*, S65-S70.

Helmle, K. P., Dodge, R. E., Swart, P. K., Gledhill, D. K., & Eakin, C. M. (2011). Growth rates of Florida corals from 1937 to 1996 and their response to climate change. *Nature Communications, 2*, 215.

Hetzinger, S., Pfeiffer, M., Dullo, W.-C., Keenlyside, N., Latif, M., & Zinke, J. (2008). Caribbean coral tracks Atlantic Multidecadal Oscillation and past hurricane activity. *Geology, 36*(1), 11-14.

Highsmith, R. C. (1981). Coral bioerosion: damage relative to skeletal density. *The American Naturalist, 117*(2), 193-198.

Hoegh-Guldberg, O., Mumby, P. J., Hooten, A. J., Steneck, R. S., Greenfield, P., Gomez, E., . . . Caldeira, K. (2007). Coral reefs under rapid climate change and ocean acidification. *Science, 318*(5857), 1737-1742.

Hubisz, M. J., Falush, D., Stephens, M., & Pritchard, J. K. (2009). Inferring weak population structure with the assistance of sample group information. *Molecular Ecology Resources, 9*(5), 1322-1332.

Hudson, J. H. (1981). Growth rates in *Montastraea annularis*: a record of environmental change in Key Largo Coral Reef Marine Sanctuary, Florida. *Bulletin of Marine Science, 31*(2), 444-459.

Hudson, J. H., Hanson, K. J., Halley, R. B., & Kindinger, J. L. (1994). Environmental implications of growth rate changes in *Montastrea annularis*: Biscayne National Park, Florida. *Bulletin of Marine Science, 54*(3), 647-669.

Hudson, J. H., Shinn, E. A., Halley, R. B., & Lidz, B. (1976). Sclerochronology: a tool for interpreting past environments. *Geology, 4*(6), 361-364.

Hughes, A. D., & Grottoli, A. G. (2013). Heterotrophic compensation: a possible mechanism for resilience of coral reefs to global warming or a sign of prolonged stress? *PloS one, 8*(11), e81172.

Hughes, T. P., Anderson, K. D., Connolly, S. R., Heron, S. F., Kerry, J. T., Lough, J. M., . . . Bridge, T. C. (2018). Spatial and temporal patterns of mass bleaching of corals in the Anthropocene. *Science, 359*(6371), 80-83.

Hughes, T. P., & Tanner, J. E. (2000). Recruitment failure, life histories, and long-term decline of Caribbean corals. *Ecology, 81*(8), 2250-2263.

Idjadi, J., & Edmunds, P. (2006). Scleractinian corals as facilitators for other invertebrates on a Caribbean reef. *Marine Ecology Progress Series, 319*, 117-127.

Jackson, J., Donovan, M., Cramer, K., & Lam, V. (2014). *Status and trends of Caribbean coral reefs: 1970-2012*: Global Coral Reef Monitoring Network.

Jakobsson, M., & Rosenberg, N. A. (2007). CLUMPP: a cluster matching and permutation program for dealing with label switching and multimodality in analysis of population structure. *Bioinformatics, 23*(14), 1801-1806.

Jokiel, P., & Coles, S. (1977). Effects of temperature on the mortality and growth of Hawaiian reef corals. *Marine Biology, 43*(3), 201-208.

Kemp, D. W., Oakley, C. A., Thornhill, D. J., Newcomb, L. A., Schmidt, G. W., & Fitt, W. K. (2011). Catastrophic mortality on inshore coral reefs of the Florida Keys due to severe low-temperature stress. *Global Change Biology, 17*(11), 3468-3477.

Kenkel, C. D., Almanza, A. T., & Matz, M. V. (2015). Fine-scale environmental specialization of reef-building corals might be limiting reef recovery in the Florida Keys. *Ecology, 96*(12), 3197-3212.

Kenkel, C. D., Goodbody-Gringley, G., Caillaud, D., Davies, S., Bartels, E., & Matz, M. (2013). Evidence for a host role in thermotolerance divergence between populations of the mustard hill coral (*Porites astreoides*) from different reef environments. *Molecular Ecology, 22*(16), 4335-4348.

Kenkel, C. D., & Matz, M. V. (2017). Gene expression plasticity as a mechanism of coral adaptation to a variable environment. *Nature Ecology & Evolution, 1*(1), 0014.

Kimes, N. E., Grim, C. J., Johnson, W. R., Hasan, N. A., Tall, B. D., Kothary, M. H., . . . Green, L. (2012). Temperature regulation of virulence factors in the pathogen *Vibrio coralliilyticus*. *ISME J, 6*(4), 835.

Knowlton, N. (2001). The future of coral reefs. *Proceedings of the National Academy of Sciences, 98*(10), 5419-5425.

Knowlton, N., Mate, J., Guzman, H., Rowan, R., & Jara, J. (1997). Direct evidence for reproductive isolation among the three species of the Montastraea annularis complex in Central America (Panama and Honduras). *Marine Biology, 127*(4), 705-711.

Koop, K., Booth, D., Broadbent, A., Brodie, J., Bucher, D., Capone, D., . . . Harrison, P. (2001). ENCORE: the effect of nutrient enrichment on coral reefs. Synthesis of results and conclusions. *Marine Pollution Bulletin, 42*(2), 91-120.

Kuffner, I. B., Lidz, B. H., Hudson, J. H., & Anderson, J. S. (2015). A century of ocean warming on Florida Keys coral reefs: historic in situ observations. *Estuaries and Coasts, 38*(3), 1085-1096.

Kuta, K., & Richardson, L. (1996). Abundance and distribution of black band disease on coral reefs in the northern Florida Keys. *Coral Reefs, 15*(4), 219-223.

Kwiatkowski, L., Cox, P. M., Economou, T., Halloran, P. R., Mumby, P. J., Booth, B. B., . . . Guzman, H. M. (2013). Caribbean coral growth influenced by anthropogenic aerosol emissions. *Nature Geoscience, 6*(5), 362.

Lindo-Atichati, D., Curcic, M., Paris, C., & Buston, P. (2016). Description of surface transport in the region of the Belizean Barrier Reef based on observations and alternative high-resolution models. *Ocean Modelling*.

Lirman, D., & Fong, P. (2007). Is proximity to land-based sources of coral stressors an appropriate measure of risk to coral reefs? An example from the Florida Reef Tract. *Marine Pollution Bulletin, 54*(6), 779-791.

Lirman, D., Schopmeyer, S., Manzello, D., Gramer, L. J., Precht, W. F., Muller-Karger, F., . . . Bourque, A. (2011). Severe 2010 cold-water event caused unprecedented mortality to corals of the Florida reef tract and reversed previous survivorship patterns. *PloS one, 6*(8), e23047.

Lough, J., & Barnes, D. (2000). Environmental controls on growth of the massive coral Porites. *Journal of Experimental Marine Biology and Ecology, 245*(2), 225-243.

Lugo-Fernández, A., Deslarzes, K. J., Price, J. M., Boland, G. S., & Morin, M. V. (2001). Inferring probable dispersal of Flower Garden Banks coral larvae (Gulf of Mexico) using observed and simulated drifter trajectories. *Continental Shelf Research, 21*(1), 47-67.

Lunz, K., Landsberg, J., Kiryu, Y., & Brinkhuis, V. (2017). *Investigation of the Coral Disease Outbreak Affecting Scleractinian Coral Species along the Florida Reef Tract*. Miami, FL: FL DEP.

Macintyre, I. G., & Pilkey, O. H. (1969). Tropical Reef Corals: Tolerance of Low Temperatures on the North Carolina Continental Shelf. *Science, 166*(3903), 374-375.

MacNeil, M. A., Mellin, C., Matthews, S., Wolff, N. H., McClanahan, T. R., Devlin, M., . . . Graham, N. A. (2019). Water quality mediates resilience on the Great Barrier Reef. *Nature Ecology & Evolution*, 1.

Manica, A., & Carter, R. (2000). Morphological and fluorescence analysis of the Montastraea annularis species complex in Florida. *Marine Biology, 137*(5-6), 899-906.

Manzello, D. P. (2015). Rapid recent warming of coral reefs in the Florida Keys. *Scientific Reports, 5*.

Manzello, D. P., Berkelmans, R., & Hendee, J. C. (2007). Coral bleaching indices and thresholds for the Florida Reef Tract, Bahamas, and St. Croix, US Virgin Islands. *Marine Pollution Bulletin, 54*(12), 1923-1931.

Manzello, D. P., Enochs, I. C., Kolodziej, G., & Carlton, R. (2015). Recent decade of growth and calcification of *Orbicella faveolata* in the Florida Keys: an inshore-offshore comparison. *Marine Ecology Progress Series, 521*, 81-89.

Manzello, D. P., Enochs, I. C., Melo, N., Gledhill, D. K., & Johns, E. M. (2012). Ocean acidification refugia of the Florida Reef Tract. *PloS one, 7*(7), e41715.

Marron, J. S., Todd, M. J., & Ahn, J. (2007). Distance-weighted discrimination. *Journal of the American Statistical Association, 102*(480), 1267-1271.

Marszalek, D., Babashoff, G., Noel, M., & Worley, D. (1977). Reef distribution in south Florida. *Proceedings of the 3rd International Coral Reef Symposium, 2*, 223-229.

Marubini, F., & Atkinson, M. (1999). Effects of lowered pH and elevated nitrate on coral calcification. *Marine Ecology Progress Series, 188*, 117-121.

McCulloch, M., Falter, J., Trotter, J., & Montagna, P. (2012). Coral resilience to ocean acidification and global warming through pH up-regulation. *Nature Climate Change, 2*(8), 623.

Meirmans, P. G., & Hedrick, P. W. (2011). Assessing population structure: FST and related measures. *Molecular Ecology Resources, 11*(1), 5-18.

Mendes, J., & Woodley, J. (2002). Effect of the 1995-1996 bleaching event on polyp tissue depth, growth, reproduction and skeletal band formation in Montastraea annularis. *Marine Ecology Progress Series, 235*, 93-102.

Miller, K., & Mundy, C. (2003). Rapid settlement in broadcast spawning corals: implications for larval dispersal. *Coral Reefs, 22*(2), 99-106.

Miller, M., Bourque, A., & Bohnsack, J. (2002). An analysis of the loss of acroporid corals at Looe Key, Florida, USA: 1983-2000. *Coral Reefs, 21*(2), 179-182.

Mollica, N. R., Guo, W., Cohen, A. L., Huang, K.-F., Foster, G. L., Donald, H. K., & Solow, A. R. (2018). Ocean acidification affects coral growth by reducing skeletal density. *Proceedings of the National Academy of Sciences, 115*(8), 1754-1759.

Morgan, K. M., Perry, C. T., Johnson, J. A., & Smithers, S. G. (2017). Nearshore turbid-zone corals exhibit high bleaching tolerance on the great barrier reef following the 2016 ocean warming event. *Frontiers in Marine Science, 4*, 224.

Muller, E., van Woesik, R., & Sartor, C. (2018). *Spatial Epidemiology Modeling of the Florida Coral Disease Outbreak*. Retrieved from

Muscatine, L., & Porter, J. W. (1977). Reef corals: mutualistic symbioses adapted to nutrient-poor environments. *Bioscience, 27*(7), 454-460.

Endangered and Threatened Wildlife and Plants: Final Listing Determinations on Proposal To List 66 Reef-Building Coral Species and To Reclassify Elkhorn and Staghorn Corals, 0648-XT12 C.F.R. (2014).

Nei, M., & Chesser, R. K. (1983). Estimation of fixation indices and gene diversities. *Annals of Human Genetics, 47*(3), 253-259.

Okazaki, R. R., Towle, E. K., Hooidonk, R., Mor, C., Winter, R. N., Piggot, A. M., . . . Swart, P. K. (2017). Species-specific responses to climate change and community composition determine future calcification rates of Florida Keys reefs. *Global Change Biology, 23*(3), 1023-1035.

Palumbi, S. R. (2003). Population genetics, demographic connectivity, and the design of marine reserves. *Ecological Applications*, S146-S158.

Palumbi, S. R., Barshis, D. J., Traylor-Knowles, N., & Bay, R. A. (2014). Mechanisms of reef coral resistance to future climate change. *Science, 344*(6186), 895-898.

Paris, C. B., Chérubin, L. M., & Cowen, R. K. (2007). Surfing, spinning, or diving from reef to reef: effects on population connectivity. *Marine Ecology Progress Series, 347*, 285-300.

Paris, C. B., & Cowen, R. K. (2004). Direct evidence of a biophysical retention mechanism for coral reef fish larvae. *Limnology and Oceanography, 49*(6), 1964-1979.

Paris, C. B., Cowen, R. K., Lwiza, K. M., Wang, D.-P., & Olson, D. B. (2002). Multivariate objective analysis of the coastal circulation of Barbados, West Indies: implication for larval transport. *Deep Sea Research Part I: Oceanographic Research Papers, 49*(8), 1363-1386.

Peakall, R., & Smouse, P. E. (2006). GENALEX 6: genetic analysis in Excel. Population genetic software for teaching and research. *Molecular Ecology Notes, 6*(1), 288-295.

Pebesma, E. J. (2004). Multivariable geostatistics in S: the gstat package. *Computational Geosciences, 30*(7), 683-691.

Pespeni, M. H., & Palumbi, S. R. (2013). Signals of selection in outlier loci in a widely dispersing species across an environmental mosaic. *Molecular Ecology, 22*(13), 3580-3597.

Pinheiro, J., Bates, D., DebRoy, S., Sarkar, D., & R Core Team. (2012). nlme: Linear and nonlinear mixed effects models. *R package version, 3*(0).

Porter, J. W., Dustan, P., Jaap, W. C., Patterson, K. L., Kosmynin, V., Meier, O. W., . . . Parsons, M. (2001). Patterns of spread of coral disease in the Florida Keys *The Ecology and Etiology of Newly Emerging Marine Diseases* (Porter, J.W. ed., Vol. 159, pp. 1-24). Dordrecht: Springer.

Porter, J. W., Torres, C., Sutherland, K. P., Meyers, M. K., Callahan, M. K., Ruzicka, R., & Colella, M. (2011). Prevalence, severity, lethality, and recovery of dark spots syndrome among three Floridian reef-building corals. *Journal of Experimental Marine Biology and Ecology, 408*(1-2), 79-87.

Porto-Hannes, I., Zubillaga, A., Shearer, T., Bastidas, C., Salazar, C., Coffroth, M., & Szmant, A. (2015). Population structure of the corals Orbicella faveolata and Acropora palmata in the Mesoamerican Barrier Reef System with comparisons over Caribbean basin-wide spatial scale. *Marine Biology, 162*(1), 81-98.

Pratchett, M. S., Anderson, K. D., Hoogenboom, M. O., Widman, E., Baird, A. H., Pandolfi, J. M., . . . Lough, J. M. (2015). Spatial, temporal and taxonomic variation in coral growth—implications for the structure and function of coral reef ecosystems. *Oceanography and Marine Biology: An Annual Review, 53*, 215-295.

Precht, W. F., Gintert, B. E., Robbart, M. L., Fura, R., & Van Woesik, R. (2016). Unprecedented disease-related coral mortality in Southeastern Florida. *Scientific Reports, 6*, 31374.

Pritchard, J. K., Stephens, M., & Donnelly, P. (2000). Inference of population structure using multilocus genotype data. *Genetics, 155*(2), 945-959.

R Core Team. (2017). R: A language and environment for statistical computing. Vienna, Austria: R Foundation for Statistical Computing. Retrieved from https://www.r-project.org/

Rasband, W. S. ImageJ. U. S. National Institutes of Health, Bethesda, Maryland, USA, https://imagej.nih.gov/ij/, 1997-2018.

Raymond, M., & Rousset, F. (1995). GENEPOP (version 1.2): population genetics software for exact tests and ecumenicism. *Journal of Heredity, 86*(3), 248-249.

Rhein, M., Rintoul, S. R., Aoki, S., Campos, E., Chambers, D., Feely, R. A., . . . Wang, F. (2013). *Observations: Ocean*. Retrieved from Cambridge University Press, Cambridge, United Kingdom and New York, NY, USA.:

Richardson, L. L., Goldberg, W. M., Carlton, R. G., & Halas, J. C. (1998). Coral disease outbreak in the Florida Keys: plague type II. *Revista de Biología Tropical, 46*(5), 187-198.

Richardson, P. (2005). Caribbean Current and eddies as observed by surface drifters. *Deep Sea Research Part II: Topical Studies in Oceanography, 52*(3), 429-463.

Ries, J. B., Cohen, A. L., & McCorkle, D. C. (2009). Marine calcifiers exhibit mixed responses to CO2-induced ocean acidification. *Geology, 37*(12), 1131-1134.

Ries, J. B., Cohen, A. L., & McCorkle, D. C. (2010). A nonlinear calcification response to CO2-induced ocean acidification by the coral *Oculina arbuscula*. *Coral Reefs, 29*(3), 661-674.

Rippe, J. P., Baumann, J. H., De Leener, D., Aichelman, H. E., Friedlander, E. B., Davies, S. W., & Castillo, K. D. (2018). Corals sustain growth but not skeletal density across the Florida Keys Reef Tract despite ongoing warming. *Global Change Biology, 24*(11), 5204-5217.

Risk, M. J. (1972). *Fish diversity on a coral reef in the Virgin Islands*: Smithsonian Institution.

Roques, S., Sévigny, J. M., & Bernatchez, L. (2001). Evidence for broadscale introgressive hybridization between two redfish (genus Sebastes) in the North-west Atlantic: a rare marine example. *Molecular Ecology, 10*(1), 149-165.

Rosenberg, N. A. (2004). DISTRUCT: a program for the graphical display of population structure. *Molecular Ecology Notes, 4*(1), 137-138.

Rousset, F. (1997). Genetic differentiation and estimation of gene flow from F-statistics under isolation by distance. *Genetics, 145*(4), 1219-1228.

Rousset, F. (2008). genepop'007: a complete re-implementation of the genepop software for Windows and Linux. *Molecular Ecology Resources, 8*(1), 103-106.

Ruiz-Moreno, D., Willis, B. L., Page, A. C., Weil, E., Cróquer, A., Vargas-Angel, B., . . . Harvell, C. D. (2012). Global coral disease prevalence associated with sea temperature anomalies and local factors. *Diseases of aquatic organisms, 100*(3), 249-261.

Ruzicka, R. R., Colella, M., Porter, J., Morrison, J., Kidney, J., Brinkhuis, V., . . . Meyers, M. (2013). Temporal changes in benthic assemblages on Florida Keys reefs 11 years after the 1997/1998 El Niño. *Marine Ecology Progress Series, 489*, 125-141.

Ruzicka, R. R., Semon, K., Colella, M., Brinkhuis, V., Kidney, J., Morrison, J., . . . Colee, J. (2010). Coral Reef Ecological Monitoring Program 2009 Final Report. *Fish & Wildlife Research Institute/Florida Fish & Wildlife Conservation Commission*.

Scoffin, T., Tudhope, A., Brown, B., Chansang, H., & Cheeney, R. (1992). Patterns and possible environmental controls of skeletogenesis of Porites lutea, South Thailand. *Coral Reefs, 11*(1), 1-11.

Selkoe, K., & Toonen, R. J. (2011). Marine connectivity: a new look at pelagic larval duration and genetic metrics of dispersal. *Marine Ecology Progress Series, 436*, 291-305.

Severance, E. G., & Karl, S. A. (2006). Contrasting population genetic structures of sympatric, mass-spawning Caribbean corals. *Marine Biology, 150*(1), 57-68.

Severance, E. G., Szmant, A. M., & Karl, S. A. (2004). Microsatellite loci isolated from the Caribbean coral, Montastraea annularis. *Molecular Ecology Notes, 4*(1), 74-76.

Shanks, A. L. (2009). Pelagic larval duration and dispersal distance revisited. *The Biological Bulletin, 216*(3), 373-385.

Shi, W., & Wang, M. (2010). Characterization of global ocean turbidity from Moderate Resolution Imaging Spectroradiometer ocean color observations. *Journal of Geophysical Research: Oceans, 115*(C11).

Slate, J., David, P., Dodds, K., Veenvliet, B., Glass, B., Broad, T., & McEwan, J. (2004). Understanding the relationship between the inbreeding coefficient and multilocus heterozygosity: theoretical expectations and empirical data. *Heredity, 93*(3), 255-265.

Somerfield, P., Jaap, W., Clarke, K., Callahan, M., Hackett, K., Porter, J., . . . Yanev, G. (2008). Changes in coral reef communities among the Florida Keys, 1996–2003. *Coral Reefs, 27*(4), 951-965.

Soto, I., Muller Karger, F., Hallock, P., & Hu, C. (2011). Sea surface temperature variability in the Florida Keys and its relationship to coral cover. *Journal of Marine Biology, 2011*.

Swearer, S. E., Shima, J. S., Hellberg, M. E., Thorrold, S. R., Jones, G. P., Robertson, D. R., . . . Warner, R. R. (2002). Evidence of self-recruitment in demersal marine populations. *Bulletin of Marine Science, 70*(1), 251-271.

Szmant, A. (1991). Sexual reproduction by the Caribbean reef corals Mon tastrea ann ularis and M. ca vernosa. *Marine Ecology Progress Series, 7*(4), 13-25.

Szmant, A., & Forrester, A. (1996). Water column and sediment nitrogen and phosphorus distribution patterns in the Florida Keys, USA. *Coral Reefs, 15*(1), 21-41.

Szmant, A., & Meadows, M. (2006). *Developmental changes in coral larval buoyancy and vertical swimming behavior: implications for dispersal and connectivity.* Paper presented at the Proceedings of the 10th International Coral Reef Symposium.

Szmant, A., & Miller, M. (2006). *Settlement preferences and post-settlement mortality of laboratory cultured and settled larvae of the Caribbean hermatypic corals Montastraea faveolata and Acropora palmata in the Florida Keys, USA.* Paper presented at the Proceedings of the 10th International Coral Reef Symposium.

Szmant, A., Weil, E., Miller, M., & Colon, D. (1997). Hybridization within the species complex of the scleractinan coral Montastraea annularis. *Marine Biology, 129*(4), 561-572.

Tambutté, E., Venn, A., Holcomb, M., Segonds, N., Techer, N., Zoccola, D., . . . Tambutté, S. (2015). Morphological plasticity of the coral skeleton under CO 2-driven seawater acidification. *Nature Communications, 6*, 7368.

Tang, L., Sheng, J., Hatcher, B. G., & Sale, P. F. (2006). Numerical study of circulation, dispersion, and hydrodynamic connectivity of surface waters on the Belize shelf. *Journal of Geophysical Research: Oceans, 111*(C1).

Tanzil, J. T., Brown, B. E., Dunne, R. P., Lee, J. N., Kaandorp, J. A., & Todd, P. A. (2013). Regional decline in growth rates of massive Porites corals in Southeast Asia. *Global Change Biology, 19*(10), 3011-3023.

Tanzil, J. T., Brown, B. E., Tudhope, A. W., & Dunne, R. P. (2009). Decline in skeletal growth of the coral *Porites lutea* from the Andaman Sea, South Thailand between 1984 and 2005. *Coral Reefs, 28*(2), 519-528.

Taylor, R., Barnes, D., & Lough, J. (1993). Simple models of density band formation in massive corals. *Journal of Experimental Marine Biology and Ecology, 167*(1), 109-125.

Tebben, J., Motti, C., Siboni, N., Tapiolas, D., Negri, A., Schupp, P., . . . Harder, T. (2015). Chemical mediation of coral larval settlement by crustose coralline algae. *Scientific Reports, 5*.

Thomson, D., & Frisch, A. (2010). Extraordinarily high coral cover on a nearshore, high-latitude reef in south-west Australia. *Coral Reefs, 29*(4), 923-927.

Underwood, J. N., Smith, L. D., Van Oppen, M. J., & Gilmour, J. P. (2009). Ecologically relevant dispersal of corals on isolated reefs: implications for managing resilience. *Ecological Applications, 19*(1), 18-29.

van Hooidonk, R., Maynard, J., & Planes, S. (2013). Temporary refugia for coral reefs in a warming world. *Nature Climate Change, 3*(5), 508-511.

van Woesik, R., & McCaffrey, K. R. (2017). Repeated thermal stress, shading, and directional selection in the Florida Reef Tract. *Frontiers in Marine Science, 4*, 182.

van Woesik, R., Scott, W. J., & Aronson, R. B. (2014). Lost opportunities: coral recruitment does not translate to reef recovery in the Florida Keys. *Marine Pollution Bulletin, 88*(1), 110-117.

Vega Thurber, R. L., Burkepile, D. E., Fuchs, C., Shantz, A. A., McMinds, R., & Zaneveld, J. R. (2014). Chronic nutrient enrichment increases prevalence and severity of coral disease and bleaching. *Global Change Biology, 20*(2), 544-554.

Venables, W. N., & Ripley, B. D. (2002). *Modern Applied Statistics with S. Fourth Edition.* New York: Springer.

Vize, P. D. (2006). Deepwater broadcast spawning by Montastraea cavernosa, Montastraea franksi, and Diploria strigosa at the Flower Garden Banks, Gulf of Mexico. *Coral Reefs, 25*(1), 169-171.

Vollmer, S. V., & Palumbi, S. R. (2007). Restricted gene flow in the Caribbean staghorn coral Acropora cervicornis: implications for the recovery of endangered reefs. *Journal of Heredity, 98*(1), 40-50.

Wagner, D. E., Kramer, P., & Van Woesik, R. (2010). Species composition, habitat, and water quality influence coral bleaching in southern Florida. *Marine Ecology Progress Series, 408*, 65-78.

Wahlund, S. (1928). Zusammensetzung von Populationen und Korrelationserscheinungen vom Standpunkt der Vererbungslehre aus betrachtet. *Hereditas, 11*(1), 65-106.

Waples, R. S. (2014). Testing for Hardy–Weinberg proportions: have we lost the plot? *Journal of Heredity*, esu062.

Wei, J., Lee, Z., & Shang, S. (2016). A system to measure the data quality of spectral remote-sensing reflectance of aquatic environments. *Journal of Geophysical Research: Oceans, 121*(11), 8189-8207.

Wei, S., Lee, C., Wichers, L., & Marron, J. (2016). Direction-projection-permutation for high-dimensional hypothesis tests. *Journal of Computational and Graphical Statistics, 25*(2), 549-569.

Weil, E. (2004). Coral reef diseases in the wider Caribbean *Coral Health and Disease* (pp. 35-68): Springer.

Weil, E., & Knowton, N. (1994). A multi-character analysis of the Caribbean coral Montastraea annularis (Ellis and Solander, 1786) and its two sibling species, M. faveolata (Ellis and Solander, 1786) and M. franksi (Gregory, 1895). *Bulletin of Marine Science, 55*(1), 151-175.

Wellington, G., & Fitt, W. (2003). Influence of UV radiation on the survival of larvae from broadcast-spawning reef corals. *Marine Biology, 143*(6), 1185-1192.

Wiedenmann, J., D'Angelo, C., Smith, E. G., Hunt, A. N., Legiret, F.-E., Postle, A. D., & Achterberg, E. P. (2013). Nutrient enrichment can increase the susceptibility of reef corals to bleaching. *Nature Climate Change, 3*(2), 160.

Wilkinson, C. R., & Souter, D. (2008). Status of Caribbean coral reefs after bleaching and hurricanes in 2005.

Wood, S. N. (2011). Fast stable restricted maximum likelihood and marginal likelihood estimation of semiparametric generalized linear models. *Journal of the Royal Statistical Society: Series B (Statistical Methodology), 73*(1), 3-36.

Wood, S. N. (2017). *Generalized Additive Models: An Introduction with R (2nd Edition)*: Chapman and Hall/CRC press.

Wood, S. N., Pya, N., & Säfken, B. (2016). Smoothing parameter and model selection for general smooth models. *Journal of the American Statistical Association, 111*(516), 1548-1563.

Wooldridge, S. A. (2009). Water quality and coral bleaching thresholds: Formalising the linkage for the inshore reefs of the Great Barrier Reef, Australia. *Marine Pollution Bulletin, 58*(5), 745-751.

Wooldridge, S. A. (2013). A new conceptual model of coral biomineralisation: hypoxia as the physiological driver of skeletal extension. *Biogeosciences, 10*(5), 2867.

Wooldridge, S. A. (2014). Formalising a mechanistic linkage between heterotrophic feeding and thermal bleaching resistance. *Coral Reefs, 33*(4), 1131-1136.

Zimmer, B., Duncan, L., Aronson, R., Deslarzes, K., Deis, D., Robbart, M., . . . Weil, E. (2010). Long-term monitoring at the East and West Flower Garden Banks, 2004-2008 *Technical Report* (Vol. 1): US Dept. of the Interior, Bureau of Ocean Energy Management, Regulation and Enforcement, Gulf of Mexico OCS Region New Orleans, Louisiana.